INFORMATION TO USERS

This manuscript has been reproduced from the microfilm master. UMI films the text directly from the original or copy submitted. Thus, some thesis and dissertation copies are in typewriter face, while others may be from any type of computer printer.

The quality of this reproduction is dependent upon the quality of the copy submitted. Broken or indistinct print, colored or poor quality illustrations and photographs, print bleedthrough, substandard margins, and improper alignment can adversely affect reproduction.

In the unlikely event that the author did not send UMI a complete manuscript and there are missing pages, these will be noted. Also, if unauthorized copyright material had to be removed, a note will indicate the deletion.

Oversize materials (e.g., maps, drawings, charts) are reproduced by sectioning the original, beginning at the upper left-hand corner and continuing from left to right in equal sections with small overlaps.

ProQuest Information and Learning
300 North Zeeb Road, Ann Arbor, MI 48106-1346 USA
800-521-0600

Université d'Ottawa • University of Ottawa

SEISMIC TESTING OF UNREINFORCED MASONRY BUILDING WITH FLEXIBLE DIAPHRAGM

by

Jocelyn Paquette

Thesis submitted to the Faculty of Graduate and Post Doctoral Studies
in partial fulfillment of the requirements for the
Doctor of Philosophy Degree in Civil Engineering
under the auspices of the
Ottawa-Carleton Institute for Civil Engineering

February 2002

Department of Civil Engineering, University of Ottawa

Ottawa, Canada, 2002

Abstract

Appendix 1 of the Uniform Code for Building Conservation (UCBC) presents a systematic procedure for the evaluation and seismic strengthening of unreinforced masonry (URM) bearing wall buildings having flexible diaphragms. However, even though this procedure is founded on extensive component testing, full scale testing of an entire 3-D building having wood diaphragms has not been conducted. Such a test would complement the computer simulations and small-scale shake table tests done by other researchers. For those reasons, a full-scale one-story unreinforced brick masonry specimen having a wood diaphragm was subjected to earthquake excitations using pseudo-dynamic testing. The specimen was designed to better understand the flexible-floor/rigid-wall interaction, the impact of wall continuity at the building corners and the effect of a relatively weak diaphragm on the expected seismic behavior. The unreinforced masonry walls of this building were also repaired with fiberglass materials and re-tested. The dynamic response of the shear walls with piers having a rocking and/or a sliding behavior is analyzed, as well as the response of the wood diaphragm and its interaction with the shear walls. These results are compared with predictions from existing seismic evaluation methodologies and demonstrate how fiberglass strips can be used to improve the rocking behavior.

Furthermore, for masonry walls subjected to out-of-plane seismic forces, while it is required to anchor the wall at every floor as a minimum, questions arise as to whether it is also necessary to retrofit the walls between floors. Notably for the facade of many older (circa 1900) residential buildings in North America in which a single wythe exterior masonry wall was tied only with nails to the timber structure, leaving an irregular gap between the masonry and timber walls. To partly answer these questions, three specimens were extracted from an existing building, and were tested using a shake table, submitting them to multiple ground motions of progressively larger intensity until structural failure. Different retrofit methods to increase out-of-plane stiffness and strength were investigated, and various analytical procedures to explain the observed behavior are discussed.

À ma mère Gisèle et ma soeur Sylvie

À la mémoire de mon père Léo

Acknowledgments

My special thanks go to my supervisor, Dr. Michel Bruneau for his support, advice and patience, without his directions, this thesis could not have been done. I would like to thank Dr. S. Nikolic-Brzev for her collaboration, comments and suggestions with the fiberglass rehabilitation, and Dr. A. Filiatrault for his extensive contribution to Chapter 5. Dr. N.J. Gardner is greatly acknowledged for his additional assistance. Thanks are also due to my fellow graduate students for their help during this project, in particular to Mr. Majid Sarraf for his help on the pseudo-dynamic system.

Also, I would like to thank all the Structures laboratory technicians, machine shop and supporting staffs in the Civil Engineering Department for their kindness and help all the time. The assistance of the Structures laboratory technicians at Ecole Polytechnique in Montreal is also appreciated as well as the collaboration of Mr. Claude Guertin. For the construction of the specimen, I acknowledge the donation of materials and labour by Brampton Brick, Fitzgerald Building Supplies (1996) Limited, Ottawa Region Masonry Contractors Association, International Union of Brick Layers and Allied Craftsmen (Industrial Promotion Fund), Canadian Portland Cement Association, George and Asmussen Limited, R.J. Watson Inc., Cintec Canada Ltd., Composite Retrofit International (Tyfo S Fibrwrap System) and Fyfe Co. L.L.C.

Je tiens à remercier profondément mes parents Léo et Gisèle ainsi que ma soeur Sylvie qui m'ont soutenu tout au long de mes études et qui ont fait en sorte, par leur amour, leur tendresse et leur soutien financier, que je puisse avoir les meilleures conditions possibles pour que je termine mes études universitaires. Enfin, mes pensées vont à mon père décédé en février 1998. Qu'il trouve ici toute ma gratitude et mon amour pour lui.

Table of Contents

CHAPTER 3

CHAPTER 4

List of Tables

List of Figures

Notations

A	mortared area, mm^2
A_n	net mortared area, mm^2
b	diaphragm width, mm
c	fraction of strength loss for secondary element, dimensionless
c	reduced strength parameter for diaphragm, dimensionless
d	inelastic drift percentage deformation capacity for primary element, dimensionless
d	parameter for maximum possible deflection at yield strength, dimensionless
d_1,	diaphragm's width, mm
d_2	diaphragm's width, mm
D	in-plane width dimension of masonry, mm
D	diaphragm's width, mm
e	inelastic drift percentage deformation capacity for secondary element, dimensionless
e	parameter for maximum deflection at a reduced strength, dimensionless
e	mid-span deformation of diaphragm, mm
E_m	modulus of elasticity of masonry, MPa
f_{ae}	expected vertical compressive stress, MPa
f'_{br}	brick compressive strength, MPa
f'_{dt}	diagonal tension strength, MPa
f'_m	masonry compressive strength, MPa
f'_{me}	expected masonry compressive strength, MPa
f'_{mort}	mortar compressive strength, MPa
f_t	tensile strength of masonry, MPa
F	foundation factor in NBCC, dimensionless
F(e)	force at the diaphragm's end, kN
F_u	ultimate force (asymptote), kN
G_d	diaphragm shear stiffness, N/mm

h height of unreinforced masonry wall measured between wall anchorage level, mm

h_{eff} effective height of pier reflecting crack pattern, mm

H least clear height of opening on either side of pier, mm

I importance factor in NBCC, dimensionless

k_1 diaphragm's initial stiffness, kN/mm

k_2 diaphragm's initial stiffness, kN/mm

k_i initial stiffness for diaphragm, kN/mm

l_1 diaphragm's length, mm

l_2 diaphragm's length, mm

L length of pier, mm

L diaphragm span, mm

P_{CE} expected vertical axial compressive force on pier, kN

P_D superimposed dead load at the top of the pier under consideration, kN

t wall thickness, mm

V_a shear strength of unreinforced masonry pier, kN

V_{bfs1} shear strength with bond plus friction, kN

V_{bfs2} shear strength with friction only, kN

V_{cr} strength to initiate cracking in a masonry pier, kN

V_{dt} diagonal tension capacity for unreinforced masonry pier, kN

V_p normal force through wall anchors, kN

V_r pier rocking capacity, kN

V_s shear force through wall anchors, kN

V_{tc} toe crushing capacity, kN

W_d total dead load tributary to a diaphragm including walls perpendicular to the direction of motion, kN

W_n tributary weight of wall from mid-height of the storey above to mid-height of storey below, kN

W_{wx} dead load of unreinforced masonry wall assigned to level x halfway above and below the level under consideration, kN

z' effective zonal velocity ratio, dimensionless

α factor for fixed-fixed or fixed-free pier, dimensionless

β coefficient for pier aspect ratio, dimensionless

Δ diaphragm's deflection, mm

v maximum shear in the direction under consideration for diaphragm, N/mm

v zonal velocity ratio, dimensionless

v' effective velocity ratio, dimensionless

v_a allowable shear stress for unreinforced masonry, psi

v_m shear strength for unreinforced masonry, MPa

v_{me} expected masonry shear strength, MPa

v_t mortar shear strength, MPa

v_{te} mortar bond strength, MPa

v_u unit shear strength of a diaphragm, kN/mm

ABBREVIATIONS

ABK	Agbabian, Barnes, and Kariotis joint venture
CGSEEB	Canadian Guidelines for Seismic Evaluation of Existing Buildings
CP	Collapse prevention
DCR	Demand-capacity ratio
DOF	Degree of freedom
FEMA	Federal Emergency Management Agency
IO	Immediate occupancy
LS	Life safety
LVDT	Linear voltage displacement transducer
NBCC	National building code of Canada
NEHRP	National earthquake hazards reduction program
PGA	Peak ground acceleration

PGV	Peak ground velocity
PHA	Peak horizontal acceleration
UCBC	Uniform Code for Building Conservation
URM	Unreinforced masonry

CHAPTER 1

Introduction

1.1 General

The seismic hazard posed by old unreinforced masonry buildings (URM) has been long recognized. The deficient seismic strength and/or ductility of many older existing URM buildings is a very critical problem in most of eastern and western North America, and many URM buildings would suffer damage or even collapse in the event of a severe earthquake. However, as reported during major earthquakes, URM buildings can perform surprisingly well under certain circumstances. Thus, the evaluation of the seismic resistance of URM is of prime importance in a seismic hazard mitigation strategy. In a general way, the objective of the research presented here is to conduct full scale experiments that are needed to enhance the existing knowledge on this topic and to verify existing analysis and evaluation procedures.

1.2 Unreinforced Masonry Buildings with Flexible Diaphragms

The Uniform Code for Building Conservation (UCBC) (International Conference of Building Officials (ICBO) 1997) *Seismic Strengthening Provisions for Unreinforced Masonry Bearing Wall Buildings* presents a systematic procedure for the evaluation and seismic strengthening of unreinforced masonry (URM) bearing wall buildings having flexible diaphragms. This special procedure, adapted from one developed by the Agbabian, Barnes, and Kariotis (ABK) joint venture (ABK 1984, Federal Emergency Management Agency (FEMA) 1992), used extensively in the Los Angeles area, and described in detail by Bruneau (1994a, 1994b), has made it economically possible to significantly reduce the seismic hazard posed by these buildings, as evidenced by the considerably less damage suffered by seismically retrofitted

URM buildings in recent earthquakes, compared to non-retrofitted ones (Bruneau 1990, 1995, Rutherford and Chekene 1991). However, even though this procedure is founded on extensive component testing, full scale testing of an entire URM building having wood diaphragms has not been conducted. Such a test would complement the computer simulations and small-scale shake table tests done by other researchers (Costley and Abrams 1995).

In this research program, one such test was conducted on a full scale 4.1 m x 5.7 m x 2.7 m single story URM building designed with the objective of better understanding the flexible-floor/rigid-wall interaction and the impact of wall continuity at the building corners on the expected seismic behavior. The building was cycled up to its ultimate limit state, repaired using fiberglass strips, and retested.

1.3 Out-of-Plane Seismic Resistance of Existing Masonry Walls

A construction technique widely used for the facade and common walls of many older (circa 1900) residential buildings in North America consisted of laying a single wythe exterior masonry wall along the wood structure. This was partly done as a fire-propagation prevention measure in dense urban areas. Generally, the wood building would consist of stacked rough-cut timber planks laterally supported by vertical (wind) posts. The masonry walls typically resisted their own weights over the height of the building (usually 3 to 4 stories) and were tied only with nails to the wood backing. The nail heads were embedded in mortar joints, every four or five brick layers, and spaced horizontally at approximately 300 mm. This construction procedure left an irregular gap between the masonry and the timber wall.

Such buildings have been constructed in parts of eastern North America where large but infrequent earthquakes are expected to occur. It has been repeatedly shown, following earthquakes worldwide, that unreinforced masonry walls can be particularly vulnerable to strong ground shaking, and the type of construction described above should be no exception. It may thus be assumed that, as a minimum seismic retrofit measure, walls would have to be

anchored at the floor/roof levels using standard seismic-resistant details (e.g. as specified in ICBO 1997). However, because the interaction between the masonry and timber backing is not well understood for this type of construction subjected to out-of-plane seismic excitation, questions arise as to whether it is also necessary to retrofit the walls between floors. In particular, having access to only one side of the masonry surface may require that new retrofit schemes be developed. Given that such buildings commonly provide low-cost housing in regions of low seismic awareness, excessive structural interventions are unlikely to be implemented.

In that perspective, out-of-plane shake table tests were conducted on three unreinforced masonry walls and wood backing assemblies extracted from an older existing residential building. The availability of this building provided a special opportunity since reproducing the actual conditions and properties of these older structures with new materials in the laboratory would have been difficult. The first wall was tested in its original condition, while the two others were retrofitted with different methods prior to testing.

1.4 Outline of the Thesis

Chapter 2 presents a review of prior research findings on the seismic resistance and behavior of masonry components and structures, and wood diaphragms.

Chapter 3 presents the characteristics of the specimen (and the concepts underlying its design), and the results of the test program.

Chapter 4 presents the analysis of the results from these tests, for the diaphragm and for the shear walls, and compares them with expected performance predicted by different codified equations, notably those from the FEMA 273 and 306 documents.

Chapter 5 presents out-of-plane shake table tests conducted on three existing unreinforced masonry walls with wood backing assemblies. Different retrofit methods to increase out-of-plane stiffness and strength were investigated, and various analytical procedures to explain the observed behavior are discussed.

Chapter 6 presents a summary of research findings and gives suggestions for future research.

CHAPTER 2

Literature Review

2.1 General

Numerous tests have been conducted around the world to examine the seismic behavior of unreinforced masonry. Generally, these tests have been conducted to study and analyse the response of unreinforced masonry components, i.e., shear walls and piers subjected to in-plane loading and the resistance of wall panels tested out-of-plane. Additionally, the dynamic seismic behavior of unreinforced masonry structures has also been investigated in some small-scale shake table tests. However, a full scale testing of an entire URM building having flexible wood diaphragms has not been conducted.

2.2 Previous Masonry Research

A summary of the available literature on masonry research was conducted by Abrams and Costley in 1995. Notably, the authors summarized static and dynamic tests performed on masonry components and structures. In brief, failure modes of walls with different aspect ratios, generally range from flexural cracking and rocking for slender walls, to diagonal cracking for stockier piers (Epperson and Abrams 1989; Anthoine et al. 1994). Other variables considered for failure modes were axial loads and mortar strengths. Dynamic tests also showed rigid body rocking for piers as well as for wall panels tested in the out-of-plane direction (Clough et al. 1979; Bariola et al. 1990; Magenes and Calvi 1994). Additionally, shake table tests on small scale unreinforced masonry structures demonstrated the importance of "how well the floor system was connected to the shear walls and how well the walls were

tied together" (Tomazevic et al. 1992). It was shown "that adding ties to the buildings with wooden floor systems can prevent serious damage to the out-of-plane walls".

Finally, Costley and Abrams (1995) performed shake table tests on two reduced-scale two stories URM buildings with flexible diaphragms. The tests showed that pier rocking in the first story provided considerable strength and deformation, exhibiting some ductility. Also, the wall displacements were amplified by the flexible diaphragm but after cracking, "diaphragm displacements relative to the walls were greatly diminished and interstory drift above cracking was largely reduced". However, in these tests, the diaphragm was modelled with steel bars and was designed to remain elastic. The authors concluded by pointing out the need for future research, notably: "further investigations of the dynamic response of unreinforced masonry buildings with flexible floor and roof diaphragm", "the effect of the out-of-plane walls on the rocking and shear strengths of corner piers", and effect of shear walls "mixing stocky and slender piers in an unsymmetric arrangement".

In a 1994 paper, Bruneau summarized the results of experimental and analytical research on the seismic behavior of unreinforced masonry buildings. Tests showed that after initial flexural cracking, if the compressive strength is not exceeded, "a stable rigid-body rocking motion" could be developed (ABK 1984; Epperson and Abrams 1990; Prawel and Lee 1990). Other tests reported that a shear sliding friction failure can produce "large relative deformations (with ductilities of up to 4) and little strength degradation" (Konig et al. 1988; Abrams 1992).

Analytical investigations of the seismic behavior using finite element models were also reported. Research using discrete-crack and smeared-crack models with special elements for nonlinear effect and opening and closing of cracks has been conducted. However, Bruneau noted that, one must have knowledge of the potential location and orientation of cracks and that "none of the above finite element analysis strategies seems to have matured to the level of sturdiness and reliability required to be readily used by practising engineers".

More recently, an analytical model has been developed to study the nonlinear dynamic response of unreinforced masonry subjected to in-plane loads (Zhuge et al. 1998). The model, using a ubiquitous joint model to account for weak bed joint plane, was implemented in a nonlinear finite element program and a failure envelope was developed to predict joint sliding and cracking and/or crushing failure modes. The results from the analytical model were compared with some experimental data, and reasonably good agreement has been found when an unloading parameter was calibrated with the experimental results. However, further research is required to improve the model.

In 1995, Bruneau described the possible various failure modes of URM buildings. Common failure modes, based largely in part on damage observed after earthquakes, include: lack of anchorage, anchor failure, in-plane failures, combined in-plane and out-of-plane effects, and diaphragm-related failures. The author then reviewed the adequacy and limitations of different codes and guidelines to design and evaluate the seismic resistance of unreinforced masonry buildings in Canada and the United States. A special procedure, the ABK methodology (ABK 1984), developed in California, incorporated in Appendix 1 of the Uniform Code for Building Conservation (UCBC 1997), and adjusted for Canada in Appendix A of the Canadian Guidelines for Seismic Evaluation of Existing Buildings (CGSEEB) (NRC 1992), is specifically intended to aid the engineer in the seismic evaluation of unreinforced masonry bearing wall buildings. In brief, the evaluation of URM walls subjected to lateral forces applied in-plane is performed by calculating the capacities corresponding to each possible individual modes of behavior, the lowest value being the governing failure mode.

Recently, the lateral behavior of a two stories unreinforced masonry wall with openings has been conducted (Irimies and Bia 2000). The shear wall was constructed with plain bricks and low strength lime mortar. Because of the low vertical load applied and weak mortar, cracks developed along bed and head mortar joints producing stair-step diagonal cracks through piers. After cracking, the resistance of the shear wall was limited to the sliding friction along the bed joints, yet the shear wall was shown to behave in a ductile manner with large

deformation at a constant strength. These tests confirmed that URM walls can exhibit substantial deformation capacity past initial cracking.

2.3 Wood Diaphragms

Research has also been conducted on wood diaphragms. Lateral tests on diaphragms covered with plywood panels and different types of lumber sheathing arrangements have been performed to evaluate the strength, stiffness and failure modes (Johnson 1954, 1955; Doyle 1955, 1960).

More recently, wood diaphragm tests have been performed as part of the ABK research program (ABK 1981) whose objective was to develop a methodology for the mitigation of seismic hazards in existing URM buildings. The study showed that typical flexible diaphragms have a highly nonlinear hysteretic stiffness. This nonlinear behavior reduces the diaphragm's peak accelerations and velocities at mid-span, thus reducing the out-of-plane excitation imparted on the head walls.

Currently, a research program is underway at the Mid-America Earthquake Center to examine the seismic behavior of wood diaphragms commonly used in pre-1950 unreinforced masonry buildings. Quasi-static cyclic tests have been performed on three large-scale wood diaphragms built with pre-1950 URM construction details, then the specimens were retrofitted and retested again. The results will be used to assess the resistance of existing and rehabilitated wood diaphragms. A final report documenting the results is forthcoming.

2.4 Summary

The literature review done on this project has shown that very little experimental data exist to validate expectations on the ultimate seismic resistance of existing unreinforced masonry buildings at the system level as opposed to the ultimate behavior of individual masonry

components. Thus, there is a need for further investigations of the dynamic response of a full scale 3-D unreinforced masonry building with flexible diaphragms. Such a test would complement the computer simulations and small-scale shake table tests done by other researchers, and would permit to better understand the flexible-floor/rigid-wall interaction, the impact of wall continuity at the building corners and the effect of a relatively weak diaphragm on the expected seismic behavior.

CHAPTER 3

Unreinforced Masonry Building with Flexible Diaphragm

3.1 General

This chapter presents the characteristics of the unreinforced brick masonry specimen having a flexible wood diaphragm (and the concepts underlying its design), and the results of the test program for the as-is and repaired conditions. Interpretation, analysis and discussion of the results follow in Chapter 4.

3.2 Design of Specimen - Objectives and Constraints

The design of the unreinforced masonry specimen was dictated by several objectives and constraints. First, the original intent was to have shear walls with some piers developing rocking while others would develop diagonal shear cracking. However, calculations showed that to develop diagonal shear cracking, a high axial load and/or aspect ratio was required, as shown in Fig. 3.1. Therefore, piers were instead designed to all undergo rocking, but with aspect ratios (and rocking resistance) that varied as much as possible. Second, an important objective was to choose an adequate wood floor diaphragm that would yield while piers are rocking, in order to investigate the postulate that a weak floor diaphragm is desirable to limit the force transmitted to the shear walls. Force-deformation envelopes for different types of diaphragms were generated to select an appropriate diaphragm for the tests (Fig. 3.2), using the second-order equation developed by the ABK joint-venture (ABK 1982):

$$F(e)=\frac{F_u\, e}{\frac{F_u}{k_i}+e} \tag{3.1}$$

where $F(e)$ is the force at the diaphragm's end, e is the mid-span deformation, k_i is the initial stiffness, and F_u is the ultimate force (asymptote). The ultimate force, F_u, is given by the unit shear strength of the diaphragm, v_u, multiplied by its width, D. Properties of typical diaphragms are given in Table 3.1. Scaling of the initial stiffness given in Table 3.1 for diaphragms with different sizes can be performed using the following relationship (ABK 1982):

$$k_2 = \frac{d_2 \, l_1}{d_1 \, l_2} k_1 \tag{3.2}$$

where k_1 is the initial stiffness of a diaphragm of size l_1 x d_1, and k_2 is the initial stiffness of a diaphragm of size l_2 x d_2.

Assuming the newly constructed specimen to be in pristine condition prior to testing (which may not be necessarily the case in an old existing building), calculations predicted that piers would first crack, then rock. This meant that a high lateral load was required to initiate pier cracking, with the capacity dropping to the rocking strength afterwards. Hence, it was decided to make the tested shear walls load-bearing to reduce their cracking-to-rocking ratios. A sufficiently strong diaphragm also had to be provided to attain the cracking loads which limited the amount of diaphragm inelastic behavior that could develop once rocking occurs. Fig. 3.2 shows some diaphragms theoretical force-displacement curves overlaid on the walls cracking/rocking behavior for comparison purposes. A typical masonry tension strength of 0.5 MPa was assumed in calculations during specimen design, but plans were made to increase the number of plywood overlays to increase the diaphragm strength in case an unusual high tension strength was obtained (e.g. Abrams and Costley (1995) reported an unusually high value of 1.26 MPa).

Additionally, preliminary calculations to evaluate the seismic in-plane loading on the shear walls using equations from the Canadian Guidelines for the Seismic Evaluation of Existing Buildings (CGSEEB) (NRC 1992), indicated that a ground acceleration of approximately

1.55g was needed to reach the cracking load (additional details are given in Appendix A). To reduce this value, additional mass was provided on the diaphragm, modeling the effects of a live load. This measure also increased the pier rocking strength.

Finally, the overall dimensions of the specimen were also limited by the space available in the structure laboratory, and the maximum size (38 mm x 286 mm) and length (6.1 m) of wood joists readily available for construction of the wood diaphragm.

3.2.1 Description of specimen

As shown in Figs. 3.3, 3.4, and 3.5, the full-scale single story unreinforced building specimen was approximately 4 m x 5.6 m in plan, with wall height and thickness of 2.7 m and 190 mm, respectively. Dimensions of the load-bearing shear walls (4 m x 2.7 m) limited the practical number of openings to two: a window and a door.

Shear walls were designed such that all piers would successively develop a pier-rocking behavior during seismic response, as shown in Fig. 3.6. The initial portion of the curve is the linear elastic stiffness of the shear wall, while the second portion has a zero slope representing the rocking behavior of the piers in the shear wall. This rigid-body mechanism is recognized by the UCBC to be a favorable stable failure mechanism.

A diagonal board plus straight sheathing overlay diaphragm was selected. It was designed to be sufficiently strong to resist the larger lateral load required to crack the masonry walls, and still provide some inelastic deformation during the pier rocking behavior.

At the corners of the building at one of its ends (west shear wall), gaps were left between the shear wall and its perpendicular walls. At the other end (east shear wall), walls were continuous over the building corners. This permits a comparison between the plane models considered by many engineers and the actual behavior at building corners, and allows to assess

the significance of this discrepancy on seismic performance, particularly when piers are rocking. To some extent, it also permits to observe the impact of in-plane rotation of the diaphragm's ends on wall corners.

3.2.2 Preliminary analyses

Prior to testing, non-linear inelastic analyses provided some valuable observations on expected seismic behavior of the specimen, particularly on diaphragm response respective to wall response, and it was possible to considerably simplify the originally planned pseudo-dynamic test set-up (additional details are given in Appendix B). For a first series of analyses, elastic floor diaphragm response was considered. For the El Centro earthquake, the entire structure would remain elastic until 0.5g, when first occurrence of inelastic rocking was observed. Displacement time histories of the floor diaphragm at mid-span are compared with that at the top of the shear wall in Fig. 3.7 (note that in Figs. 3.7 to 3.9, only approximately 10 seconds of the entire time-history response is plotted to better show the relative behavior of the structural elements of interest). The wood diaphragm, being more flexible, dominates the response as expected, with peak displacement of 26.5 mm versus 0.953 mm for the wall (response of the walls is magnified by 100 to make it visible on the same figure). The walls, with considerably shorter period, are thus driven by the floor behavior, clearly vibrating in phase with them, as shown in Fig. 3.7. The only exception occurs at 2.62 seconds when rocking of the wall occurs. Upon return from its rocking excursion, the wall motion damps itself rapidly as a consequence of its high natural frequency (logarithmic decrement of peak amplitudes occurs over a relatively short absolute time for a high frequency structural element).

More evidence of wall rocking is visible when earthquakes having more significant velocity pulses are used. This is consistent with the empirical evidence and somewhat addressed by the existing methodologies for the seismic evaluation of unreinforced masonry buildings. For example, for the Northridge earthquake Newhall fire station record (a near-fault record with

large peak-ground-velocity), at a peak-ground-acceleration of 0.583g, considerably more rocking takes place. Response for that case and still elastic diaphragm is shown in Fig. 3.8, with a peak wall displacement of 20.5 mm (peak diaphragm displacement, not shown here, is 53 mm). Note that the scale of rocking response makes the wall response prior and after rocking barely visible. Seismic response was then calculated using the same Newhall fire station record but considering inelastic response of the diaphragm. For this purpose, the wood floor diaphragm considered is a 19 mm x 140 mm diagonal with 19 mm x 140 mm straight sheathing overlay (having a shear strength of 29.8 kN/m). As seen in Fig. 3.8, inelastic response of this rather weak diaphragm limits the force transmitted to the walls, to a magnitude below that needed to initiate significant pier rocking. A maximum wall displacement of 1.73 mm is observed, even though the peak diaphragm displacement (not shown here) remains 53 mm.

3.2.3 Pseudo-dynamic test set-up

A first logical actuator configuration for the test of interest here would be to use one actuator to excite the tributary mass at each end-wall location, and another to displace the tributary mass at the diaphragm center-span. This is referred to as a three degree-of-freedom model (3 DOF). However, in light of the analytical results that show how wall response is largely driven by the diaphragm response, sufficiently accurate seismic response can be captured by using only a single actuator acting at the diaphragm center-span, i.e. using a single-degree-of-freedom model (1 DOF). Although all analyses conducted to validate this concept and determine the effective tributary mass that would match the fundamental period of the specimen are not shown here, results for the Newhall record are presented in Fig. 3.9. As shown in that figure, most of the instances and magnitudes of pier rocking observed using the 3 DOF analytical model are captured using the 1 DOF model. The high frequency wall vibrations that follow rocking, visible when using a 3 DOF model, are obviously missed by the 1 DOF model, but the previous discussion as well as Fig. 3.9 shows these to be of no significance. Given the supporting evidence from analytical studies, and the fact that using a

single actuator results in a simpler test set-up, with considerable savings, the 1 DOF configuration is used in this testing program.

3.2.4 Ground motion

Non-linear inelastic analyses were conducted to determine an appropriate seismic input motion representative of Eastern North America seismicity and that would initiate significant pier rocking from the diaphragm response. The selected input motion is a synthetic ground motion for La Malbaie, Canada, with a peak ground acceleration (PGA) of 0.453g, as shown in Fig. 3.10. The simulated analytical shear wall response to La Malbaie scaled to 0.8g produced the numerous desired pier rocking cycles, as shown in Fig. 3.11.

3.3 Construction and Material Properties

The single-story full-scale unreinforced brick masonry building constructed for this experimental program is shown in Fig. 3.12. A rectangular reinforced concrete pad was designed and constructed to provide a foundation for the specimen, as shown in Fig. 3.13. No mechanical connectors were used between the foundation and specimen. Construction of the walls then proceeded with two wythes solid brick walls (collar joint filled). The bricks were laid by four skilled bricklayers in running and American bond in which a header course was laid at every sixth course, tying the two wythes together as shown in Fig. 3.14. The bricks used were standard metric modular 90 mm x 57 mm x 190 mm. Type O mortar was used to replicate old construction methods and materials with cement:lime:sand in 1:2:9 proportion. The mortar was manually mixed on site by a skilled mixer as shown in Fig. 3.15. The east shear wall was constructed with continuous corners at its ends as in common practice, while the west wall had discontinuous corners, whereas a gap was deliberately left at the corners as shown in Fig. 3.16. Pre-made reinforced concrete lintels were provided above the openings. Appendix C gives additional details on the sequence of construction (and testing) and provides a list of materials.

3.3.1 Wood diaphragm

The specimen has a flexible diaphragm constructed with wood joists covered with diagonal boards with a straight board overlay. All framing and sheathing lumber were Construction grade spruce, and common 8d nails were used. The ten 38 mm x 286 mm joists at 406 mm on center were supported by the interior wythe of the masonry, as shown in Fig. 3.17, and 38 mm x 286 mm blockings were provided between joists at each end, and 38 mm x 89 mm at 1.22 m on center elsewhere. The diagonal and straight sheathings consisted of 19 mm x 140 mm boards, joined with three nails at ends of each board and two nails at all other support.

3.3.2 Masonry wall anchorage

According to the CGSEEB, the unreinforced masonry walls should be anchored at the diaphragm level for out-of-plane forces and diaphragm shear transfer. To resist out-of-plane forces, tension bolts through the wall are required. The minimum force acting normal to the wall, V_p, is given by:

$$V_p = 2.5 v' W_n \tag{3.3}$$

where v' is the effective velocity ratio, taken as 0.4 for the most severe seismic zone in Canada, and W_n is the tributary weight of the wall from the mid-height of the story above to the mid-height of the story below, calculated to be 31.9 kN. Thus, (3.3) gives 31.9 kN for V_p. From Table A-4 in the CGSEEB (1992), strength value for two wythes wall is 12 kN per bolt (bolts to be 12.7 mm minimum in diameter). Hence, at least three bolts would be needed. However, the maximum anchor spacing required is six times the wall thickness, i.e., 6 x 190 mm = 1140 mm. Since the wall length is 5.69 m, four 19 mm diameter bolts at 1138 mm center to center were installed.

For the diaphragm shear transfer, V_s, connections should be able to resist the lesser of:

$$V_s = v' W_d / 2 \tag{3.4}$$

or

$$V_s = v_u D \tag{3.5}$$

where all variables were previously defined in the document. Thus, (3.4) and (3.5) give 22.9 kN and 109.1 kN, respectively. Strength values for bolts in shear, as specified in the CGSEEB, are 6 kN, 9 kN, and 13 kN, for 12.7 mm, 15.8 mm and 19 mm diameter bolt, respectively. However, in the event of an unusual high masonry tensile force, it was decided to provide enough capacity to resist a maximum shear transfer. Thus, a maximum of nine 19 mm diameter bolts were provided between each joist on each shear wall, for a shear transfer of 117 kN. The maximum shear bolt spacing is six times the wall thickness, 1140 mm. The center to center bolt spacing distance was 406 mm.

Anchor bolts, both tension and shear, were centered in a 64 mm diameter hole with non-shrink grout around, and secured on both sides with 150 mm x 150 mm x 6.0 mm steel bearing plates, as shown in Fig. 3.18.

Once the diaphragm framing system was anchored to the walls, the joists were covered with 19 mm x 140 mm boards laid diagonally, as shown in Fig. 3.19, and covered with a 19 mm x 140 mm straight sheathing overlay. A parapet was built above the wood joist, and additional gravity load on the diaphragm was provided by plastic containers filled with water, simulating a 2.4 kPa live load.

3.3.3 Masonry properties

Masonry properties were obtained from simple component tests. The brick and mortar compressive strengths were determined by crushing five half-bricks and five mortar cubes, respectively. The resulting compressive strengths of the brick (f'_{br}) and mortar (f'_{mort}) were 109 MPa and 9.24 MPa, respectively. Brick prisms were made during construction of the specimen. Five prisms consisting of five-stacked-bricks with mortar joints in between were

tested in compression, while five seven-stacked-brick prisms were used in a three-point flexural bending test to determine the tensile strength of the masonry, as shown in Figs. 3.20 and 3.21, respectively. The resulting compressive (f'_m) and tensile (f_t) strengths of the masonry were 22.2 MPa and 0.18 MPa, respectively. A modulus of elasticity of masonry, E_m, of 850f'_m MPa = 18 870 MPa was assumed (which is less than the maximum of 20 000 MPa permitted by CSA 1994). To provide an estimate of the mortar shear strength along bed joints, five triplet components were tested, and four in-place shear tests were performed directly on the specimen after testing, as shown in Fig. 3.22. The obtained shear strength for triplet tests and in-place shear tests were 0.52 MPa and 0.418 MPa, respectively.

3.3.4 Theoretical response

Prior to the pseudo-dynamic tests, the expected strength of the URM specimen was assessed using the Canadian Guidelines for the Seismic Evaluation of Existing Buildings (CGSEEB) (NRC 1992) and masonry properties obtained from material tests. The CGSEEB procedure is very similar to the UCBC procedure, as described in Chapter 4.

First, the in-plane seismic resistance of each pier was determined, namely, the resistance to rocking, V_r, and shear failure, V_a:

$$V_r = 0.9\frac{D}{H}P_D \tag{3.6}$$

where P_D is the axial load on the pier, and D and H are the pier width and height, respectively, and:

$$V_a = v_m Dt/1.5 \tag{3.7}$$

where v_m is the masonry shear strength, and t is the thickness of the wall.

The lateral load required to initiate cracking at the pier's top and bottom, V_{cr}, was calculated as:

$$V_{cr}=f_t\frac{tD^2}{3H}+\frac{P_D D}{3H} \tag{3.8}$$

where f_t is the tensile strength of the masonry.

The results of these calculations are summarized in Table 3.2. For all piers, the rocking resistance is less than the shear resistance, and the total rocking resistance for each shear wall is therefore the sum of the resistance of the individual components, i.e. $\sum V_r = 46.7$ kN

Second, the maximum force transmitted by the diaphragm to the shear walls was determined. For this purpose, the total load tributary to the diaphragm, including walls perpendicular to the direction of motion, $W_d = 114.5$ kN , and the tributary load of each shear wall, $W_{wx} = 21.1$ kN, was calculated. The corresponding expected in-plane seismic load, F_{wx}, on a shear wall for an effective velocity ratio, v' taken as 0.4 for the most severe seismic zone encountered in Canada, is:

$$F_{wx}=v'(W_{wx}+W_d/2)=31.3\ kN \tag{3.9}$$

Because this is less than the shear wall rocking resistance of 46.7 kN previously calculated, this specimen would theoretically be able to resist the highest seismic lateral force expected in Canada. However, this equation assumes that the ground motion applied at the diaphragm's edges is unamplified by the end-walls.

Note that the force distributed to a shear wall cannot exceed:

$$F_{wx}=v'W_{wx}+v_u D \tag{3.10}$$

where $v_u D$, is the maximum shear strength of the diaphragm. In this case, the unit shear strength of a diagonal with straight sheathing overlay diaphragm is 29.8 kN/m based on values from the CGSEEB procedure. Thus, for a 3.66 m x 5.28 m diaphragm, the seismic lateral force distributed to the shear wall is limited by the shear yielding strength of the diaphragm:

$$F_{wx}=0.4(21.3)+29.8(3.66)=117.5\ kN \tag{3.11}$$

3.4 Experimental Procedure and Instrumentation

3.4.1 Test setup

The unreinforced brick masonry specimen was secured to a strong floor by four high strength bolts affixed at each corner of the reinforced concrete foundation. A MTS hydraulic actuator was connected to the specimen's south wall at center span, and at the wood diaphragm level. The actuator was supported by a rigid steel reaction frame as shown in Fig. 3.23. The head of the actuator was connected on a built-up steel section made of plates welded together, and attached with four long steel rods running through the entire width of the building above and below the wood diaphragm and connected to a similar built-up steel section on the north wall. Those rods were used to avoid pulling on the south wall, and to instead push on the north wall when reverse loading was applied. The rods below the diaphragm ran through the 38 mm x 286 mm joists in which 38 mm diameter holes were cut out, as shown in Fig. 3.24. Calculations showed that this reduction in cross-section, i.e., a net section of 86.7% of the gross section, did not significantly decrease the member's resistance. A global view of the test setup is shown in Fig. 3.25.

When connecting the actuators to the rods, some unexplained equipment malfunction generated a slight push from the actuator, which resulted in noticeable cracking through several mortar joints and bricks at some location around the building, particularly on the south-east and north-west corners of the specimen. Thus, a masonry restoration engineering firm was hired to proceed with masonry repointing. The damaged mortar joints were cut from both sides of the wall with a circular saw, and the remaining mortar removed with chisels. New mortar was put in, and damaged bricks were also removed and replaced with new ones, as shown in Fig. 3.26.

3.4.2 Pseudo-dynamic testing

The testing plan was to subject the specimen to the same La Malbaie synthetic time history described previously, scaled to progressively increasing intensity. The pseudo-dynamic method was used for many of the tests conducted on the specimen. The characteristics of this on-line computer-controlled testing technique have been extensively described elsewhere (Shing and Mahin 1987a, 1987b, 1990, Shing and Vannan 1990). In summary, this approach allows for the testing of structures or components under real earthquake excitations but at a relatively slow speed, thus allowing to observe the evolution of damage. The dynamic characteristics of the structure (mass and damping) are numerically simulated on a computer model, while the restoring force characteristics are directly measured from the tested specimens. The pseudo-dynamic testing algorithm by Shing et al. (1991) has been implemented by MTS in its controllers, and has proven to be reliable. A MTS Testar controller system with this pseudo-dynamic capability was used at the University of Ottawa for this research. The algorithm is presented in detail in Appendix D.

3.4.3 Instrumentation

The time-history response of the specimen was measured by a variety of instruments. As shown in Fig. 3.27, the displacement of the diaphragm was measured at the quarter points by three MTS displacement transducers called temposonics, the mid-span displacement being the controlling variable for the pseudo-dynamic test. The displacement of both shear walls at the diaphragm level was recorded by Linear Voltage Displacement Transducers (LVDT). Due to the limited number of instruments available, only the west shear wall of the specimen was closely instrumented during the early test runs. However, some tests were repeated with instruments moved to the east shear wall. As shown in Fig. 3.28, a pair of LVDTs was placed on the central pier to monitor shear deformation. Also, the in-plane deformation of the diaphragm was measured by displacement transducers (Celesco) located diagonally across half of the diaphragm. Finally, as shown in Fig. 3.28, twelve special clip gages were installed at

expected crack locations around all the piers to record crack opening and closing during the pier's rocking cycle. Additional details on the design of those special clip gages are given in Appendix E. All data were recorded automatically by a data acquisition system.

3.5 Experimental Results

Description and visual observations made during testing are presented in this section. First, the specimen was subjected to a series of pseudo-dynamic simulated free vibration tests to determine the period of vibration of the specimen and its damping ratio. Note that the specimen did not vibrate freely but this was truly a pseudo-dynamic test as per the algorithm in Appendix D. An initial displacement of 1 mm gave insufficient data points. Displacements of 2 mm and 3 mm yielded sufficient information to calculate the period and damping ratio that were found to be 0.12 s and 15%, respectively, as shown in Fig. 3.29 using the logarithmic decrement method (Clough and Penzien, 1993).

The specimen was then subjected to the first 10 seconds of La Malbaie earthquake with its intensity multiplied by 0.25. During this test run, both shear walls and the diaphragm responded elastically. Then, the specimen was tested with La Malbaie x 0.5. As shown in Fig. 3.30, a different stiffness response was noticeable for the two shear walls. Interestingly, the stiffness softening of each shear wall at large deformation is also different depending on the direction of the force. The full-scale La Malbaie earthquake was then applied creating additional cracking. Clip gages recorded maximum crack opening ranging from 0.18 mm to 4.00 mm, as shown in Fig. 3.31. The earthquake excitation was then increased to La Malbaie x 1.5; some cracking noise was heard and additional cracks were discovered. Sliding of the central pier was noticed on the west shear wall, as shown in Fig. 3.32(a). All clip gages, except two that were not located over a crack, recorded maximum crack opening ranging from 0.5 mm to 8.0 mm, and rocking of the door pier was clearly evident, as shown in Fig. 3.32(b). Finally, the specimen was subjected to La Malbaie x 2. The hysteretic response of the west and east wall is shown in Figs. 3.33(a) and 3.33(b), respectively. Additional cracks

on the shear walls and a longitudinal crack appeared between the 7th and 8th row of bricks on the north head wall. On the west wall, a triangular piece of bricks was created and started to separate due to the combined rocking and sliding motion of the central pier, as shown in Fig. 3.34. Recorded maximum crack openings ranged from 2.5 mm to 13.0 mm. The pier's rocking motion is clearly shown in Fig. 3.35(a), where the crack opens when the force acts in one direction and remains closed in the reverse direction. The resulting crack pattern for the west and east wall is shown in Figs. 3.36(a) and 3.36(b), respectively.

The clip gages monitoring the cracks on the west wall were then installed on the east wall, and the displacement transducers (Celesco) were moved on the eastern half of the diaphragm. The unreinforced masonry building was then re-tested with La Malbaie x 1.0 and x 1.5. The maximum crack openings varied from 0.5 mm to 1.3 mm, and from 0.5 mm to 2.9 mm for La Malbaie x 1.0 and x 1.5, respectively. A global view of the URM specimen after this first series of tests is shown in Fig. 3.37.

As stated above, a different stiffness for the east and west walls was observed at the beginning, during low intensity seismic motion. However, as the cracking pattern fully developed, the hysteretic curves during a higher intensity seismic motion, La Malbaie x 2.0, became very similar, as shown in Figs. 3.33(a) and 3.33(b). This suggests that the effect of continuous/discontinuous corners becomes somehow negligible during high intensity seismic motion.

After this first series of tests, it was observed that the diaphragm remained elastic throughout the tests, as shown in Fig. 3.38. This is confirmed by Fig. 3.2 using the 0.18 MPa value for f_t obtained from material tests after the specimen was constructed. Therefore, to force the diaphragm into the inelastic range and to investigate the effectiveness of a repair procedure, it was decided to reinforce the shear walls with fiberglass materials.

3.6 Repair

The shear walls were repaired using Tyfo fiberglass strips as shown in Fig. 3.39 Note that these strips are frequently used to enhance the out-of-plane performance of unreinforced masonry walls (Tyfo Systems 1997). The in-plane rocking behavior of unreinforced masonry walls is generally perceived as a stable desirable behavior, but there may be instances where the available rocking strength of such walls may still be inadequate. In that perspective, Tyfo strips were applied to the shear walls to increase their in-plane capacity.

This masonry rehabilitation was designed in collaboration with Professor Svetlana Brzev (private communication, 1998), a professional engineer having practical experience on the seismic retrofit of unreinforced masonry structures and familiar with the Tyfo system. A simple analytical model based on strain compatibility was developed (additional details are given in Appendix F). The Tyfo strip was modeled as a wire mesh reinforcement using a linear elastic stress-strain relation for the Tyfo material and a rectangular stress block for masonry at ultimate. The model can determine the ultimate moment transmitted by a section and the corresponding rocking force capacity. The strips were designed to increase the rocking force capacity of each pier, but to keep that rocking capacity below the pier shear capacity. Hence, the objective of this repair strategy is to use the Tyfo strips to preserve the desirable pier rocking mode and avoid the possibility of changing the mode of failure from rocking (deformation-controlled mode) to diagonal tension (force-controlled mode). This strategy both increases the capacity and enhances the displacement ductility of the repaired shear walls. The corners of the continuous and discontinuous walls were wrapped with Tyfo WEB to increase their shear resistance. This fabric not only provides additional shear strength, but also maintains the wall's integrity by preventing spalled portions of the wall from breaking off and becoming safety hazards.

Two types of glass fabric were used: Tyfo SEH 51 for the tension strips and Tyfo WEB for added in-plane shear capacity. The ultimate tension strength and elastic modulus of Tyfo SEH

51 and Tyfo WEB are 552 MPa and 27 579 MPa, and 207 MPa and 13 790 MPa, respectively. Fiberglass strips 100 mm wide were applied on the left and right sides of each pier, and on both wall faces (i.e., both inside and outside the building). The strips were extended to the top of the parapet, and wrapped along the concrete foundation horizontal base and vertical edge at the bottom of the walls to ensure sufficient anchorage length. Tyfo anchors were used only at the base of the door pier to enhance anchorage at that location because the rocking crack was expected at or near the concrete foundation at that location.

3.7 Experimental Results of Repaired Specimen

An initial pseudo-dynamic free vibration test was performed to determine any change in the dynamic properties of the repaired specimen. The period of vibration and the damping ratio of the repaired specimen were 0.12 s and 14.4%, respectively. The specimen was re-tested with the same input motion as before. For La Malbaie x 0.5 and x 1.0, the displacements of both shear walls were considerably reduced while maintaining the same level of force as before. The shear walls were also able to resist more load during La Malbaie x 1.5 and x 2.0 for a reduced displacement, as shown in Figs. 3.40(a) and 3.40(b), for La Malbaie x 2.0. The rocking motion was also significantly reduced as shown in Fig. 3.35(b). Throughout the tests, some noise was heard indicating partial de-bonding of the Tyfo WEB. The specimen was then subjected to La Malbaie x 3.0 during which new cracks appeared, a Tyfo strip started de-bonding, and more noise was heard coming from the Tyfo WEB. Due to some unexplained equipment malfunction, the data from that latter test were not fully recovered; therefore, La Malbaie x 3.0 was run a second time. In this second test, some strips as well as the Tyfo WEB at the corner, developed a shearing tear due to the increasing sliding behavior of some piers in both shear walls. Additional cracks were formed near the concrete foundation below the central pier on the west wall. Finally, the specimen was subjected to La Malbaie x 4.0. The corresponding hysteretic curves for the west and east wall are shown in Figs. 3.41(a) and 3.41(b), respectively. Additional de-bonding and tearing of the Tyfo material (strips and WEB) were observed and more cracks appeared, as shown in Figs. 3.42(a) and 3.42(b).

The clip gages monitoring the cracks on the west wall were then installed on the east wall, and the displacement transducers were moved on the other half of the diaphragm. The unreinforced masonry building was then re-tested with La Malbaie x 3.0 and x 4.0. The Tyfo strips and WEB completely de-bonded in some location and some strips were torn apart. Note that the hysteretic curves obtained for the west and east walls are fairly similar, as shown in Figs. 3.41(a) and 3.41(b), respectively.

Strengthening the shear walls with Tyfo materials did increase the force on the diaphragm, as shown in Fig. 3.43, comparing diaphragm response with shear walls as-is and repaired with Tyfo for La Malbaie x 2.0. At La Malbaie x 4.0 for the repaired specimen, some nonlinear diaphragm behavior initiated, as seen in Fig. 3.44. However, due to the state of damage on the shear walls, and for safety reasons, it was decided at this point to proceed further using conventional quasi-static cyclic tests, by simply increasing the center-span displacement instead of keeping increasing the intensity of the input motion in pseudo-dynamic tests.

3.7.1 Cyclic-testing

The center-span displacement of the specimen was increased by pushing with the actuator with a predetermined set of displacements i.e., 1.0, 1.5, 2.5, and 3.0% drift until a large proportion of the Tyfo materials (strips and WEB) were almost completely de-bonded from the shear wall surface, as shown in Fig. 3.45. The hysteretic curves and the final crack pattern are shown in Figs. 3.46 and 3.47, respectively. However, because most of the Tyfo materials had de-bonded and became ineffective in strengthening the shear walls, the diaphragm did not experience any additional nonlinear inelastic behavior, and thus simply slid like a rigid body on the top of the shear walls, as seen in Fig. 3.48 where the center-span response of the diaphragm is shown. After the test, examination showed that the diaphragm remained relatively intact. Damage was limited to some popped out nails at each end of the diaphragm, as shown in Fig. 3.49.

3.8 Summary

A full-scale one-story unreinforced brick masonry specimen having a flexible wood diaphragm was tested pseudo-dynamically. Test results have shown that stable combined rocking and sliding mechanisms formed and large deformations developed without significant strength degradation. The diaphragm remained, however, essentially elastic throughout. The difference in wall response due to the presence of continuous or discontinuous corners was somehow negligible during high intensity seismic excitation producing inelastic wall response. The specimen was repaired using Tyfo fiberglass strips, which increased the lateral strength of the shear walls while significantly reducing the displacements. While subjected to higher force, the diaphragm showed some nonlinear inelastic behavior.

CHAPTER 4

Analysis of Results

4.1 General

In this chapter the dynamic response of the shear walls with piers having a rocking and/or a sliding behavior is analyzed, as well as the response of the wood diaphragm and its interaction with the shear walls. Following an overview of existing methodologies for the seismic evaluation of unreinforced masonry (URM) buildings, the experimentally obtained results are compared with predictions from these methodologies, in particular, the one contained in the FEMA 273 document "NEHRP Guidelines for the Seismic Rehabilitation of Buildings" (FEMA 1997a). The objective is to determine whether these codified procedures adequately capture the experimentally obtained behavior and identify shortcomings if any.

4.2 Seismic Evaluation of URM Buildings

4.2.1 Existing documents

The seismic evaluation and strengthening of unreinforced masonry bearing wall buildings is addressed specifically in various documents such as the Uniform Code for Building Conservation (UCBC) (ICBO 1997), the NEHRP Handbook for Seismic Evaluation of Existing Buildings (FEMA 178) (FEMA 1992b), the Canadian Guidelines for Seismic Evaluation of Existing Buildings (CGSEEB) (NRC 1992), the NEHRP Guidelines for the Seismic Rehabilitation of Buildings (FEMA 273) (FEMA 1997a), and FEMA 306 (FEMA 1999a) entitled Evaluation of Earthquake Damaged Concrete and Masonry Wall Buildings.

The NEHRP FEMA 178 document and its companion, the NEHRP Handbook of Techniques for the Seismic Rehabilitation of Existing Buildings (FEMA 172) (FEMA 1992a), are intended to aid the engineer in the seismic evaluation of existing buildings, to identifying structural deficiencies and life-safety hazards. The methodology uses a set of true or false statements to identify the flaws and weaknesses of a building. Additionally, the evaluation of unreinforced masonry bearing wall buildings is specifically addressed in Appendix C. Appendix 1 of the UCBC is similar to the FEMA 178 document but is based on allowable stress values, i.e. working stress design. The CGSEEB is also directly based on the FEMA 178 document, with some adjustments for compatibility with Canadian codes and practice. Similarly, Appendix A addresses the seismic evaluation of URM.

Published subsequently to FEMA 178, FEMA 273, and its Commentary volume (FEMA 274) (FEMA 1997b), provide steps to rehabilitate existing buildings to attain the different performance levels of immediate occupancy, life safety, and collapse prevention. It requires a preliminary evaluation of the building, which can be performed using FEMA 178, or alternatively, by using the methods presented in FEMA 273.

The more recent document, FEMA 306, provides a basic procedure to evaluate the observed damage specifically caused by an earthquake to URM and concrete structures. Additional information on the basis and use of FEMA 306 is provided in FEMA 307 (FEMA 1999b), and information on repairing and upgrading earthquake-damaged concrete and masonry buildings can be found in FEMA 308 (FEMA 1999c).

Note that the seismic evaluation procedure for URM buildings in all of these documents has evolved from the same fundamental approaches first presented by ABK (1984), with some levels of refinements and improvements. However, some notable differences exist and will be outlined in the following section.

4.2.2 Evaluation procedure

The evaluation of URM walls subjected to lateral forces applied in-plane is performed by calculating the capacities corresponding to each possible individual modes of behavior, the lowest value being the governing failure mode. All behavior modes described below, are summarized in Table 4.1, showing in which documents they are addressed.

Pier Rocking

As the lateral force is increased, flexural cracks will develop along a bed joint at the top and base of a relatively slender wall, and the pier will start to rock. The rocking capacity is given by:

$$V_r = 0.9\alpha P_{CE}\frac{L}{h_{eff}} \tag{4.1}$$

where α is a factor equal to 0.5 for fixed-free cantilever wall, or equal to 1.0 for a fixed-fixed pier; P_{CE} is the expected vertical axial compressive force; and L and h_{eff} are the length and effective height reflecting crack patterns, respectively.

Eq. (4.1) is found in FEMA 273, FEMA 306, and in a similar form in FEMA 178, and the CGSEEB. In the UCBC 1997 context, i.e. using allowable values, pier rocking is given by:

$$V_r = 0.5P_D\frac{D}{H} \tag{4.2}$$

Sliding Shear Resistance

For squat walls, a diagonal shear crack can develop through bed and head mortar joints. Neglecting the tensile capacity of the head joints, the horizontal stair-stepped shear capacity of a pier having such cracking is given by:

$$V_a = v_m\frac{Dt}{1.5} \tag{4.3}$$

where t is the thickness of the wall, and v_m is the masonry shear strength given by:

$$v_m = 0.56 v_t + 0.75 \frac{P_D}{A} \tag{4.4}$$

where v_t is the mortar shear strength determined by in-place shear tests (also known as "push-tests"), and A is the mortared area, or equivalently, the pier's width (D) times its thickness (t). Note that the push-test measures the force required to displace a single brick by sliding on its bed joints.

Eqs. (4.3) and (4.4) are found in FEMA 178 and the CGSEEB. If (4.4) is substituted into (4.3), it gives:

$$V_d = 0.373 v_t A + 0.5P \tag{4.5}$$

A similar equation is found in FEMA 273 and FEMA 306, which acknowledges two forms of bed joint sliding: a stair-stepped diagonal crack as mentioned above, and sliding on a horizontal plane. In FEMA 273 and FEMA 306, both sliding behaviors are termed bed joint sliding with bond plus friction (V_{bjsl}), and the corresponding resistance is given by:

$$V_{bjsl} = v_{me} A_n \tag{4.6}$$

where A_n is the area of net mortared section, and v_{me} is the bond plus friction strength of mortar, given by:

$$v_{me} = \frac{0.75\left(0.75 v_{te} + \frac{P_{CE}}{A_n}\right)}{1.5} \tag{4.7}$$

where v_{te} is the mortar bond strength obtained from push tests.

Substituting (4.7) into (4.6), gives:

$$V_{bjs1}=0.375v_{te}\,A+0.5P \tag{4.8}$$

which is identical to (4.5).

In UCBC 1997, (4.3) and (4.4) simply become:

$$V_a=v_aA \tag{4.9}$$

and

$$v_a=0.1v_t+0.15\frac{P_D}{A} \tag{4.10}$$

A special case of (4.6) is given in FEMA 306. At lateral drifts of 0.3 to 0.4%, a strength degradation most likely due to a complete erosion of the bond capacity has been observed experimentally. Thus, after the bond capacity in (4.6) has eroded, the strength is then based only on the friction portion of the equation. This behavior is termed "bed joint sliding with friction only" (V_{bjs2}), and is given by:

$$V_{bjs2}=\frac{0.75\left(\frac{P_{CE}}{A_n}\right)}{1.5}(A_n)=0.5P_{CE} \tag{4.11}$$

Note that Eq. (4.11) is not found in FEMA 178, FEMA 273, UCBC 1997, and the CGSEEB.

Diagonal Tension and Toe Crushing

Additionally, two other behavior modes, diagonal tension, and toe crushing, are recognized only in FEMA 273 and FEMA 306.

Typically, diagonal tension X-shaped cracking develops under high compressive stress when strong mortar and weak masonry units are used. In this type of damage, double diagonal

cracks form suddenly through the units, and the pier rapidly loses its vertical load carrying capacity. Diagonal tension (V_{dt}) is given by:

$$V_{dt}=f_{dt}'A_n(\beta)\left(1+\frac{f_{ae}}{f_{dt}'}\right)^{\frac{1}{2}} \tag{4.12}$$

where f'_{dt} is the diagonal tension strength, assumed as v_{me} in lieu of better available data; f_{ae} is the expected vertical axial compressive stress; and $\beta = 0.67$ for $L/h_{eff} < 0.67$, $\beta = L/h_{eff}$ when $0.67 \le L/h_{eff} \le 1.0$, and $\beta = 1.0$ when $L/h_{eff} > 1$.

Under high axial loads and the overturning moment due to a lateral load, a localized compression failure can occur at the toe of the pier. Toe crushing resistance (V_{tc}) is given by:

$$V_{tc}=\alpha P_{CE}\left(\frac{L}{h_{eff}}\right)\left(1-\frac{f_{ae}}{0.7f_{me}'}\right) \tag{4.13}$$

where f'_{me} is the expected masonry compressive strength. When determining the lower bound strength, a low estimate of the vertical compressive strength must be used and may be estimated by dividing f'_{me} by 1.6.

4.3 Push Over Analyses

The single-story URM building specimen tested as reported in the previous chapter was designed in 1996, using the CGSEEB methodology to assess its strength and expected seismic response. Recall that the CGSEEB is essentially similar to the FEMA 178 Appendix C procedure, and Appendix 1 of the UCBC 1997. As the FEMA 273, and FEMA 306 documents became available after the specimen was constructed, it is worthwhile to compare the theoretical response of the URM specimen obtained from these various seismic evaluation procedures. Consequently, the strengths for each individual modes of behavior for each pier were calculated using the experimentally obtained compressive, tensile, and shear material properties reported in Chapter 3, and summarized in Table 4.2.

4.3.1 FEMA 273

Following the procedure outlined in FEMA 273, the expected lateral strength of each pier is the lesser of its rocking (V_r) and bed-joint sliding shear (V_{bjs1}). As shown in Table 4.2, for all piers, rocking governs. The lower bound lateral strength is the lesser of diagonal tension (V_{dt}) and toe crushing (V_{tc}). Again, from Table 4.2, toe crushing governs for all piers. Since for all piers rocking is less than toe crushing, rocking governs. For that mode of failure, piers are considered as deformation-controlled components, being able to sustain large lateral deflections as strengths remain almost constant. Thus, the lateral capacity for each shear wall is the summation of each individual pier rocking capacity, and is equal to 46.7 kN, a value identical to that computed using the CGSEEB, as reported in Chapter 3.

4.3.2 FEMA 306

FEMA 306 gives a procedure to evaluate lateral capacity based on observed damage caused by an earthquake. As such, it requires to use the effective height (h_{eff}) of pier reflecting the observed crack pattern. Therefore, the capacities for the individual modes of behavior for each pier shown in Table 4.2, were re-calculated using the crack pattern observed after pseudo-dynamic tests. The effective heights used and resulting capacities are presented in Table 4.3.

Based on the piers' aspect ratios and the applied vertical stresses, the governing modes of behavior are determined. According to FEMA 306, for piers with aspect ratio (L/h_{eff}) less or equal to 1.25, and for a vertical stress (f_{ue}) less than 0.69 MPa (100 psi), the predicted mode of failure is rocking if V_r or V_{tc} are the lowest values of V_r, V_{bjs1}, V_{bjs2}, V_{dt}, and V_{tc}. For the tested URM specimen, all piers have an aspect ratio less than 1.25 and V_r is the governing mode of failure, except for the central pier whose strength is governed by bed joint sliding with friction only, V_{bjs2}. In such case, the lateral load capacity for each shear wall is given by the summation of the governing strength of each individual pier. For the west and east wall, it

is 23.0 kN and 22.2 kN, respectively. Both rocking and bed joint sliding are considered to be deformation-controlled behaviors able to sustain large lateral deformations while strength remains almost constant.

4.4 Comparison with Experimental Results

4.4.1 Masonry walls

Results and observations during the test and presented in the previous chapter show that all piers in the west wall started to rock during the first low amplitudes tests. Then, upon reaching a maximum negative lateral load of approximately 29 kN during La Malbaie x 1.5 (negative meaning pushing towards the south wall), the central pier behavior gradually switched from rocking to bed-joint sliding during La Malbaie x 2.0, reducing the strength to approximately 23 kN, which matches the push-over analysis results calculated with FEMA 306 in the preceding section, as shown in Fig. 4.1(a). However, when the force was acting in the opposite direction, the behavior was slightly different. During testing, the portion of the wall above the door pier was observed to lift, creating a gap across the entire width at the top of the door pier. Therefore, this pier became ineffective in providing resistance against lateral loads. That pier's share of gravity load resistance was thus transferred to the central pier, increasing its rocking resistance. The capacity of the west wall for a positive force is therefore given by adding the rocking capacity of the window pier (3.97 kN) to the increased rocking capacity of the central pier (approximately 35.1 kN), with no contribution from the door pier. A maximum strength of approximately 33 kN has been reached (Fig. 4.1(a)), and slightly higher values might have been obtained if testing had not stopped due to damage under negative lateral loads.

From test results and observations, the lateral capacity of the east wall for a positive force is given by the sum of the rocking capacity of each pier, and equal to 34.95 kN. As shown in Fig. 4.1(b), a maximum lateral strength of approximately 33 kN was also reached for that

wall. The lateral capacity for a negative force is slightly different. As observed during the test, both the door and window pier were rocking but the diaphragm was simply sliding on the central pier. Therefore, the estimated lateral strength is the rocking capacity of the door (5.48 kN) and window pier (3.77 kN) plus the strength of the diaphragm sliding on top of the central pier (10.5 kN), which adds up to 19.8 kN. Note that the diaphragm sliding value is not explicitly addressed by FEMA but is an interpretation of the models embedded in FEMA. As shown in Fig. 4.1(b), the maximum load reached is approximately 23 kN.

The FEMA 273 nonlinear static procedure was used to establish the idealized nonlinear force-deflection relation for the wall, as shown in Fig 4.2. In this procedure, permissible deformations are established as drift percentages for primary elements (walls considered to be part of the lateral-force system) and secondary elements (walls not considered as part of the lateral-force-resisting system but supporting gravity loads) for the different performance levels of immediate occupancy (IO), life safety (LS), and collapse prevention (CP) as per Table 4.4. For comparison purposes, here, the walls are treated as primary elements. Permissible drift limits for the shear walls were calculated using an average pier's height and length. The expected capacities for FEMA 273 (46.7 kN), and FEMA 306 (23.0 kN and 22.2 kN for the west and east wall, respectively) are used.

The idealized nonlinear force-deflection is plotted against the hysteretic response of the west wall and east wall in Figs. 4.1(a) and 4.1(b), respectively. As shown here and noted in FEMA 307, the experimentally obtained displacements that occurred under a stable rocking mechanism exceed the proposed "d" drift value for collapse of $0.4h_{eff}/L$, and equal to 0.52% for primary element, as specified in FEMA 273. Furthermore, as also noted in FEMA 307 and observed here, the rocking capacity does not drop to a "c" value of 60% of the initial capacity as proposed by FEMA 273. Finally, FEMA 307 comments that a sequence of different behaviors is common in experiments. The rocking shifting to bed-joint sliding for the central pier, observed when pushing the building in the south direction, is consistent with this expectation.

Given the reasonable agreement between experimental results and the above calculations which neglect the presence of continuous corners at the east end, and comparing results for both building ends, it appears that pier continuity at the corner has no beneficial effect on behavior.

4.4.2 Repaired walls

For the same level of excitation as before, the repaired shear walls were able to resist higher lateral force while displacements and rocking motion were considerably reduced as shown in Chapter 3. For comparison, the time history of the diaphragm center-span displacement before and after the Tyfo repair is shown in Fig. 4.3 for La Malbaie x 2.0. The intensity of the earthquake was then increased to La Malbaie x 3.0, then to x 4.0. As the level of excitation was increased, some strips started to de-bond, yet still providing enough deformation capacity to allow rocking as shown in Fig. 4.4, where a crack opening of 10 mm is visible. However, for the pier having a bed-joint sliding behavior, the Tyfo strips provided limited resistance, as shown in Fig. 4.5, and failed in shear. As for the Tyfo WEB, it de-bonded mostly around cracks created by pier rocking and sliding.

The shear walls with Tyfo were able to develop higher strength for the same lateral displacements. However, the repeated rocking and sliding behavior of the piers induced tears and de-bonding, limiting the capacity to approximately 66 kN, which resulted in increased lateral displacement, as observed in Fig. 4.6, where two successive responses, La Malbaie x 3.0 and 4.0, are shown. Some tearing was also observed in the Tyfo WEB wrapping the corners due to out-of-plane tensile cracks, as shown in Fig. 4.7. Finally, the specimen was subjected to more conventional cyclic-testing, by increasing the center-span displacement until a large proportion of the Tyfo materials (strips and WEB) were almost completely de-bonded from the shear wall surface.

4.5 Wood Diaphragm

4.5.1 Models and theoretical values

The dynamic response of the wood diaphragm was also investigated. In the CGSEEB, FEMA 178, and the UCBC 1997, the dynamic response is essentially assessed by calculating a normalized demand-capacity ratio (DCR). Given that the CGSEEB, FEMA 178, and UCBC 1997 requirements are essentially similar, for the sake of brevity, equations and calculations are shown for the CGSEEB only. Thus, the DCR is given by:

$$DCR=\frac{2.5v'W_d}{\sum v_u D} \tag{4.14}$$

where v_u, W_d, D and v' are respectively the unit shear, the total load tributary to the diaphragm, the width of the diaphragm, and an effective velocity ratio defined by:

$$v'=\frac{vIF}{1.3} \leq 0.4I \tag{4.15}$$

where v is the zonal velocity ratio, I the importance factor, and F the foundation factor typically found in the National Building Code of Canada (NBCC) (NRC 1995). For the special evaluation methodology to be applicable, any given point defined by the DCR and the span, L, must fall within the boundaries of the graph in Fig. 4.8. This figure has been developed to control the severity of the diaphragm displacements and velocities at mid-span. It also ensures that the horizontal deflection of the diaphragm does not produce instability of the out-of-plane walls by providing limits on slenderness ratios derived from dynamic stability concepts. The figure is divided into three regions, namely: region 1, where h/t ratios for buildings with cross walls may be used if qualifying cross walls are present in all stories; region 2, where h/t ratios for buildings with cross walls may be used whether or not qualifying cross walls are present; and region 3, where h/t ratios for other buildings shall be used whether or not qualifying cross walls are present.

Using v'=0.4, W_d=114.5 kN, v_u=29.8 kN/m, and D=3.66 m for the tested specimen, the DCR is 1.05, and given the diaphragm span of 5.28 m, it is confirmed that the point (1.05, 5.28) falls in region 3 of Fig. 4.8.

FEMA 273 defines the capacity of a diaphragm by its yield shear capacity. Typical values for chorded and unchorded (i.e. presence or not of perimeter chord or flange members) wood diaphragm having diagonal sheathing with straight sheathing overlay are 13.13 kN/m (900 lb/ft) and 9.12 kN/m (625 lb/ft), respectively (FEMA 1997a).

The elastic maximum deflection of a wood diaphragm is given by:

$$\Delta = \frac{vL^4}{G_d\, b^3} \tag{4.16}$$

where v is the maximum shear in the direction under consideration, L and b are the diaphragm's span and width, respectively, and G_d is the diaphragm shear stiffness taken as 315 234 kN/m (1,800,000 lb/in) and 157 617 kN/m (900,000 lb/in) for chorded and unchorded diagonal sheathing with straight sheathing, respectively (FEMA 1997a).

The non-linear inelastic deformation of the diaphragm is determined by a normalized force-deflection curve defined by parameters d, e, and c, as shown in Fig. 4.9, where d is the maximum possible deflection at yield strength, and e is the maximum deflection at a reduced strength c. These values are given in Table 4.5, for a diaphragm with straight sheathing over diagonal sheathing.

Alternatively, the ABK methodology expresses force-deformation envelopes for different type of wood diaphragms by the second-order curve defined by Eq. 3.1 in Chapter 3. For a wood diaphragm having diagonal sheathing with straight sheathing overlay, the initial stiffness from Table 3.1 is 10.7 kN/mm for a 6.1 m x 6.1 m diaphragm. Using Eq. 3.2, the initial stiffness for

a 3.66 m x 5.28 m diaphragm is:

$$k_2 = \frac{(3.66)(6.1)}{(6.1)(5.28)} 10.7 = 7.42 \ kN/mm \tag{4.17}$$

The unit shear strength, 29.8 kN/m (from Table 3.1) multiplied by the diaphragm's width, 3.66 m, gives the ultimate force, F_u = 109.1 kN, for the diaphragm's dimensions considered here.

4.5.2 Comparison with experimental results

Using the data recorded by the three temposonics located across the span of the diaphragm as well as the LVDTs on each shear wall, the lateral force-deformation relationship of the diaphragm was investigated. The hysteretic response of the wood diaphragm during La Malbaie x 2.0 is shown in Fig. 4.10. The response is essentially linearly elastic and the stiffness is in agreement with the initial stiffness of the ABK force-deformation envelope. The maximum floor deformation (center relative to ends) recorded at mid-span was 5.54 mm under a 66.5 kN force. Using (4.16) from FEMA 273, the calculated mid-span deflections are 0.457 mm and 0.914 mm for chorded and unchorded diaphragm, respectively, which are significantly less than the experimental values.

Using the force-deformation envelope from ABK, Eq. 3.1, and rearranging the terms, gives:

$$e = \frac{\frac{F_u}{k_1} F(e)}{F_u - F(e)} \tag{4.18}$$

Thus, for a force of 33.25 kN (i.e., 66.5/2 kN) at the end of the diaphragm, the calculated deflection, using (4.18) is 6.45 mm, which matches more closely the experimentally obtained deflection. Even though, the diaphragm was restricted by continuous corners on one side, the experimentally obtained in-plan deflected shape of the diaphragm is nearly symmetric and close to that of a pinned-pinned beam model, as shown in Fig. 4.11. This suggests that flexural deformations dominated over shear deformations for this diaphragm.

By adding Tyfo fiberglass strips to the shear walls, their in-plane capacity was increased allowing larger forces to be applied to the system and, therefore, larger relative displacements between the diaphragm and shear walls. As observed in Fig. 4.12, a maximum mid-span deflection of 23.9 mm was recorded under a load of 133.4 kN for La Malbaie x 4.0. Corresponding deformations under such load using (4.16), are 0.916 mm and 1.833 mm for chorded and unchorded diaphragms, respectively, and 23.1 mm for the ABK model. Again, the deflection predicted by the ABK model is closer to the one obtained experimentally. The force-deformation curves for the diaphragm considered herein based on FEMA 273, and ABK are shown in Fig. 4.13. A noticeable difference exists between the two curves. FEMA 273 under estimates the diaphragm ultimate strength, predicting 13.13 kN/m, and 29.8 kN/m by the ABK model, respectively, whereas a maximum shear of 19.0 kN/m was reached experimentally. Experimental results for the diaphragm closely follow the ABK model in the linear elastic range, but since the diaphragm did not undergo very large inelastic deformations, it is not known whether it would behave as predicted by the ABK model up to its ultimate.

4.5.3 Deflected shape

Fig. 4.11 shows that the experimentally obtained in-plan deflected diaphragm shape for the repaired specimen is not symmetrical. In that case, the continuous corners seem to have restrained the rotation of the diaphragm at that end, and the deflected shape is better approximated by a fixed-pinned beam model. Assuming that the deflection can be computed using a fixed-pinned beam model, using the modulus of elasticity of Spruce (i.e. E= 9500 MPa), different models for the moment of inertia were investigated to match the experimental and analytical results.

Model 1

A first approach calculates the flexural deflection of the floor, as a composite system, but neglecting the sheathing shear deformation as shown in Fig. 4.14. As a conservative first

approach, only the two outer joists are considered in calculating the floor inertia. The corresponding moment of inertia of this section is 7.129×10^{10} mm^4. Using this value in a fixed-pinned beam model to calculate the deflection for La Malbaie x 4.0 gives 0.264 mm, significantly less than the 23.9 mm observed experimentally. This suggests that a flexural model that assumes full in-plane compositeness of the wood floor is not appropriate.

Model 2

An alternative approach assumes that the flexural stiffness of the diaphragm is given by the sum of the weak-axis flexural stiffness of the wood joists, with one of the outer joists treated as behaving in a composite manner with the adjacent brick wall as shown in Fig. 4.15. Indeed, because the joist at the outer edge of the diaphragm is continuously tied to the masonry wall by anchors, a section of the brick wall is engaged and can contribute to the stiffness of the diaphragm. Equivalent stiffness of that joist is therefore calculated using the modular ratio, transforming the effective brick wall into an equivalent height of wood. Note that, by analogy, this wood-masonry composite joist is conceptually similar in behavior to that of a reinforced concrete beam, with the wood joist acting as the reinforcing bar in tension and the brick wall as the concrete in compression. The portion of brick wall participating into the diaphragm stiffness is assessed empirically. To match the deflections obtained experimentally, a 1500 mm height of brick wall is required to contribute. This value would correspond to 286 mm over the joist depth, 258 mm for the parapet above, and an additional 956 mm of brick wall below the joist, which seems to be reasonable. Then, the inertia of the wood-masonry composite joist is 1.0483×10^9 mm^4, and the inertia of the remaining nine joists is $9 \times (1.308 \times 10^6) = 1.177 \times 10^7$ mm^4. Thus, the total inertia is 1.060×10^9 mm^4. Using a fixed-pinned beam model, it gives a mid-span deflection of 18.5 mm, matching the deflection obtained experimentally for La Malbaie x 3.0, 18.49 mm.

Thus, even though the diaphragm did not have a long span (aspect ratio = 1.44), the lateral deflection of the wood diaphragm was mostly due to flexural rather than shear deformations.

The fact that the joists were laid parallel to the long diaphragm direction as opposed to spanning the short direction, as commonly encountered, may have contributed to the observed flexural deformation, but the concept underlying Model 2 appears applicable to any aspect ratio.

4.5.4 In-plane deformation

Two Celesco displacement transducers were used to measure the in-plane deformation of the diaphragm as reported in Chapter 3. The resulting hysteretic response is shown in Figs. 4.16(a) and 4.16(b) for La Malbaie x 2.0 without Tyfo and x 4.0 with Tyfo repair, respectively. The odd response observed can be explained as follow, and is schematically illustrated in Fig. 4.17. First, the top layer of straight sheathing is assumed to bend back and forth following the imposed displacement in the north-south direction without contributing much to the diaphragm strength or stiffness. Therefore, the displacement transducers are assumed to measure displacements as affected by the diagonal sheathing. As such, the transducer parallel to the bottom layer of diagonal sheathing (labelled "celesco north" in Fig. 4.17) measures plank elongations in tension or compression, which explains the relatively high rigidity observed by that instrument, while the perpendicular displacement transducer (labelled "celesco south") measures the lateral separation of these planks, which explains the lesser rigidity and larger displacement observed in that direction. The same behavior was observed when the displacement transducers were installed on the other half of the diaphragm.

4.6 Summary

Pseudo-dynamic tests have been conducted on a single-story URM building with a wood diaphragm. The theoretical seismic response was calculated using different codified evaluation methodologies. It was found that the FEMA 273 procedure predicted the same behavior for the shear walls as the CGSEEB, i.e. a rocking mode for all piers but strengths in excess of experimentally obtained results. The FEMA 306 procedure, used to evaluate the

lateral capacity of concrete and masonry buildings after an earthquake, gave results that closely matched the observed behavior. None of the codified procedure account for the presence of continuous corners, but this continuity was observed to have a negligible impact on the lateral strength of the shear wall during high intensity input motion.

The wood diaphragm exhibited some inelastic deformation. Although not tested to its ultimate capacity, it was shown to deflect primarily due to flexural deformation as opposed to shear deformation as commonly assumed. Thus, the diaphragm's deflections observed experimentally were significantly greater than predicted with FEMA 273, but closely matched those predicted using the ABK model.

CHAPTER 5

Out-of-Plane Seismic Resistance of Existing Masonry Walls

5.1 General

The previous chapters focus on lateral behaviors of wall with piers, which are important modes of behavior of URM as failure can lead to collapse. However, the existing literature (Bruneau 1990, 1995, Rutherford and Chekene 1991) demonstrates that extensive damages in URM buildings have occurred due to out-of-plane failure of individual walls. For completeness of a study on a seismic response of URM building, this chapter discusses out-of-plane shake table tests conducted on three unreinforced masonry walls and wood backing assemblies extracted from an older existing residential building, and investigates the adequacy of various analytical procedures to explain the observed behavior as well as different retrofit methods to increase the out-of-plane stiffness and strength.

5.2 Specimen Retrieval and Properties

The three wall specimens were extracted from an old three-story building in Montreal, Canada, scheduled for demolition. The building, shown in Fig. 5.1, was built in the late 19th century as a wood structure and masonry walls of the type described in Section 1.3. The plan dimensions of the building were 14 m x 9 m. The timber structure consisted of stacked 75 mm x 250 mm (3 in x 10 in) rough-cut timber planks laterally supported by vertical posts at 4 m (12 ft) spacing. In addition to the four single-wythe brick masonry exterior facades of the building, two more walls of the same construction became interior walls when an addition was built a few years after the original construction. The specimens were extracted from a single interior wall for which access to both sides was facilitated, and to minimize variability of construction. Note that for

these interior walls, a thin layer of plaster covered the brick surface and had to be removed prior to the shake table tests.

Careful retrieval of the specimens was critical to maintain the integrity of the masonry wall and wood-backing assemblies during extraction and transportation. First, horizontal saw cuts, 1.2 m long and spaced at 2 m vertically, were made through each wall. Steel plates with pre-drilled holes were inserted in each cut. Four steel threaded rods were tightly bolted between the plates, on each side of the wall. A plywood sheet was placed on each surface of the wall, and wedged by timber members against the threaded rods. The bottom portion of the wall underneath the bottom cut was demolished to the floor level. A rolling cart was introduced in the opening and secured to the bottom steel plate. Finally, the vertical sections of the specimen were saw-cut. The crated specimen was rolled out of the wall and retrieved from the building by a boomed truck, as shown in Fig. 5.2.

Basic tests were conducted to determine the material properties of the masonry specimens. First, before retrieval of the specimen, an in-place shear test was performed directly on the interior wall in accordance with the special procedure of Appendix A, Uniform Code for Building Conservation (UCBC) (ICBO 1997). A mortar shear strength of 0.401 MPa was obtained, which exceeds the minimum value of 0.2 MPa for which repointing would have been required. Also, masonry specimens were cut out of the interior walls and brought to the laboratory for flexural tension and compression tests. Due to the fragility and particular geometry of the specimens available, special tests were devised to determine these basic properties. A three-point bending test was performed on two bricks bonded by an uncracked mortar joint, followed by a compression test on the same. The obtained compressive (f'_m) and tensile (f_t) strengths of the masonry were 2.50 MPa and 0.0162 MPa, respectively.

5.3 Retrofit Techniques

One of the three wall specimens was tested in its existing condition as shown in Fig. 5.3(a), the other two were retrofitted prior to testing. The first retrofit strategy consisted of adding through-thickness anchors connecting the masonry to the wood backing. The intent was to determine if it is possible to rely on the stiffness of the wood backing to reduce the height-to-thickness ratio of the wall by intermediate anchorages. Here, two bolts were used at mid-height of the specimen. Cintec bolts with socks injected with grout under pressure (Cintec 1996) were used to ensure a bearing surface over the expanded sock surface in the gap between the masonry and the timber planks.

In the second retrofit strategy, fiberglass strips (Tyfo 1997) were glued to the masonry side of the wall, to increase its out-of-plane stiffness and strength. As shown in Fig. 5.3(b), three vertical strips 100 mm wide were epoxied to the masonry surface of the wall specimen. Although retrofitting both sides of the walls with strips is typically recommended based on available testing results (e.g. Reinhorn and Madan 1995), this is not possible for the type of construction considered here. Nevertheless, the expectation for the single-side retrofit of this specimen was that the fiberglass strips would prevent dynamic out-of-plane instability of the masonry in the outward direction, and that the wood backing would preclude the same in the inward direction, in spite of the small gap present between the two walls. Such a retrofit assumption can only be experimentally verified by shake table testing.

5.4 Experimental Procedure

5.4.1 Test setup and instrumentation

The shake table tests were performed on the uniaxial earthquake simulation facility at Ecole Polytechnique in Montreal, Canada (Filiatrault et al. 1996). As shown in Fig. 5.4, a rigid steel A-frame was used to tie the top of the wall, whereas the bottom was cast into a concrete base

bolted to the shake table. This was to ensure that both the top and bottom of the wall would be subjected to the same seismic excitation, as commonly assumed for the upper stories when performing seismic evaluation of unreinforced masonry buildings incorporating wood floor diaphragms (ABK 1984; Bruneau 1994; ICBO 1997). The top of the wall was secured to the A-frame by two steel angles welded to the wall's top steel plate installed prior to transportation. This plate was bolted to a wooden belt surrounding the top edge of the wall. This belt was installed prior to removing the steel threaded rods and plywood panels used for crating. These plywood panels were saw-cut at the concrete base level and just below the wooden belt, revealing the specimen and permitting removal of the thin layer of plaster covering the brick surface. The final net dimensions of the wall specimens were approximately 1.2 m x 1.5 m. The measured thickness of the brick wall was 95 mm. The initial gap between the wood backing and the brick wall varied from 15 to 20 mm for both the as-built and Cintec specimen. The Tyfo specimen was initially in poor condition compared to the other two specimens. The brick wall had several cracks through the mortar joints and the bricks themselves. Contrary to the previous specimens, two of the timber planks in the wood backing were not continuous (i.e., a joint was present). Also, part of the wood backing was slightly charred (hinting at prior fire damage) and the initial gap between the wood and brick wall was larger, varying from 25 to 35 mm. These conditions were not repaired prior to application of the Tyfo strips and were not considered to be significant factors in the dynamic performance of the test specimens. Since the masonry walls typically resisted only their self weight in the existing building and because top story walls are typically more vulnerable during earthquakes (Bruneau 1995), no supplementary gravity load was considered for the shake table tests.

Horizontal acceleration time-histories at different locations on the specimen were measured using seven accelerometers. All except one were located on the brick wall, as shown in Fig. 5.5(a). Additionally, five displacement transducers were used to measure horizontal and vertical movements, as shown in Fig. 5.5(b). All data were recorded automatically by a data acquisition system at a sampling rate of 200 readings per second per channel.

5.4.2 Testing sequence

The three wall specimens were subjected to the same seismic input motion of progressively increasing intensity, expressed in terms of Peak Horizontal Acceleration (PHA), until structural failure was observed. Between each seismic excitation, low level impact tests were performed by hammering the wall with bare fist to capture the evolution of the wall's out-of-plane dynamic characteristics (natural frequencies, mode shapes and damping ratios). The natural frequencies were determined from power spectral density plots of the absolute acceleration records on the walls. The structural mode shapes were obtained from the amplitudes of the spectral peaks and by the phase and coherence between the measured acceleration time-histories. The first modal damping ratio of the wall specimen was then established by the logarithmic decrement method (Clough and Penzien, 1993).

In order to determine an appropriate floor-level seismic input motion for the shake table tests, linear dynamic time-history analyses were performed on a typical one-story unreinforced masonry building incorporating a wooden floor diaphragm. These analyses were performed for four different ground motions: 1) the S00E component of the 1940 El Centro Earthquake, 2) the N24E component of the ground motion recorded at Chicoutimi North during the 1988 Saguenay Earthquake in Quebec, Canada, 3) a synthetic ground motion compatible with the short periods of the recently proposed uniform hazard spectrum for Montreal, Canada (Atkinson and Beresnev 1998) and 4) a synthetic ground motion compatible with the long periods of the same uniform hazard spectrum for Montreal (Atkinson and Beresnev 1998).

Based on the results obtained, the acceleration time-history obtained at the floor level of the analyzed building under the synthetic long period accelerogram for Montreal was selected for the shake table tests. The acceleration time-history and the associated absolute acceleration response spectrum, at 5% damping, for this floor motion are presented in Fig. 5.6. It can be seen that most of the energy of the signal is concentrated in the 0.15 s period range, corresponding to the natural period of the wood diaphragm analyzed. Note also that the full-scale amplitude of the selected floor motion has a PHA value of 0.40g, corresponding to a Peak Ground Acceleration (PGA) of 0.13g.

5.5 Theoretical Strength of Wall Specimens

Prior to testing, the expected out-of-plane strength of the wall specimens was assessed using three different approaches.

First, it is possible to deduce the strength of a masonry wall subjected to out-of-plane excitation from the limits of the h/t ratio specified by code documents such as the Canadian Guidelines for Seismic Evaluation of Existing Buildings (CGSEEB) (NRC 1992) and the Uniform Code for Building Conservation (UCBC) (ICBO 1997). Here, the h/t ratio of the masonry wall in these specimens is 15.2. Specified limits in the CGSEEB indicate that the wall specimens can survive earthquakes in regions of effective zonal velocity ratio z' of 5 or less, which translates into a maximum Peak Ground Velocity (PGV) of 0.32 m/s and PGA of 0.32g. Considering implied amplification velocity values of 1.75, this corresponds to floor velocities of 0.56 m/s.

Second, a probabilistic assessment is possible by considering the data supporting the ABK methodology (ABK 1984; Bruneau 1994) from which other procedures such as the UCBC and CGSEEB are directly derived. For the given h/t ratio of 15.2, and absence of overburden on the tested wall (i.e., no axial load applied), the floor velocity applied to the wall can be related to a specified probability of survival. Here, for a 98% probability of survival, the peak floor velocity (assuming identical velocities applied at the top and bottom of the wall) is 0.538 m/s. For a 50% probability of survival, this increases to 0.574 m/s. The corresponding peak ground acceleration for 98% and 50% survival would be 0.307g and 0.328g, respectively.

Finally, using a method proposed by Priestley (Priestley 1985, Priestley and Paulay 1992) to calculate dynamic out-of-plane wall stability, the accelerations (uniformly distributed along the height of the wall) to initiate cracking and to trigger static instability were calculated to be 0.044g and 0.108g, respectively (calculations are shown in Appendix G). This result, obtained considering an elastic nonlinear model, is then converted using an equal energy approach into a corresponding value for an equivalent linear elastic model. This equivalent elastic lateral wall response acceleration to induce failure was thus calculated to be 2.58g.

Strength estimates for the wall retrofitted using Cintec anchors depend on whether the anchors provided at mid-height of the wall are effective in reducing the h/t ratio by a factor of 2. Assuming full effectiveness for the sake of comparison, then, according to the CGSEEB and UCBC, the wall could survive earthquakes in regions of effective zonal velocity ratio, z' of 6, corresponding to PGV and PGA in excess of 0.4 m/s, and 0.4g, respectively. According to the ABK methodology, for 98% and 50% survival, the peak velocity at each end of the wall would be 0.683 m/s and 0.790 m/s, respectively. The corresponding peak ground acceleration for 98% and 50% survival would be 0.390g and 0.451g, respectively. Based on Priestley's method, the equivalent elastic lateral wall response acceleration at failure would be 15.4g.

For the wall retrofitted with Tyfo fiberglass strips, ultimate capacity was computed using a reinforced concrete stress block analogy, but where the steel reinforcement is replaced by the fiberglass. The corresponding lateral wall acceleration at failure was found to be 6.02g.

5.6 Experimental Results

Description and visual observations made during the testing of each specimen are presented in this section. Each wall specimen was subjected to the same seismic input motion of progressively increasing intensity starting at 0.05g, increasing by increments of 0.05g up to 0.20g, then by increments of 0.10g up to 0.40g, and by 0.20g increments up to 1.0g, and 0.25g afterwards until failure. A video camera was used to record global specimen behavior during the tests. After each test run, the condition of each specimen and extent of cracking was noted, and photographs were taken.

5.6.1 As-built specimen

Up to a PHA of 0.15g, the response of the as-built specimen was characterized by very small vibrations, making the deflected shape barely perceptible. Minor cracks extended from existing cracks on the left side of the brick wall. At 0.15g, the dynamic response was more visible, as well as the deflected shape. Two cracks appeared in the central portion of the wall. From 0.2g to 0.6g, the brick wall deflections gradually increased, which formed new cracks and extended existing ones as shown in Fig. 5.7(a). A parabolic deflected shape could be

clearly seen during response. At 0.8g, the response became more severe and dust emanated from the plaster inside the wooden belt. A full-width crack formed at the top just below the wooden belt causing the wall to behave slightly more like a mix of a cantilever and simply-supported beam. At 1.0g, a more severe response caused the plaster cover that was hidden inside the wooden belt to crumble, creating further dust. Due to the full-width crack at the top as shown in Fig. 5.7(b), the wall was now sliding under the top row of bricks. After a PHA of 1.25g, several cracks around numerous bricks were noticeable, mostly on the upper left portion of the wall, but no bricks had fallen. However, at a PHA of 1.5g, most of these bricks fell, as shown in Fig 5.7(c), leaving the specimen in poor condition. At 1.75g, the as-built specimen completely failed, as shown in Fig. 5.8(a). Starting from the upper rows, all bricks fell down successively. The wood backing was still standing, and after close inspection, wood mortises were discovered between the 75 mm x 250 mm (3 in x10 in) planks on the right side only.

5.6.2 Cintec specimen

Up to 0.6g, response of the Cintec specimen was identical to that of the as-built specimen, with the exception that being attached with anchors, the wood backing could clearly be seen moving along with the brick wall. At 0.8g, the portion of the wall above the anchors was noticed to respond more as evidenced by the more extensive cracking developing above mid-height compared to the lower portion as shown in Figs. 5.7(d) and (e). At 1.0g, dust emanated from the upper portion of the brick wall. After a PHA of 1.25g, cracks were found almost around each brick, especially in the upper part of the wall. As shown in Fig. 5.7(f), at 1.5g, three bricks on the upper left side fell down. The mortar joints in the first four rows of brick at the top were thoroughly cracked and pieces had fallen down, leaving these bricks in precarious stability. The nails connecting the brick wall to the wood backing above the anchors were sliding freely in the mortar joints. At a PHA of 1.75g, the upper portion of the Cintec wall fell down, leaving the part below the anchors in relatively good condition, as shown in Fig. 5.8(b). No wood mortises were discovered in the wood backing.

5.6.3 Tyfo specimen

From a PHA of 0.05g to 0.20g, the wall responded almost rigidly, with almost no visible deflection. No new cracks appeared during these test runs. After a PHA of 0.30g, pieces of mortar fell down, leaving some bricks in the upper corner considerably unstable. Also, a small gap was noticed in the wooden belt between the plywood and the encased brick wall. From a PHA of 0.40g to 0.80g, the gap inside the wooden belt grew to cause the brick wall to behave more like a cantilever partially restrained at the top. During each test run, pieces of mortar were falling in the cavity between the brick and wood wall and several bricks on each side at the top became very unstable. After 0.80g, the remaining piece of crated plywood inside the wooden belt was displaced upon repeated impact, as shown in Fig. 5.9. After 1.0g, bricks fell from the upper left side and from inside of the wooden belt, as shown in Figs. 5.7(g) and (h). At 1.25g, other bricks fell from the upper and bottom right corners, as shown in Fig. 5.7(i). The accumulation of mortar debris in the cavity between the two walls was rising above mid-height. After a PHA of 1.5g, more bricks fell from the right side and from inside the wooden belt. At this point, there was a considerable gap inside the wooden belt, allowing the wall to behave first as a cantilever, until it hit the side of the belt, then as a simply-supported wall following that impact. Only the upper left portion of the wall fell at a PHA of 1.75g, tearing a Tyfo strip above mid-height in the process. The remaining portion of the wall stayed in place due to the other Tyfo strips being glued to the remaining piece of crated plywood inside the wooden belt. At 2.0g, the Tyfo strips de-bonded from the plywood, causing the remaining portion of the brick wall to fall like a rigid body held together by fiberglass strips, as shown in Fig. 5.8(c).

Although difficult to quantify, it is expected that some improvement in behaviour would have been observed if, for each specimen, the test at the highest PGA had been carried out without prior shaking at increasing amplitudes.

5.7 Variation of Dynamic Properties

5.7.1 Fundamental frequencies

As shown in Fig. 5.10(a), the fundamental frequency of the as-built specimen gradually decreased, from 6.25 Hz initially to 5.66 Hz at a PHA of 0.6g. At 0.8g, the frequency dropped to 4.59 Hz due to development of a full-width crack at the top, to reach 4.00 Hz at 1.25g. It then increased to 4.29 Hz at 1.5g as several bricks fell, thereby reducing the effective mass of the wall. After failure of the brick wall, the frequency of the wood backing alone was found to be 8.1 Hz.

The initial natural frequency of the Cintec specimen was 7.52 Hz, and did not change during the first few test runs. At a PHA of 0.15, it gradually decreased to 5.1 Hz at failure of the wall.

The initial frequency of the Tyfo specimen was 12.7 Hz. Up to 0.4g, the natural frequency remained almost constant. At 0.6g, it dropped to 7.32 Hz due to the gap created in the connection at the top, and then gradually decreased to 4.79 Hz. It increased to 5.85 Hz and 7.03 Hz at the PHA of 1.5g and 1.75g, respectively, as the specimen began to lose bricks and due to the ample accumulation of debris in the cavity between the two walls.

5.7.2 Damping ratios

The damping ratio, measured as described in an earlier section, varied considerably for each wall and between each test run, ranging from 2% to 11%, as shown in Fig. 5.10(b). The initial damping of the as-built specimen ratio was 9.3%; it dropped to about 4.5% for the first few test runs, increased to 7.5% at a PHA of 0.4g, then dropped to about 3% for the remainder of the tests. The damping ratio of the wood backing alone was found to be 3.28%. The initial damping ratio of the Cintec specimen was approximately 4%; it increased to 10% at a PHA of 0.2g, dropped to 3.6% at 0.3g, then progressively decreased from 6.5% at 0.4g to 3.5% at a PHA of 0.8g, and finally increased to 6.1% at 1.5g. The initial damping ratio of the Tyfo specimen was 4.75%; it dropped to 2.75% and to 2% at a PHA of 0.1g and 0.4g, respectively,

with some higher values recorded in between, increased to 11.2% at a PHA of 0.8g, and gradually decreased to 4% at 1.75g. The considerable variation of damping ratios is attributed to the small numbers of low amplitude cycles used to calculate these values. As such, from Fig. 5.10(b), one could argue that damping, on average, has not varied meaningfully during these tests (i.e., no clear trend could be established), and that average values of 5.2%, 5.6%, and 5.7% for the as-built, Cintec, and Tyfo specimen, respectively, could have been used.

5.7.3 Mode shapes - vertical profiles

Using the data recorded by the accelerometers located on the wall, the fundamental mode shapes were generated at various steps throughout the testing sequence. The first tests yielded a parabolic shape for the as-built specimen, as shown in Fig 5.11(a). The curvature was not perfectly symmetric about mid-height due to a less rigid connection at the top compared to the bottom, where it was cast into concrete. Based on trial and error, the mode shape and period of a fixed-pinned model more closely match the experimental results than any other simple assumption (e.g., pinned-pinned), even though some discrepancy is noted in the lower part of the mode shapes. The mode shape was constant up to a PHA of 1.0g. At a PHA of 1.25g and higher, the response of the upper part of the wall started to exceed that of mid-height, causing eventually failure of the wall.

The mode shape of the Cintec specimen is similar to the as-built specimen. As shown in Fig. 5.11(b), at a PHA of 1.0g and 1.25g, the displacement at the 3/4 height nearly equals that at mid-height and is comparable to the as-built specimen, suggesting that the anchors at mid-height did not noticeably help to prevent excessive displacement of the upper portion of the wall. Nonetheless, the flexible connection at the top caused the wall to fail prematurely.

For the first test runs of the Tyfo specimen, the mode shape was very similar to that of the previous specimen as shown in Fig. 5.11(c). However, the mode shape changed radically when a gap developed in the wooden belt. As described earlier, the wall then started to behave like a cantilever, banging at the top inside the wooden belt. The deteriorating conditions at the top subsequently led to the wall failure.

5.7.4 Mode shapes - in-plan deformations

Using the accelerometers located across the width of the specimen at mid-height, the in-plan mode shapes were generated. As shown in Fig. 5.12, some torsion was experienced by the specimens during each test. It is clearly evident on the as-built specimen, for which a larger displacement is noticed on the left side in most test runs. This is consistent with observation that cracks developed primarily on this side of the wall during testing. When the specimen was removed from the shake table, vertical wood mortises were discovered between planks only on the right side of the wall. The Cintec retrofit specimen, which had no wood mortises in the wood backing, showed a small amount of torsion compared to the as-built specimen. A similar observation can be made for the Tyfo retrofit specimen, which exhibited very little torsion in spite of the substantially poor initial conditions of the brick wall.

5.8 Analysis of Results

5.8.1 Wall response

The existing unreinforced masonry wall was able to resist significant peak horizontal accelerations without substantial damage. As shown in Figs. 5.13(a) and (b), large accelerations developed at mid-height of the wall before they collapsed out-of-plane. Note that the wall's dynamic response significantly amplified the input floor accelerations, as shown in Figs. 5.13(c) and (d). As the level of excitation increased from 0.05g to 1.25g, the amplification at mid-height of the as-built specimen decreased from 3.16 to 0.86, respectively. Based on the experimental values for the period and damping ratio, theoretical corresponding wall dynamic amplifications for each specimen were calculated and compared against the values obtained experimentally, as shown in Fig. 5.14. It can be seen in Fig. 5.14(a) that the initial period of the as-built wall was located right after the spectral peak; therefore, as the period elongated, the dynamic amplification from the wall decreased. The Cintec specimen, being more rigid (i.e., having a shorter period), had an amplification factor of 6.82 initially; it decreased accordingly as the period lengthened, even though the initial period of the Cintec wall was located just before the peak response, as shown in Fig. 5.14(b). Interestingly, the behavior of the Tyfo retrofit was different. The specimen had a considerably shorter period

than the other two specimens. As the period lengthened, the amplification factor increased from 2.28 initially to 4.87 at a PHA of 0.6g, then decreased to 1.84 at a PHA of 1.5g, as shown in Fig. 5.13(c). By looking at the response spectrum as shown in Fig. 5.14(c), one can see that the actual peak of the response spectrum as observed experimentally was found to be at a period of approx. 0.133 s instead of 0.15 s, which is concordant with the behavior observed for the Cintec and Tyfo specimens.

As shown in Figs. 5.15(a) and (b), the lateral maximum displacement at mid-height increased as the level of input seismic motion increased. This increase is almost linear in the case of the as-built and Cintec specimen, except for PHA greater than 1.0g for the as-built specimen, where maximum displacement increases more significantly. The maximum displacement of the Tyfo specimen at mid-height appears to be non-proportional and limited to a certain value (approximately 14 mm) after a PHA of 0.8g. This is explained by Fig. 5.16, where the maximum inward and outward displacements of both the brick wall and wood backing during testing are presented. It can be seen in Fig. 5.16(c) that, at a PHA of 0.8g and 1.0g, the inward displacement, which was greater than the outward displacement, was limited when the brick wall was moving towards the wood backing.

5.8.2 Wood-masonry interaction

As shown in Fig. 5.16(a), the wood backing and brick wall of the as-built specimen were moving in-phase during the first test runs (as indicated by the brick and wood displacement curves closely following each other), and moved more independently of each other as the level of excitation increased. As mentioned earlier, the wood and brick walls were connected together only by nails protruding from the wood backing and embedded in the masonry walls' mortar joints. As the level of earthquake intensity increased, these nails started to slide freely in the mortar. The gap between the wood and brick walls, originally 15 to 20 mm, expanded by an additional 29.7 mm.

As shown in Fig. 5.16(b), introducing anchors at mid-height forced the two walls to move together and kept the gap between them from increasing noticeably during the test, with the additional gap generated being only 2.0 mm. Another way to confirm this behavior is by

looking at the phase angle. By comparing the frequency content of the accelerometers located at mid-height of the brick wall and wood backing, it is possible to determine the phase relation between the two walls. A phase angle of 0° means that both walls are moving in-phase, whereas an angle of 180° indicates that they are completely out-of-phase. Thus, as observed in Fig. 5.17, the phase angle is almost zero throughout the test for the Cintec specimen compared to the as-built specimen, which increased almost exponentially after a PHA of 1.0g. Interestingly, the fiberglass retrofit apparently also helped to keep the two walls together, even though no improvements were made to the nail connection. The additional gap observed in that case was about 12.3 mm, adding to an initial gap of 25 to 35 mm, as shown in Fig. 5.16(c).

5.9 Comparison with Analytical Predictions

The base acceleration that caused collapse of the as-built wall was 1.75g, corresponding to a wall base and top velocity of 0.404 m/s and a PGA of 0.583g, given a floor amplification of 3 obtained from the diaphragm linear dynamic analyses. This result is lower than the 0.538 m/s and 0.574 m/s values for 98% and 50% probability of survival predicted by the ABK methodology. However, it exceeds the 0.32g maximum PGA capacity calculated by the CGSEEB in an earlier section. The peak acceleration value recorded at mid-height was 3.92g at a PHA of 1.75g, a value greater than 2.58g, the lateral response acceleration calculated by Priestley's method.

Specified limits in the CGSEEB indicated that the Cintec specimen could survive to a maximum PGA of 0.4g or higher if the anchors at mid-height were effective in reducing the h/t ratio by two. As exhibited by the mode shape in an earlier section, the anchors did not effectively contribute to reducing the h/t ratio, but helped to increase the structural integrity of the specimen. However, like the as-built specimen, the Cintec wall collapsed at a base acceleration of 1.75g, corresponding to a wall base and top velocity of 0.404 m/s, which is lower than the values predicted by the ABK methodology, as stated above. The peak lateral acceleration recorded at mid-height was 6.58g at a PHA of 1.75g, a value greater than 2.58g but lower than 15.4g, as calculated by Priestley's method for a wall with an h/t ratio reduced by two.

The peak lateral acceleration recorded at mid-height on the Tyfo specimen at collapse was 5.59g at a PHA of 2.0g. This result is lower than the 6.02g value predicted in an earlier section, based on a reinforced concrete stress block analogy.

It is important to remember when interpreting the experimental results that they are from wall specimens whose heights (1.5m) are not representative of actual floor to floor distance in buildings. A height of approximately of 2.5 to 3.0 m is more likely for a single wythe masonry brick wall panel spanning vertically between floor diaphragms. In such cases, the h/t ratio may range from 25 to 30, which exceeds the limit of 20 specified in the CGSEEB and UCBC. Therefore, such walls would survive earthquakes in regions of effective zonal velocity ratio z' of 1 or less, which translates into a maximum PGV of 0.08 m/s and PGA of 0.08g. According to the ABK methodology, for 98% and 50% survival, the peak velocity at each end of the wall would be 0.377 m/s and 0.413 m/s, respectively. Based on Priestley's method, the equivalent lateral response wall acceleration at failure would be 0.357g. All these values are significantly less than those calculated for the test specimens.

Various analytical procedures have been tried in attempts to model the experimental behavior observed. A model by Blaikie and Davey (2000) was first considered (additional details are given in Appendix G). They have studied the seismic behavior of face loaded unreinforced masonry walls, modeled the walls as uncracked except at the diaphragm and mid-height levels, and assessed their stability under lateral load using simple statics in the deformed configuration. The lateral load deformation calculated using this model for the as-built wall is plotted in Fig. 5.18. Note that while this model takes into account the self weight and overburden load from a parapet or any upper storey as contributing to the stability, the wall model is not restrained against vertical movements due to rigid body motions on open cracks. A model developed by Priestley includes the effects of stiff boundary conditions in which compression struts are formed as the wall cracks under lateral inertial accelerations (additional details are given in Appendix G). The corresponding membrane compression deformation relationship for the as-built wall is plotted in Fig. 5.18 and could be viewed as an upper bound limit. It appears that experimental results partly progressed toward the upper limit, as shown in Fig. 5.18, and largely exceeded the values predicted by the Blaikie and Davey model. However, it was observed during testing that while the specimens were restrained at the top,

the lack of tight fit provided by the wooden belt increased as the level of seismic excitation increased. Therefore, the resistance provided by compression membrane action diminished until the upper brick portion of the wall sustained large displacements that triggered dynamic instability, causing collapse of the wall.

5.10 Summary

Out-of-plane shake table tests have been conducted on three existing unreinforced masonry walls with wood backing assemblies. These tests have demonstrated that such walls could resist significant out-of-plane inertial accelerations without failure. Performance can be improved by different retrofit methods such as providing anchors at mid-height to force the wood and masonry wall to move as a unit, and adding fiberglass strips epoxied to the masonry wall to increase its out-of-plane stiffness and strength. The latter method proved to be more effective. However, in order to achieve such out-of-plane performances for wall panels, it is assumed that the walls are properly anchored at the floor/roof levels. Otherwise, as shown in the tests, lack of appropriate boundary conditions could considerably reduce expected performance. Various analytical methods have been used to explain the observed behavior, but the lack of tight fit at the top of the wall in the test set-up and interaction with the wood backing resulted in an intricate ultimate failure mode that could not be replicated analytically.

CHAPTER 6

Conclusion

6.1 Conclusions

Many old existing unreinforced masonry buildings (URM), built before the 1960's, were not designed to resist earthquakes. As a result, their seismic behavior may not be adequate, and they may need to be retrofitted. In the current research project, a full-scale URM specimen with a flexible diaphragm was constructed and tested pseudo-dynamically to better understand its expected seismic behavior.

The overall specimen was found to be relatively resilient to earthquake excitation, even though cracking was extensive. A stable combined rocking and sliding mechanisms formed and large deformations developed without significant strength degradation. The repair procedure using fiberglass strips to preserve pier rocking was demonstrated to enhance this behavior. While the specimen was able to resist severe levels of earthquake excitation, it should not be forgotten, that this specimen was subjected to only unidirectional earthquake excitation, and that its performance under true dynamic bi-directional excitation could have been (somewhat) worse than observed here, particularly as loose bricks might have been dislodged and projected outside the plane of the wall, leading to its accelerated degradation.

It was found that even though the diaphragm did not experience significant inelastic deformation, some (but not all) of the existing seismic evaluation methodologies accurately capture the rocking/sliding behavior that developed in the shear walls under large displacement. Notably, the FEMA 306 methodology proved the most accurate for evaluation purpose while others missed one or more points of behavior.

Additionally, shake-table tests have demonstrated that existing masonry walls with wood backing could resist significant out-of-plane inertial accelerations without failure, and their performance can be improved by different retrofit methods such as providing anchors at mid-height to force the wood and masonry wall to move as a unit, and adding fiberglass strips epoxied to the masonry wall to increase its out-of-plane stiffness and strength. The latter method proved to be more effective.

6.2 Future Research Needs

The dynamic response of existing unreinforced masonry buildings should be further investigated. Notably, additional studies should investigate the effect of the nonlinear response of diaphragms with different types of lumber sheathing arrangements, and diaphragms rehabilitated with plywood sheathing. Additional research is needed on the force-deformation relationships of old existing wood diaphragms to either confirm or contradict the models used by ABK and FEMA 273. The ongoing research project at the Mid-America Earthquake Center will undoubtedly provide useful information on this issue.

The dynamic response of a similar structure constructed with stone masonry should also be examined. This comparison between stone masonry and brick masonry buildings will permit to determine whether current knowledge on the seismic evaluation of existing unreinforced masonry buildings can be safely extended to cover stone masonry buildings.

Finally, previous research on the rehabilitation of masonry walls with fiberglass material concentrated on retrofitting the shear walls to increase either their in-plane shear resistance or out-of-plane flexural resistance. Thus, the force-deformation relationship of piers retrofitted with fiberglass strips to increase their in-plane capacity during rocking should be investigated. A detailed parametric experimental study must be conducted in order to implement this retrofit solution into a reliable design method for engineers.

REFERENCES

ABK, A Joint Venture, (1981). "Methodology for mitigation of seismic hazards in existing unreinforced masonry buildings: Diaphragm testing." *Rep. ABK-TR-03*, Agbabian & Associates, S.B. Barnes & Associates, and Kariotis & Associates, El Segundo, CA.

ABK, A Joint Venture, (1982). "Methodology for mitigation of seismic hazards in existing unreinforced masonry buildings: Interpretation of diaphragm tests." *Rep. ABK-TR-05*, Agbabian & Associates, S.B. Barnes & Associates, and Kariotis & Associates, El Segundo, CA.

ABK, A Joint Venture, (1984). "Methodology for mitigation of seismic hazards in existing unreinforced masonry buildings: The Methodology." *Rep. ABK-TR-08*, Agbabian & Associates, S.B. Barnes & Associates, and Kariotis & Associates, El Segundo, CA.

Abrams, D.P., (1992). "Strength and behaviour of unreinforced masonry elements." Proceedings of the Tenth World Conference on Earthquake Engineering, (6) 3475-3480, Madrid, Spain.

Anthoine, A., Magenes, G., Magonette, G., (1994). "Shear-compression testing and analysis of brick masonry walls." Proceedings, Tenth European conference on earthquake engineering, Vienna

Atkinson, G.M., Beresnev, I.A., (1998). "Compatible ground-motion time histories for new national seismic hazard maps." *Can. J. Civ. Engrg*, Ottawa, Canada, 25(2), 305-318.

Bariola, J., Ginocchio, J., and Quiun, D., (1990). "Out-of-plane seismic response of brick walls." Proceedings, Fifth North American masonry Conference, v. I, 429-439

Blaikie, E.L., Davey, R.A., (2000). "Seismic behaviour of face loaded unreinforced masonry walls," *12th World Conference on Earthquake Engineering*, Auckland, New Zealand, (on CD-ROM).

Bruneau, M., (1990). "Preliminary report of structural damage from the Loma Prieta (San Francisco) earthquake of 1989 and pertinence to Canadian structural engineering practice." *Can J. Civ. Engrg.*, Ottawa, Canada, 17(2), 198-208.

Bruneau, M., (1994a). "Seismic evaluation of unreinforced masonry buildings - a state-of-the-art report." *Can J. Civ. Engrg.*, Ottawa, Canada, 21(3), 512-539.

Bruneau, M., (1994b). "State-of-the-art report on the seismic performance of unreinforced masonry buildings." *J. Struct. Engrg.*, ASCE, 120(1), 230-251.

Bruneau, M., (1995). "Performance of masonry structures during the 1994, Northridge (L.A.) earthquake." *Can J. Civ. Engrg.*, Ottawa, Canada, 22(2), 378-402.

Cintec (1996). Cintec International News, *Cintec Canada Ltd.*, Nepean, Ontario.

Clough, R., Mayes, R., and Gulkan, P., (1979). "Shaking table study of single-story masonry houses, Volume 3: Summary, conclusions, and recommendations." UCB/EERC-79/25

Clough, R.W., and Penzien, J. (1993). "Dynamics of Structures. " Second Edition, McGraw-Hill, New York.

Costley, A. C., and Abrams, D.P. (1995). "Dynamic response of unreinforced masonry buildings with flexible diaphragms." *Rep. No. UILU-ENG-95-2009*, Department of Civil Engineering, University of Illinois at Urbana-Champaign, Urbana, Ill.

CSA, (1994). "Masonry Design for Buildings." CSA Standard S304.1-94, *Canadian Standards Association*, Rexdale, Ontario, Canada.

CSA, (1999). "Design and construction of building components with fibre reinforced polymers." CSA Standard S806-00 *Draft version - March 1999*, *Canadian Standards Association*, Rexdale, Ontario, Canada.

Doyle, D.V., (1955). "Diaphragm action of full-scale diagonally sheathed wood roof of floor panels." *USDA Forest Service*, Miscellaneous Publication FPL-TM 94.

Doyle, D.V., (1960). "Diaphragm action of diagonally sheathed wood panels." *USDA Forest Service Research Note*, FPL-0205.

Drysdale, R.G., Hamid, A.A., and Baker, L.R., (1994). "Masonry Structures Behavior and Design." Prentice-Hall, Englewood Cliffs, NJ.

Epperson, G., and Abrams, D., (1989). "Nondestructive evaluation of masonry buildings." ACTC No. 89-26-03.

Epperson, G.S., and Abrams, D.P., (1990). "Evaluating lateral strength of existing unreinforced brick piers in the laboratory." Proceedings of the Fifth North American Masonry Conference, Urbana-Champaign, Ill., (2), 735-746.

FEMA 172, (1992a). "NEHRP Handbook for the Seismic Rehabilitation of Existing Buildings." *Building Seismic Safety Council*, Washington, DC.

FEMA 178, (1992b). "NEHRP Handbook for the Seismic Evaluation of Existing Buildings." *Building Seismic Safety Council*, Washington, DC.

FEMA 273, (1997a). "NEHRP Guidelines for the Seismic Rehabilitation of Buildings." *Building Seismic Safety Council*, Washington, DC.

FEMA 274, (1997b). "NEHRP Commentary on the Guidelines for the Seismic Rehabilitation of Buildings." *Building Seismic Safety Council*, Washington, DC.

FEMA 306, (1999a). "Evaluation of Earthquake Damaged Concrete and Masonry Wall Buildings, Basic Procedures Manual." *The Patnership for Response and Recovery*, Washington, DC.

FEMA 307, (1999b). "Evaluation of Earthquake Damaged Concrete and Masonry Wall Buildings, Technical Resources." *The Patnership for Response and Recovery*, Washington, DC.

FEMA 308, (1999c). "Repair of Earthquake Damaged Concrete and Masonry Wall Buildings." *The Patnership for Response and Recovery*, Washington, DC.

Filiatrault, A., Tremblay, R., Thoen, B.K., and Rood, J. (1996). "A second-generation earthquake simulation system in Canada: description and performance evaluation," *11th World Conference on Earthquake Engineering*, Acapulco, Mexico, Paper No 1204 (on CD-ROM).

Glanville, J.I., Hatzinikolas, M.A., Ben-Omran, H.A. (1996). "Engineered masonry design - limit states design" Winston House, Winnipeg, Canada.

ICBO, (1997). Uniform Code for Building Conservation, *International Conference of Building Officials*, Whittier, CA.

Irimies, M.T., Bia, C.T., (2000). "Cyclic loading behavior of a perforated unreinforced masonry wall model." *12th World Conference on Earthquake Engineering*, Auckland, New Zealand, (on CD-ROM).

Johnson, J.W., (1954). "Lateral tests on full-scale lumber-sheathed roof diaphragms of various length-width ratios." *Report No. T-9*, Oregon Forest Products Laboratory, Oregon.

Johnson, J.W., (1955). "Lateral tests on 12 by 60-foot and by 80-foot lumber-sheathed roof diaphragms." *Report No. T-12*, Oregon Forest Products Laboratory, Oregon.

Konig, G., Mann, W., and Otes, A., (1988). "Experimental investigations on the behaviour of unreinforced masonry walls under seismically induced loads and lessons derived." Proceedings of the Ninth World Conference on Earthquake Engineering, (8), 1117-1122, Tokyo/Kyoto, Japan.

Magenes, G., Calvi, G., (1994). "Shaking table tests on brick masonry walls." Proceedings, Tenth European conference on earthquake engineering, Vienna.

NRC, (1992). "Guidelines for seismic evaluation of existing buildings." *Institute for Research in Construction, National Research Council*, Ottawa, Canada.

NRC, (1995). "National Building Code of Canada." *National Research Council of Canada*, Ottawa, Ontario, Canada.

Prawel, S.P., and Lee, H.H., (1990). "The performance of upgraded brick masonry piers subjected to out-of-plane motion." Proceedings of the Fourth National Conference on Earthquake Engineering, (3), 273-281, Palm Springs, CA.

Priestley, M.J.N., (1985), "Seismic behaviour of unreinforced masonry walls," Bulletin of the New Zealand National Society for Earthquake Engineering, 18(2), 191-205 and 19(1), 65-75.

Priestley, M.J.N., Paulay, T.,(1992), "Seismic design of reinforced concrete and masonry buildings." John Wiley & Sons, Inc., New York, NY.

Reinhorn, A.M., Madan, A., (1995), "Evaluation of Tyfo-W Fiber Wrap system for out-of-plane strengthening of masonry walls," *Report No. 95-AMR-0001*, Dept. of Civil Engineering, State University of New York, Buffalo, NY.

Rutherford and Chekene. (1991). "Damage to Unreinforced Masonry Buildings in the Loma Prieta Earthquake of October 17, 1989." *California Seismic Safety Commission*, Sacramento, USA, 38 p.

Shing, P. B., Mahin, S. A. (1987a). "Cumulative experimental errors in pseudo-dynamic tests." *Earthquake Engineering and Structural Dynamics*, 15, 409-424.

Shing, P. B., Mahin, S. A. (1987b). "Elimination of spurious higher-mode response in pseudo-dynamic tests." *Earthquake Engineering and Structural Dynamics*, 15, 425-445.

Shing, P. B., Mahin, S. A. (1990). "Experimental error effects in pseudo-dynamic tests." *J. Engrg. Mech.*, ASCE, 116, 805-821.

Shing, P. B., Vannan, M. (1990). "On the accuracy of implicit algorithm for pseudo-dynamic tests." *Earthquake Engineering and Structural Dynamics*, 19, 631-651.

Shing, P. B., Vannan, M., and Carter, E. (1991). "Implicit time integration for pseudo-dynamic tests." *Earthquake Engineering and Structural Dynamics*, 20, 551-576.

Tomazevic, M., Lutman, M., Weiss, P., and Velechovsky, T., (1992). "The influence of rigidity of floors on the seismic resistance of old masonry buildings: Shaking-table tests of stone-masonry houses - Summary report." ZRMK/PI-92/04, Ljubljana.

Tyfo Systems (1997)."For unreinforced masonry (URM) and reinforced concrete/masonry wall strengthening." *Fyfe Co. L.L.C.*, San Diego, CA.

Zhuge, Y., Thambiratnam, D., and Corderoy, J., (1998). "Nonlinear dynamic analysis of unreinforced masonry." *J. Struct. Engrg.*, ASCE, 124(3), 270-277.

Table 3.1 Properties of Typical Diaphragms (6.1 m x 6.1 m) based on ABK

Diaphragm type (1)	Unit shear (kN/m) (2)	Initial stiffness (kN/mm) (3)
19 mm x 140 mm straight sheathing	4.8	2.33
19 mm x 140 mm diagonal sheathing	11.6	8.27
19 mm x 140 mm diagonal sheathing + 19 mm x 140 mm straight sheathing overlay	29.8	10.7
19 mm plywood + 19 mm plywood overlay	42.1	8.66

Table 3.2 Calculation of pier in-plane seismic resistance based on CGSEEB

Pier	Aspect ratio D/H	Axial load P_D(kN)	Rocking capacity V_r (kN)	Shear capacity V_s (kN)	Force required to initiate cracking V_{cr} (kN)
(1)	(2)	(3)	(4)	(5)	(6)
Door	0.47	14.1	6.08	39.3	7.08
Central	1.48	25.9	34.5	64.5	36.6
Window	0.61	11.2	6.11	26.7	6.26

Table 4.1 Possible lateral behavior modes as per different codes and methodologies

Modes of behavior (1)	FEMA 178 (2)	CGSEEB (3)	UCBC 1997 (4)	FEMA 273 (5)	FEMA 306 (6)
Rocking	X	X	X	X	X
Shear/Bed joint sliding w/bond + friction	X	X	X	X	X
Bed joint sliding w/friction only					X
Diagonal tension				X	X
Toe crushing				X	X

Table 4.2 Calculation of pier possible behavior mode based on FEMA 273

Pier (1)	Pier's Height h (mm) (2)	Rocking V_r (kN) (3)	Bed-joint sliding V_{bjsl} (kN) (4)	Diagonal tension V_{dt} (kN) (5)	Toe crushing V_{tc} (kN) (6)
Door	1842	6.08	39.8	24.5	6.70
Central	953	34.5	65.2	59.8	37.9
Window	953	6.11	27.0	16.6	6.72

Table 4.3 Calculation of pier possible behavior mode based on FEMA 306

Wall	Pier	Effective height of pier h_{eff} (mm)	Rocking V_r (kN)	Bed joint sliding w/bond + friction V_{bjs1} (kN)	Bed joint sliding with friction only V_{bjs2} (kN)	Diagonal tension V_{dt} (kN)	Toe crushing V_{tc} (kN)
(1)	(2)	(3)	(4)	(5)	(6)	(7)	(8)
West	Door	1842	6.08	39.8	7.05	24.5	6.73
	Central	1335	24.6	65.2	12.95	59.8	27.3
	Window	1469	3.97	27.0	5.6	16.6	4.34
East	Door	2043	5.48	39.8	7.05	24.5	6.03
	Central	1278	25.7	65.2	12.95	59.8	28.3
	Window	1546	3.77	27.0	5.6	16.6	4.12

Table 4.4 FEMA 273 limiting values for idealized force-deflection relation

Mode (1)				Primary			Secondary	
	c % (2)	d % (3)	e % (4)	IO % (5)	LS % (6)	CP % (7)	LS % (8)	CP % (9)
Bed-Joint Sliding	0.6	0.4	0.8	0.1	0.3	0.4	0.6	0.8
Rocking	0.6	$0.4h_{eff}/L$	$0.8h_{eff}/L$	0.1	$0.3h_{eff}/L$	$0.4h_{eff}/L$	$0.6h_{eff}/L$	$0.8h_{eff}/L$

where c = fraction of strength loss for secondary element.
d = inelastic drift percentage deformation capacity for primary element.
e = inelastic drift percentage deformation capacity for secondary element.
IO = immediate occupancy.
LS = life safety.
CP = collapse prevention.

Table 4.5 FEMA 273 Normalized force-deflection curve coordinates for wood diaphragm with straight sheathing over diagonal sheathing.

(1)	Aspect ratio L/b (2)	d (3)	e (4)	c (5)
Chorded	< 2.0	3.0	4.0	0.2
Unchorded	< 2.0	2.5	3.5	0.3

where c = reduced strength parameter,
d = maximum possible deflection at yield strength,
e = maximum deflection at a reduced strength.

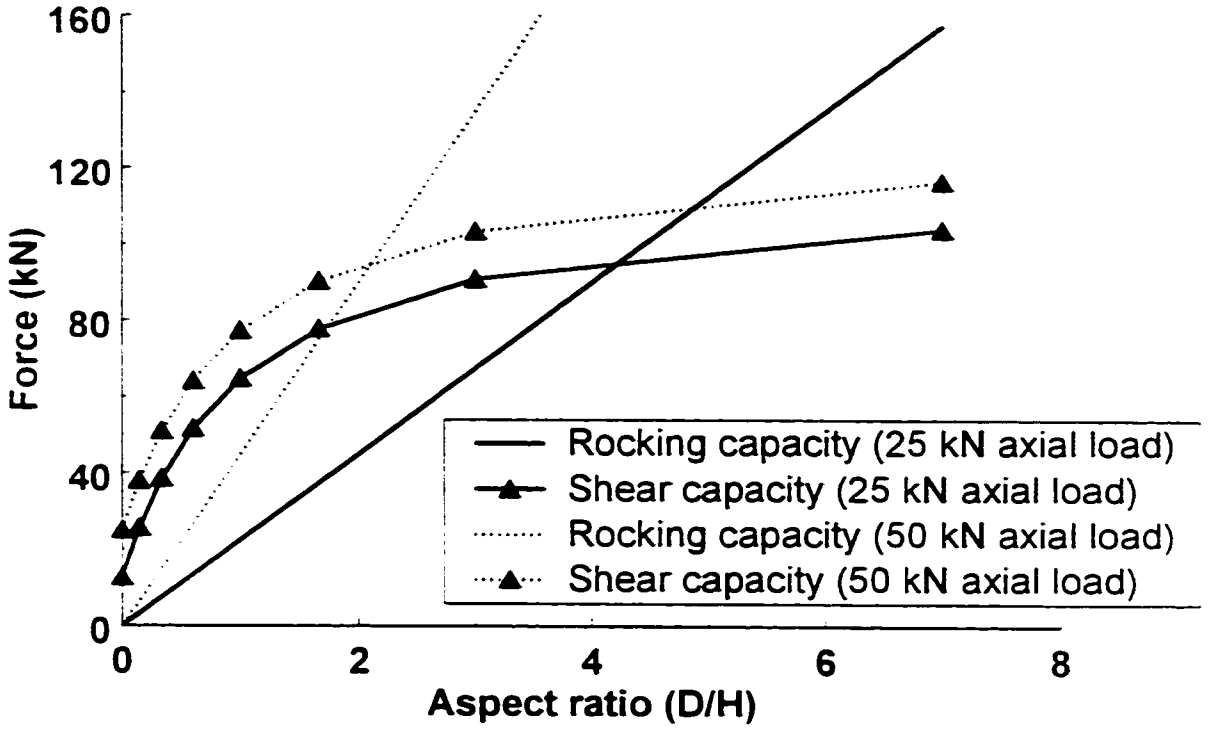

Figure 3.1 Piers rocking and shear capacity for different aspect ratios and axial loads, where D is the in-plane width dimension of masonry, and H is the least clear height of opening on either side of pier.

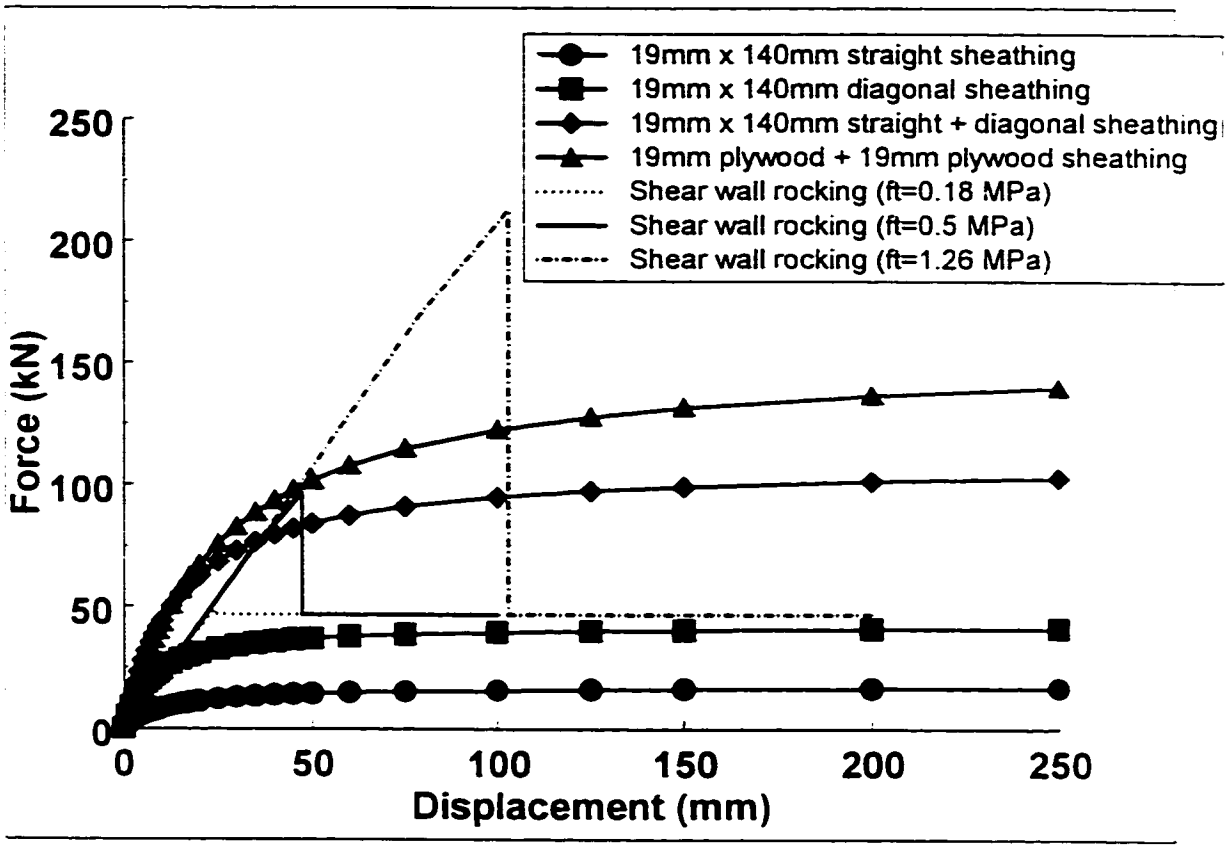

Figure 3.2 Force-deformation curves for a 3.66 m x 5.28 m diaphragm for different types of sheathing, and wall cracking/rocking behavior considering gravity on specimen's piers. Note that the shear wall rocking displacements have been magnified by 1000 to be visible on the same graph.

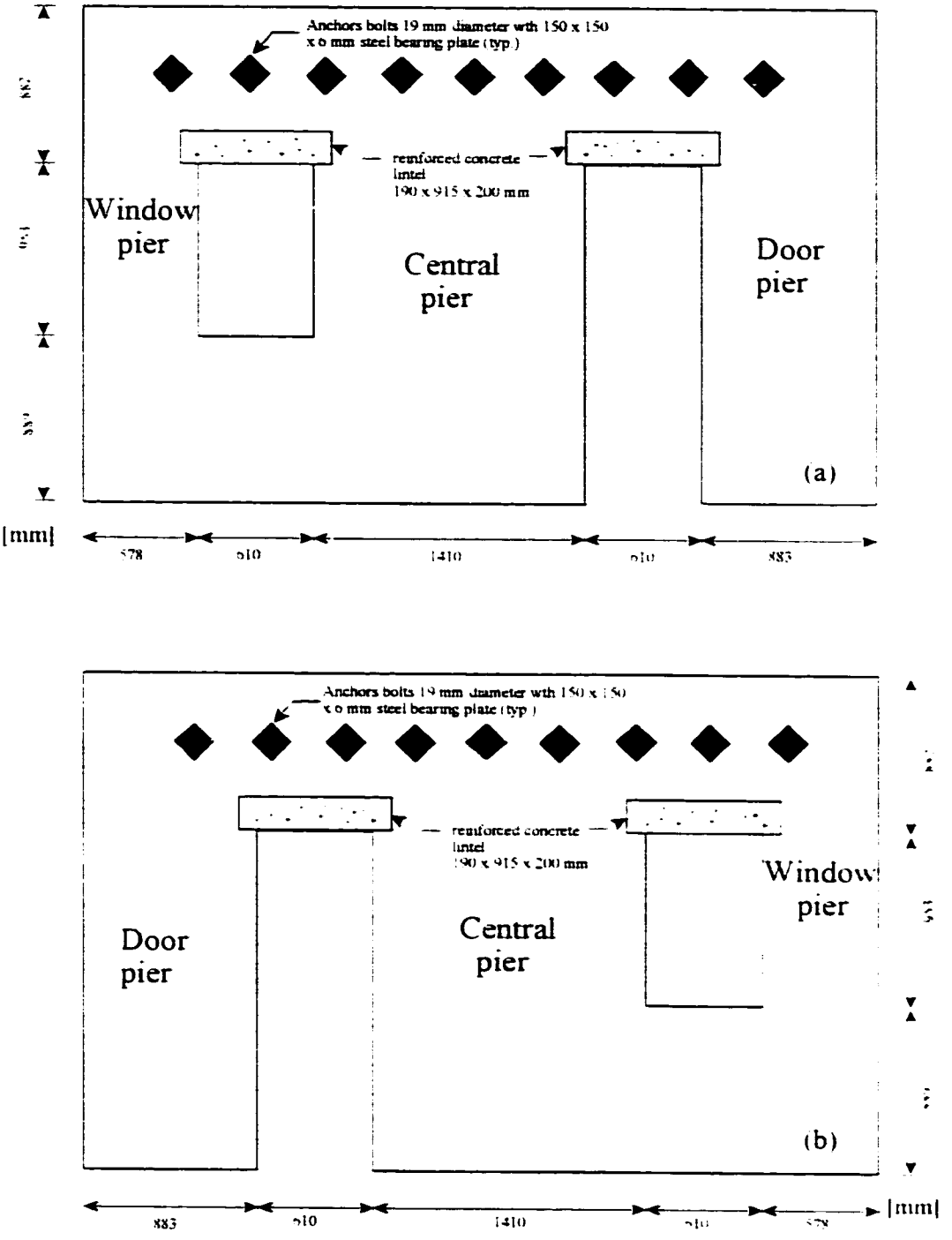

Figure 3.3 Elevation of URM specimen: (a) West wall; (b) East wall.

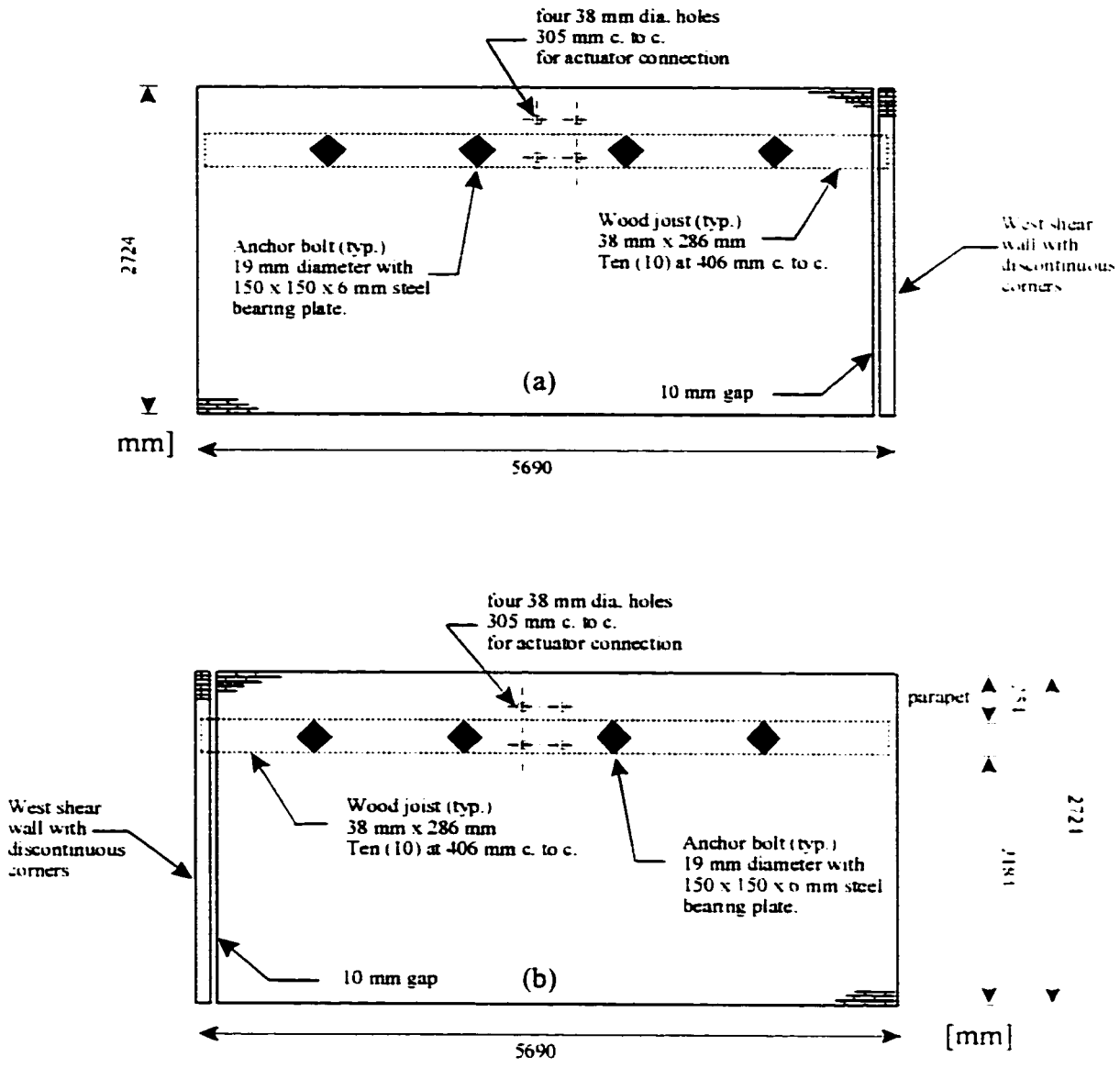

Figure 3.4 Elevation of URM specimen: (a) North wall; (b) South wall.

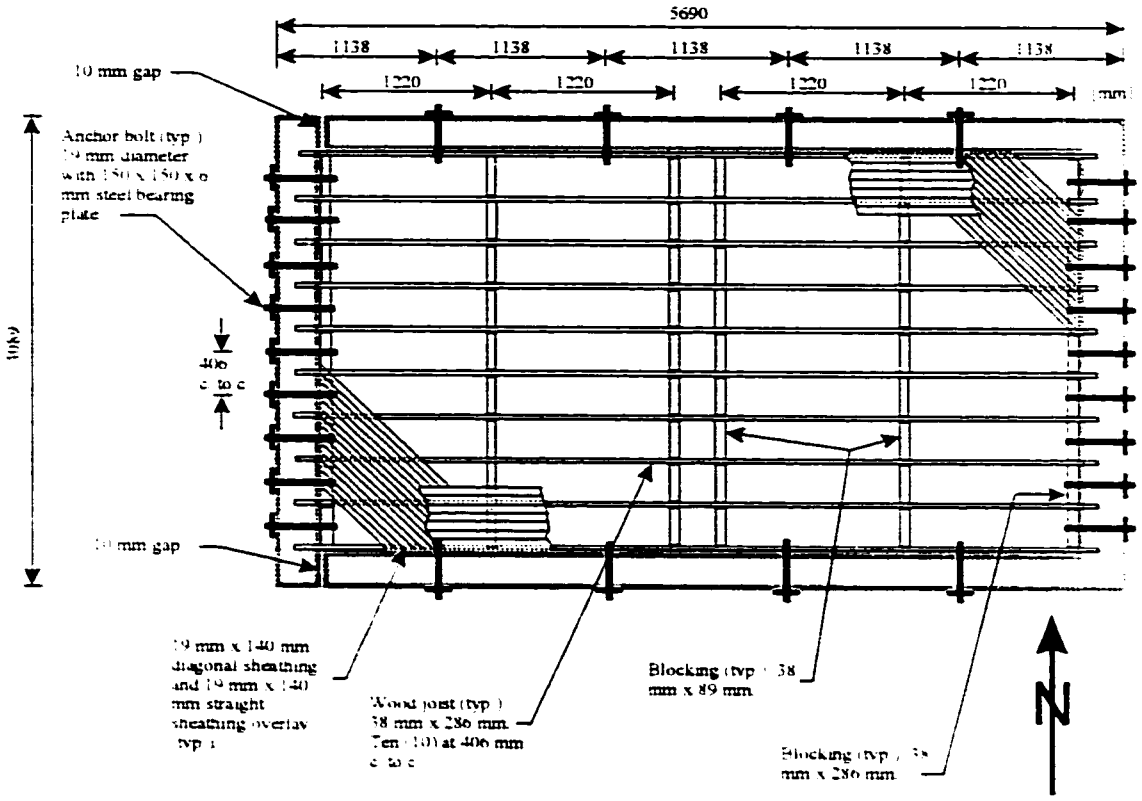

Figure 3.5 Wood sheathed diaphragm framing details.

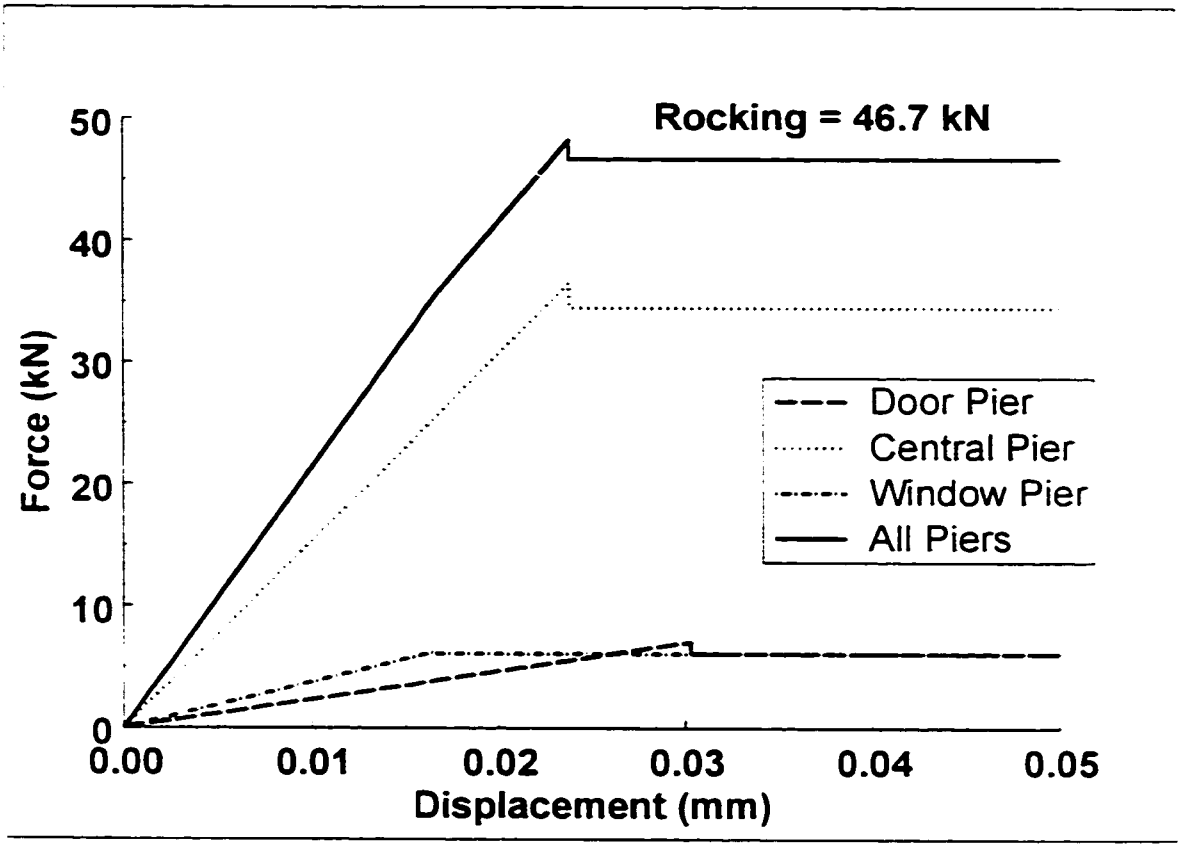

Figure 3.6 Pier rocking resistance based on CGSEEB.

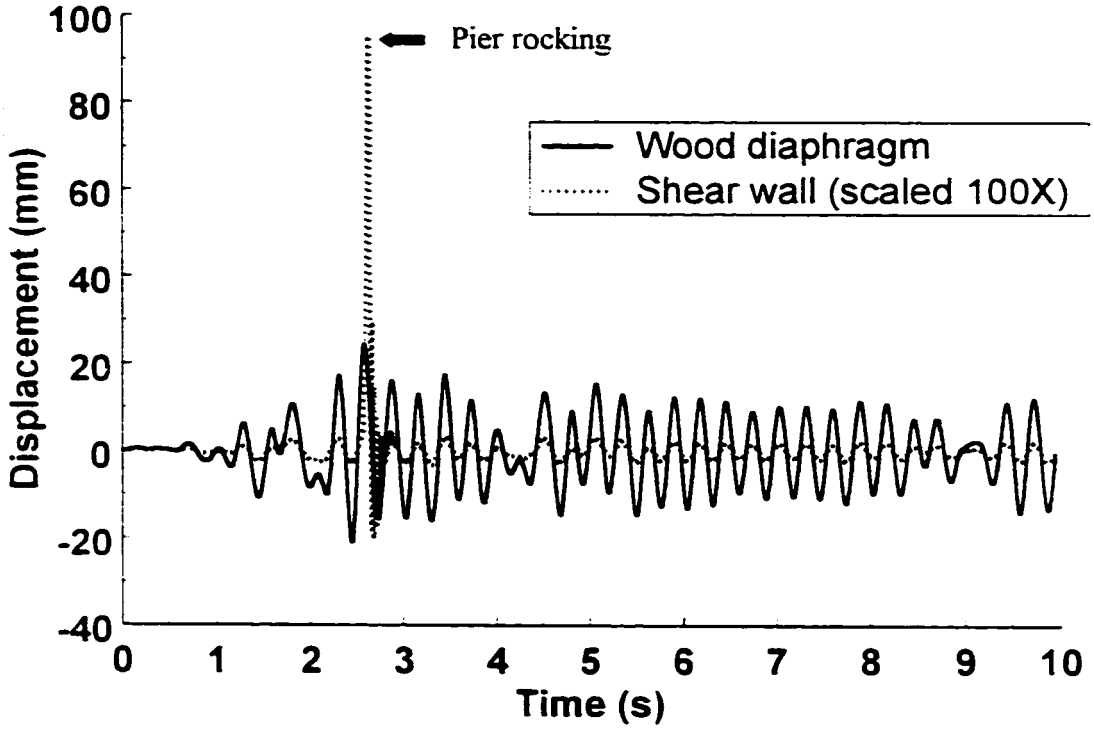

Figure 3.7 Comparison of wood diaphragm center-span response with magnified (100X) end-wall response for El Centro earthquake scaled to 0.5g.

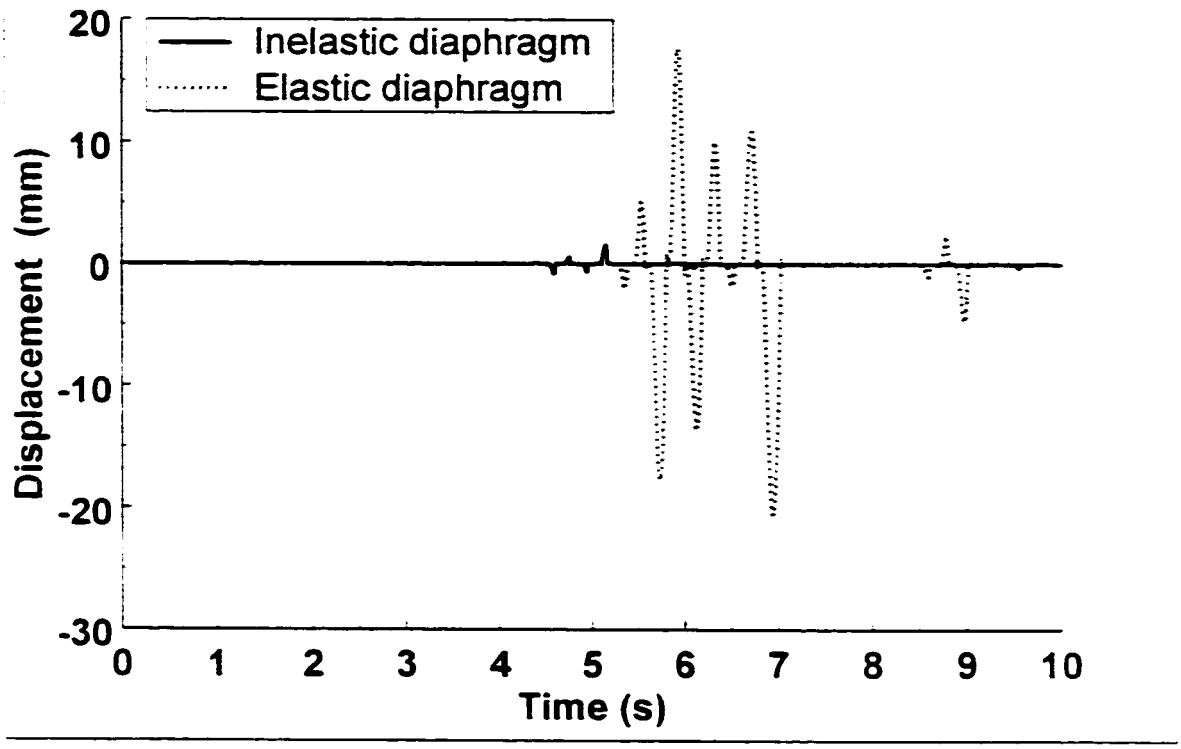

Figure 3.8 Comparison of end-wall response considering elastic or inelastic wood floor diaphragms for the Northridge earthquake Newhall fire station (peak ground acceleration of 0.583g).

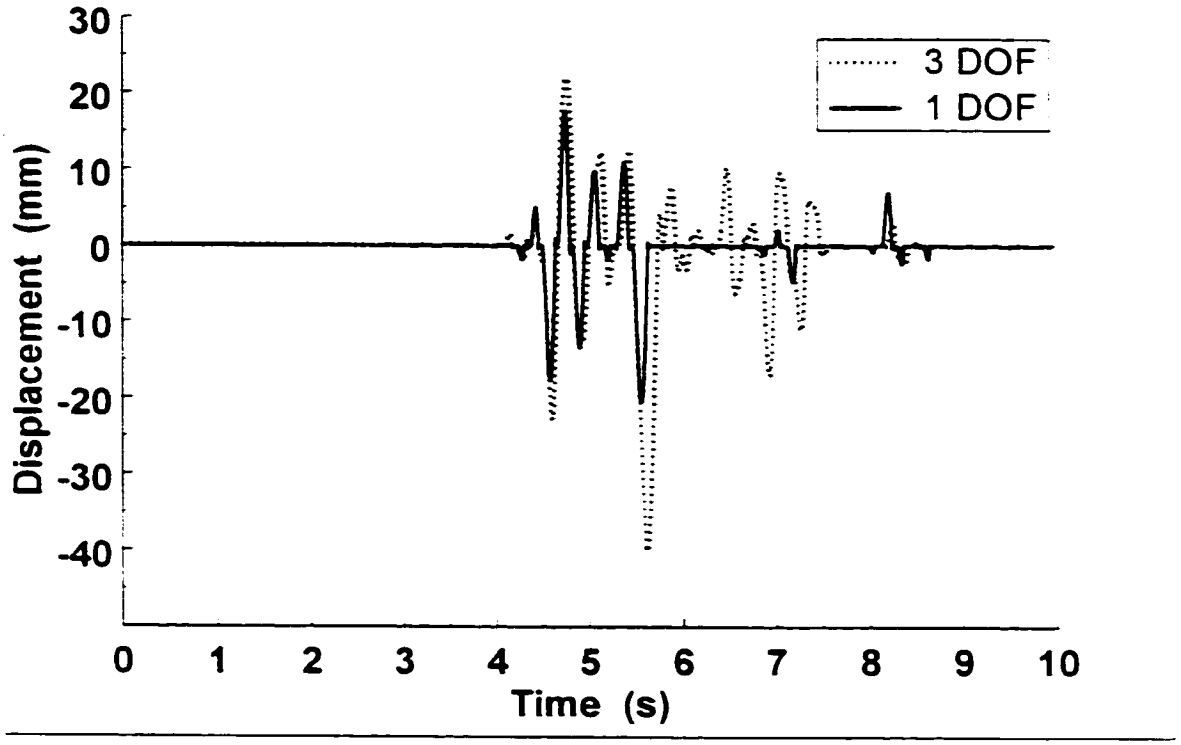

Figure 3.9 End-wall rocking response obtained considering 3 DOF or 1 DOF models for the Northridge earthquake Newhall fire station record (peak ground acceleration of 0.583g).

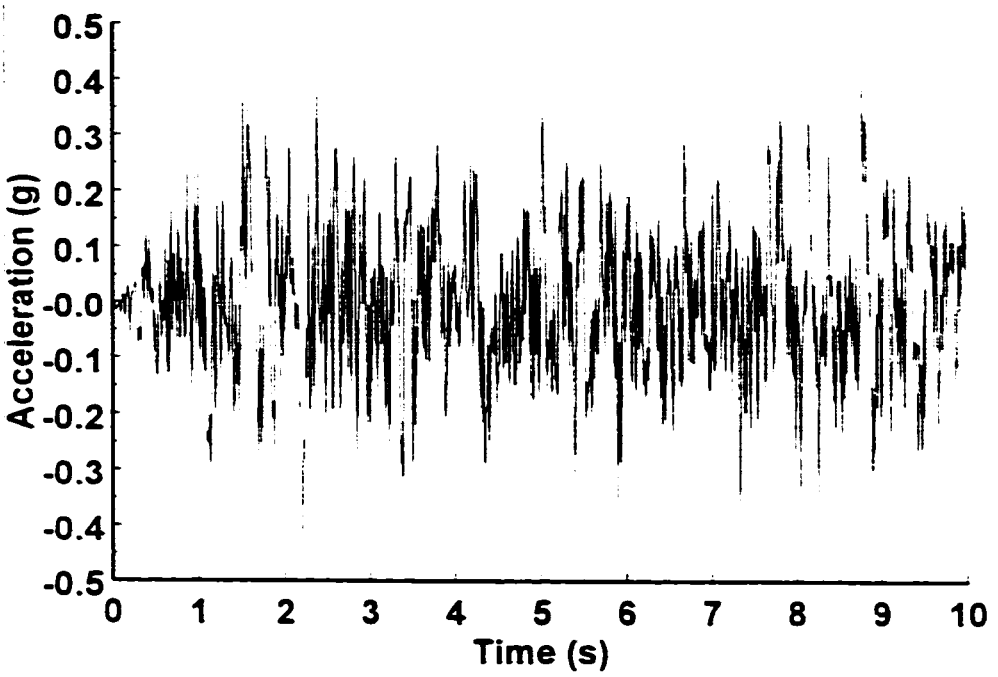

Figure 3.10 Acceleration time history for La Malbaie (peak ground acceleration of 0.453g).

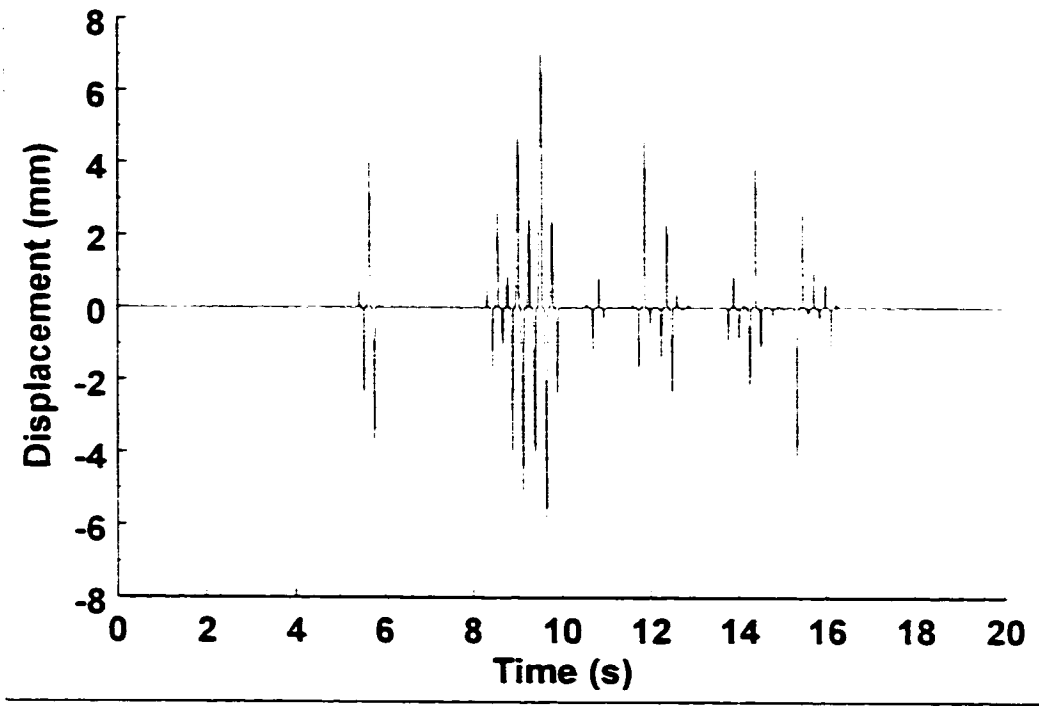

Figure 3.11 Shear wall response during La Malbaie scaled to 0.8g.

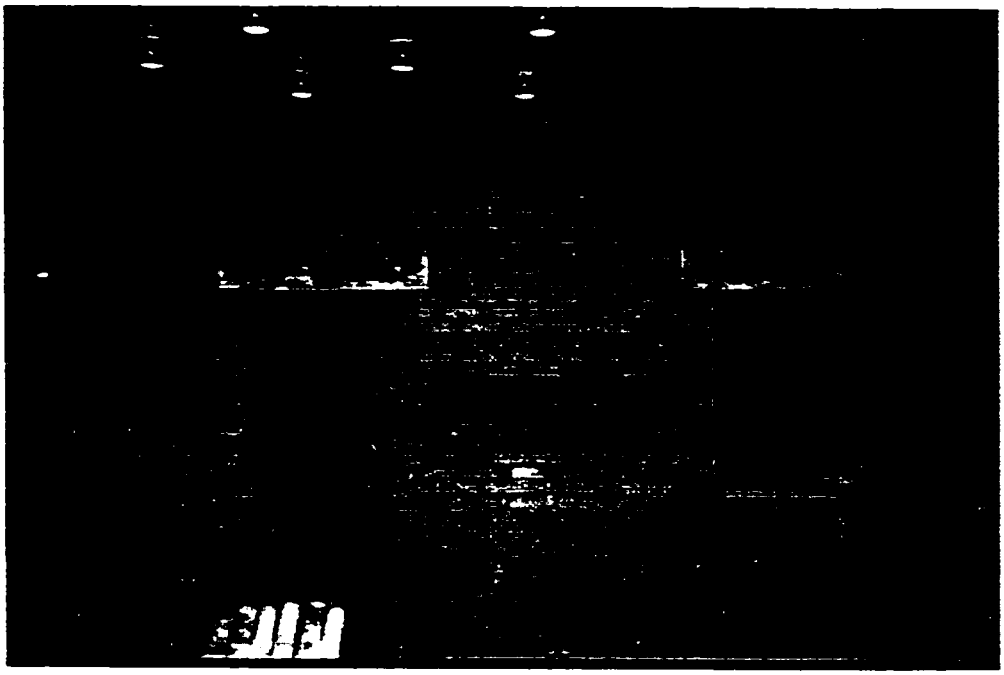

Figure 3.12 URM specimen.

Figure 3.13 Reinforced concrete foundation.

Figure 3.14 Header course.

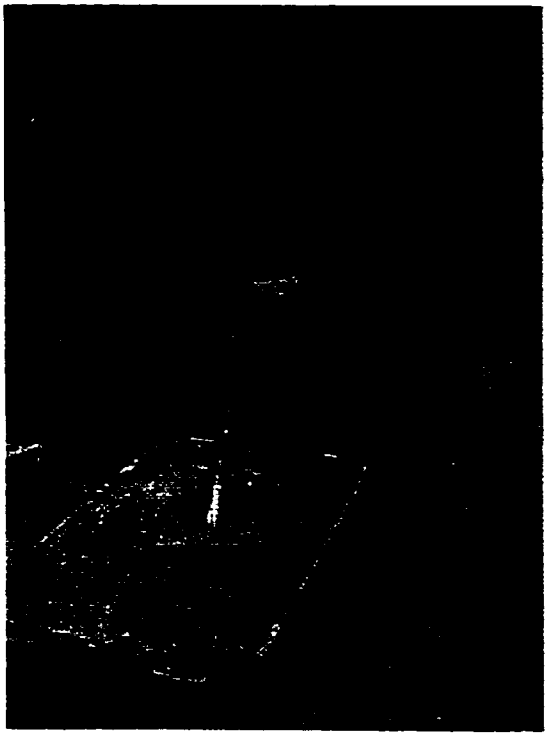

Figure 3.15 Mortar mixed manually.

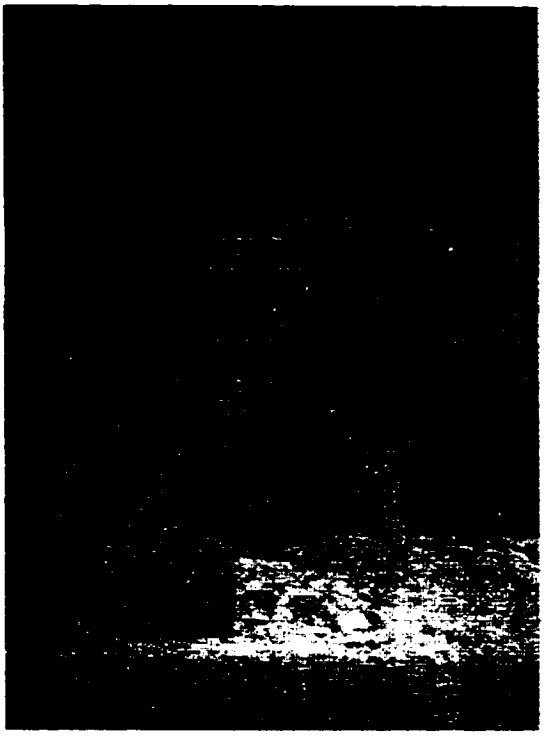

Figure 3.16 Discontinuous corner for West shear wall, 10 mm gap

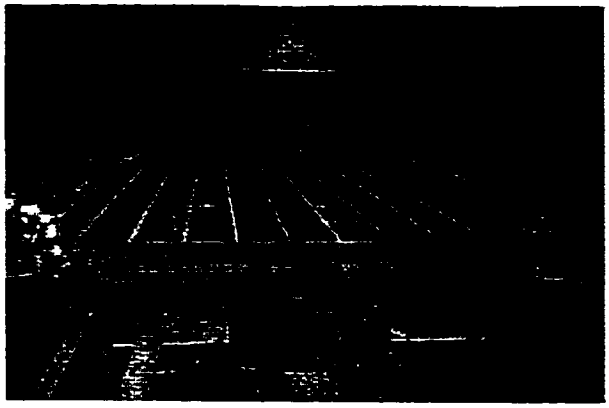

Figure 3.17 Floor joists.

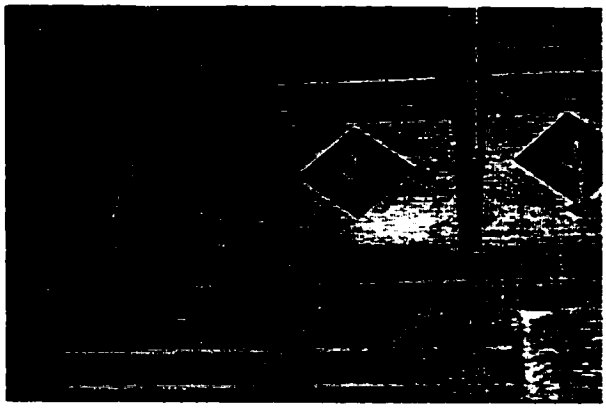

Figure 3.18 Bearing plate.

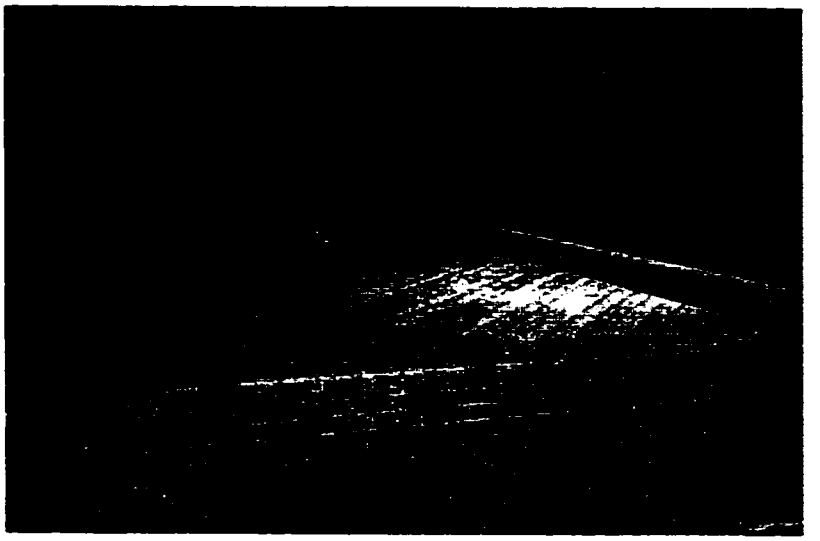

Figure 3.19 Wood floor diaphragm during construction.

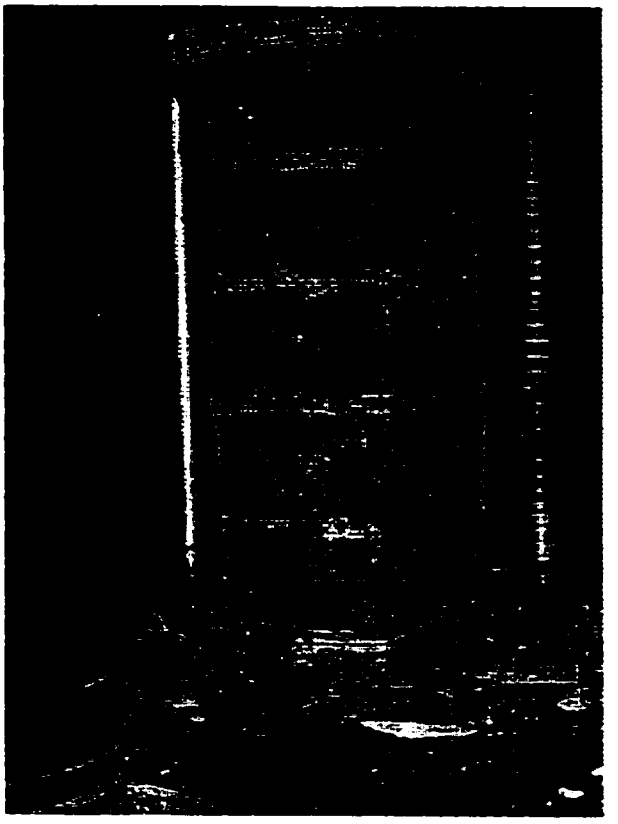

Figure 3.20 Compression test of a masonry brick prism.

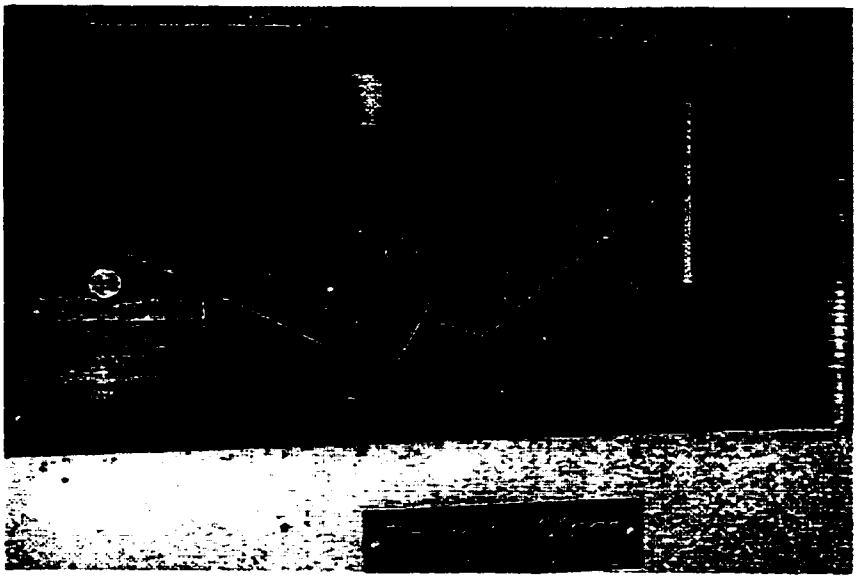

Figure 3.21 Three-point bending mortar tension-test.

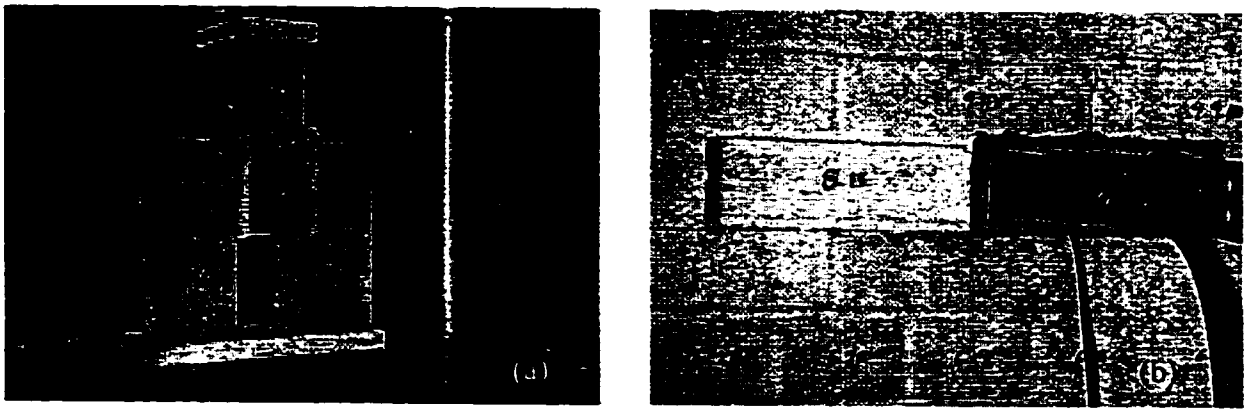

Figure 3.22 Shear test: (a) triplet test, and; (b) push test.

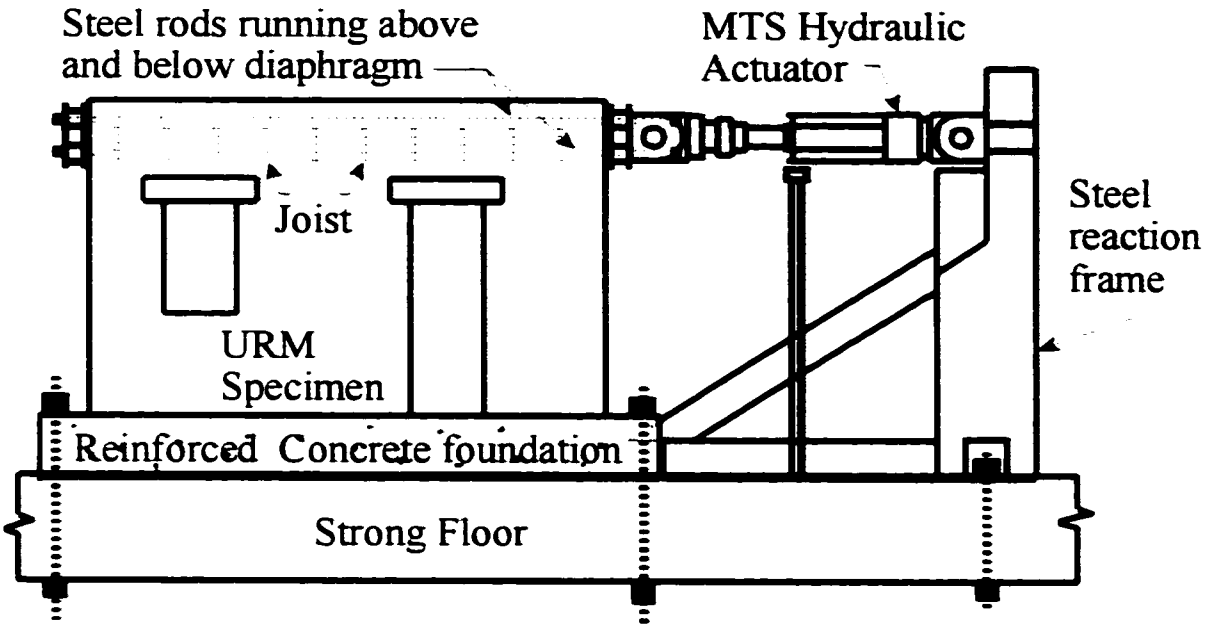

Figure 3.23 Test setup.

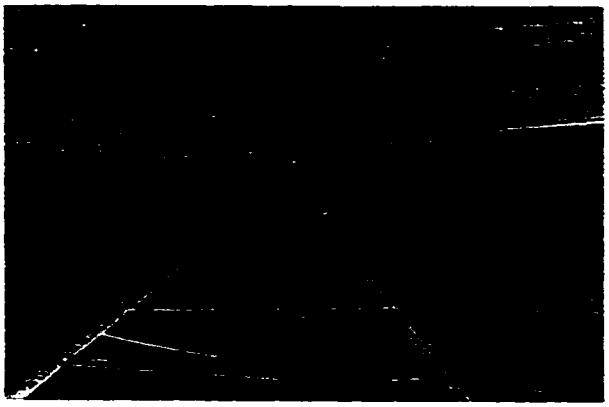

Figure 3.24 Steel rods running through the joists, and temposonic setup at midspan.

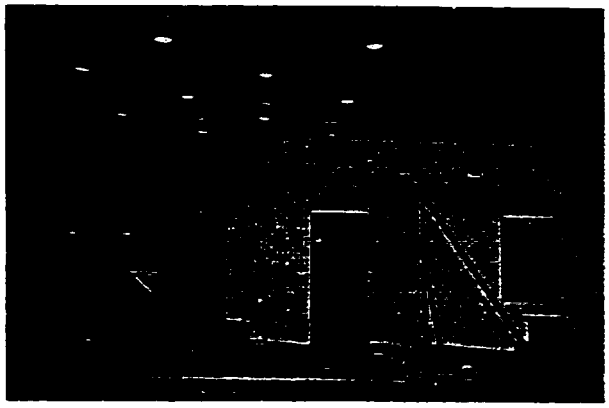

Figure 3.25 Test setup.

Figure 3.26 Masonry repointing.

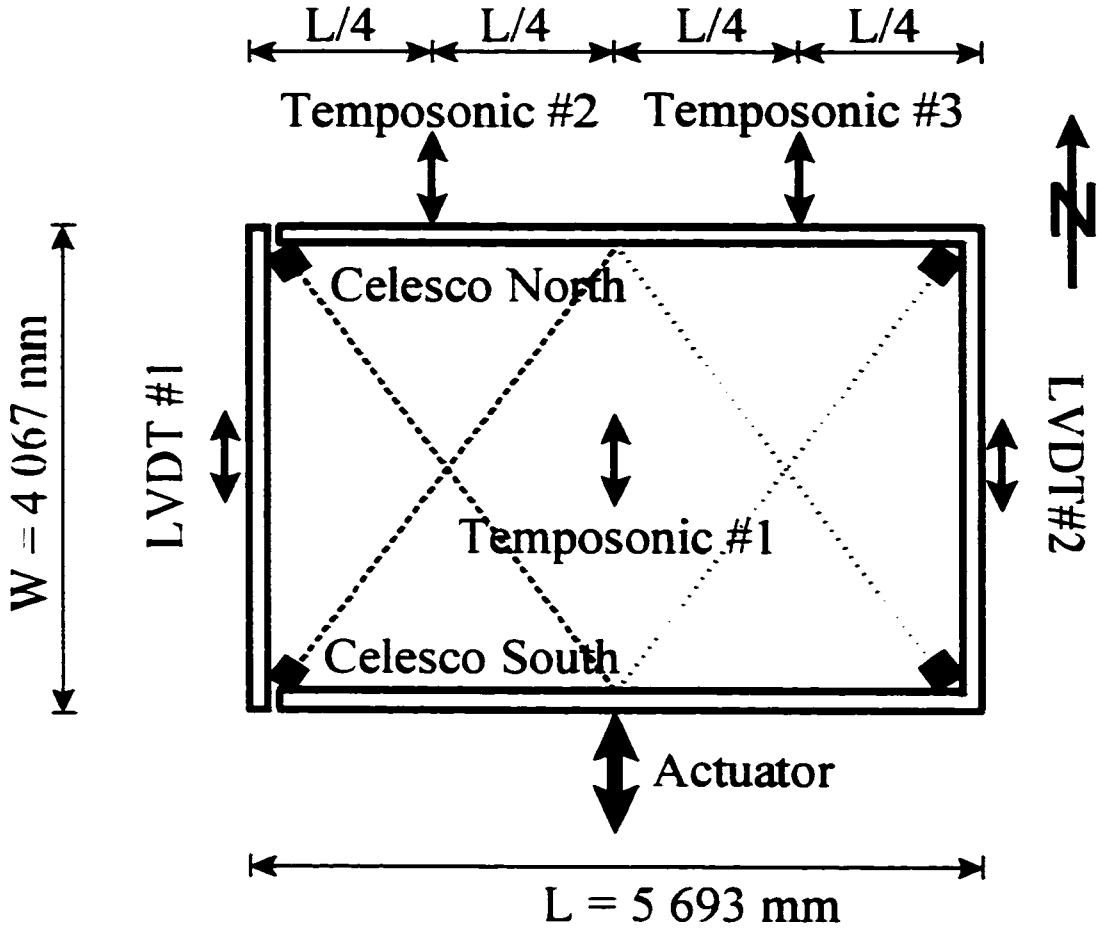

Figure 3.27 Top view and location of temposonics, LVDTs, and Celescos.

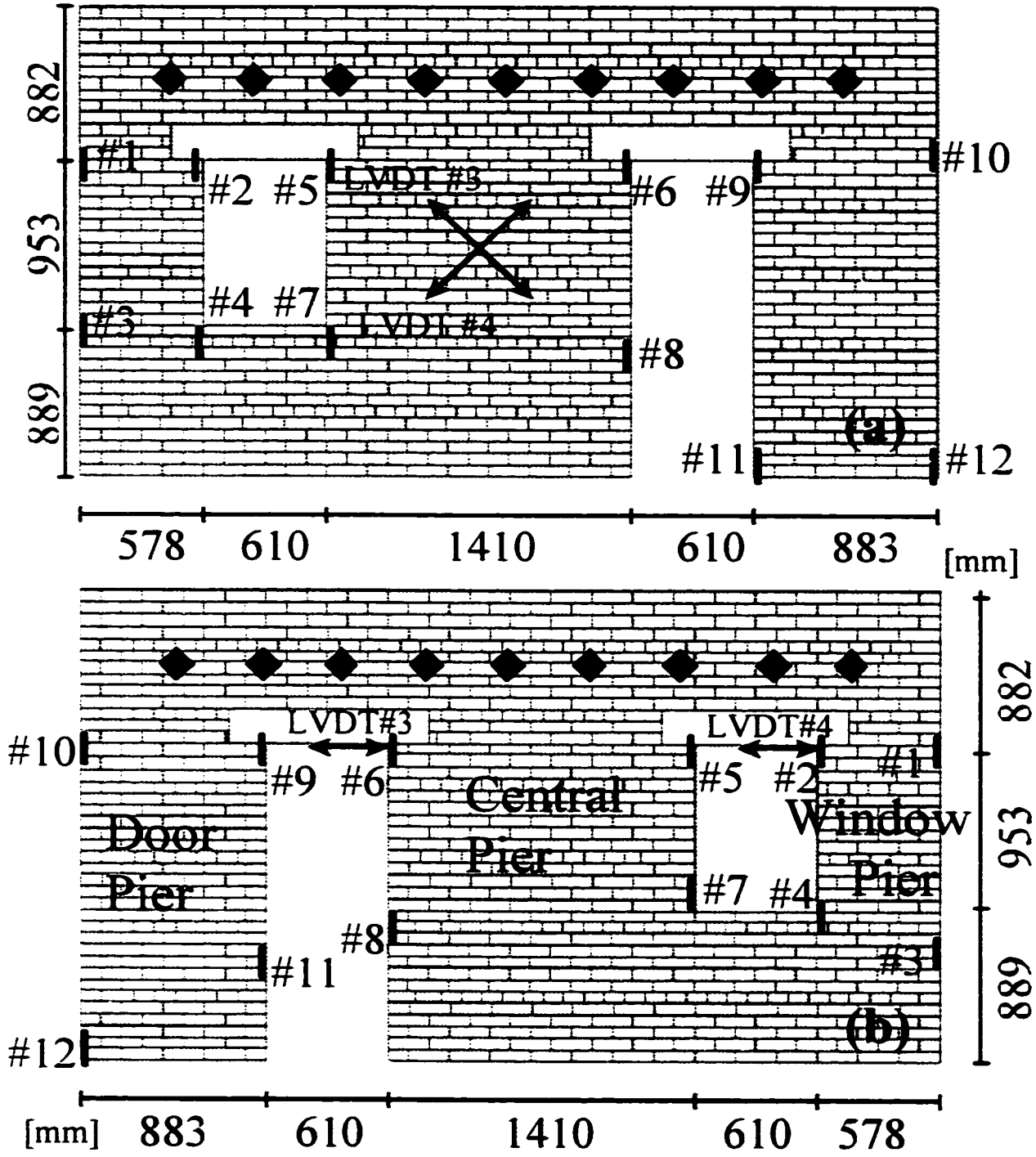

Figure 3.28 Location of LVDTs and clip gages: (a) West wall elevation; (b) East wall elevation.

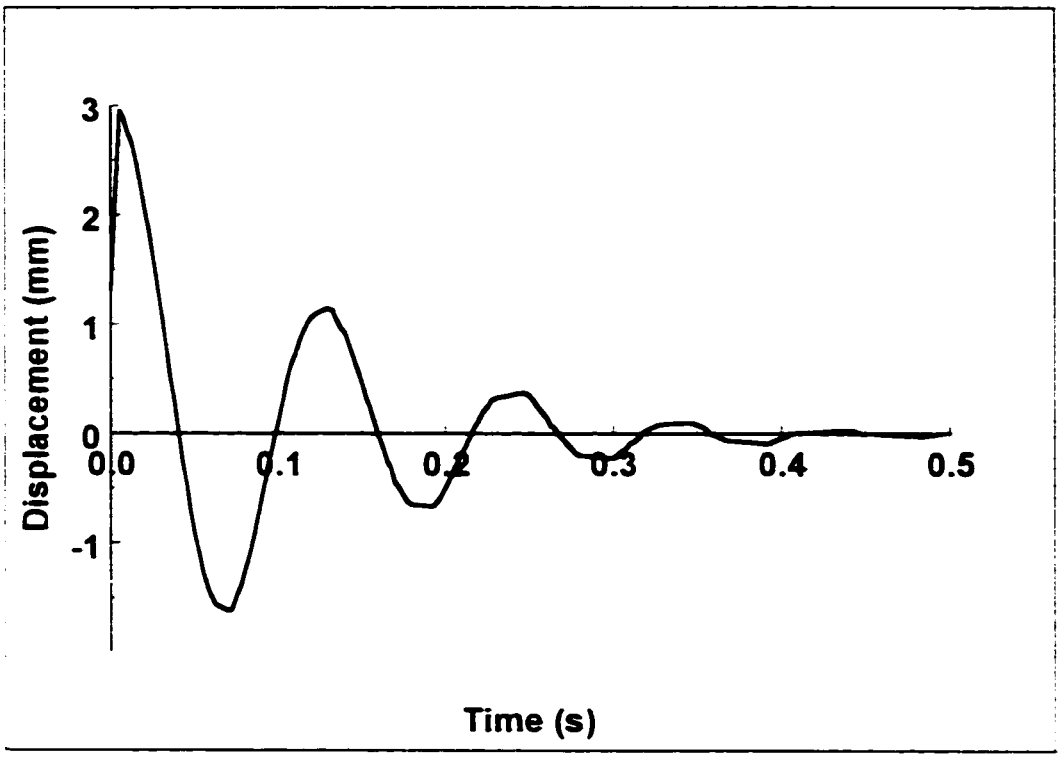

Figure 3.29 Simulation of a free vibration response of URM specimen using pseudo-dynamic testing.

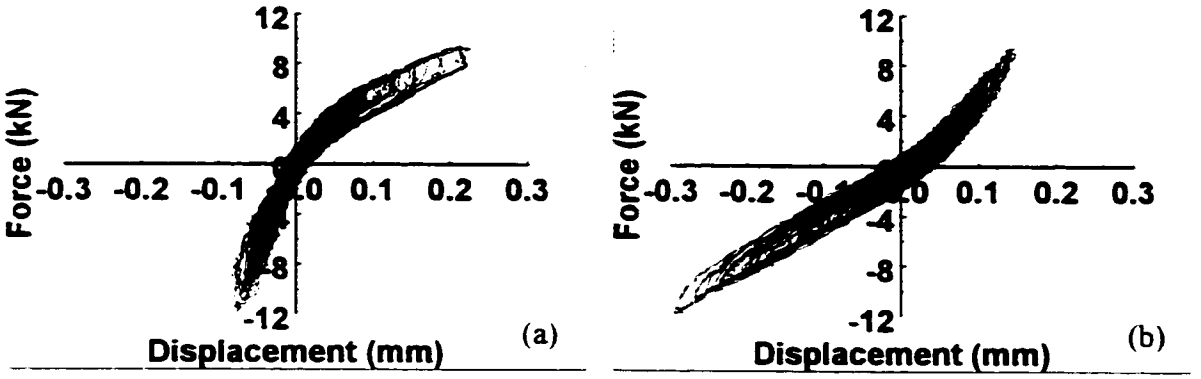

Figure 3.30 Hysteretic response during La Malbaie x 0.5 of: (a) West wall; (b) East wall.

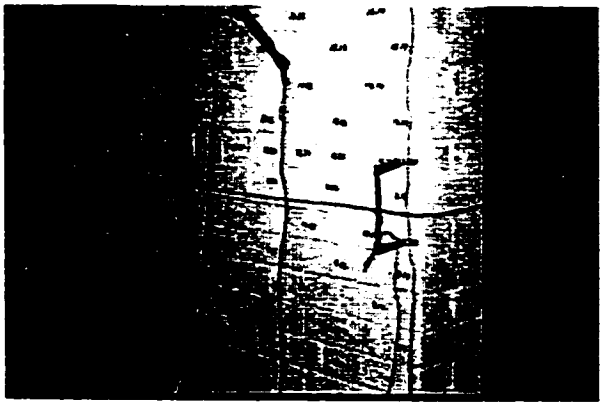

Figure 3.31 Pier rocking behavior.

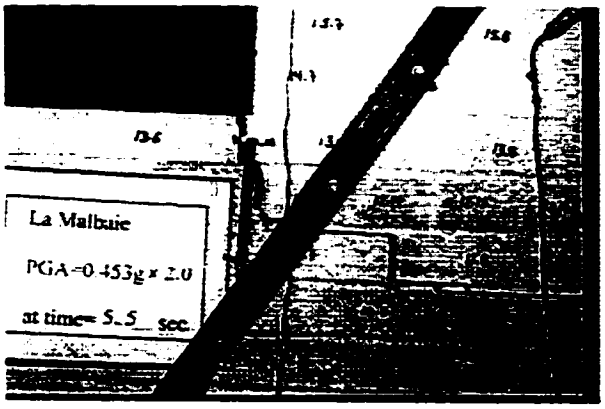

Figure 3.32(a) Pier sliding behavior.

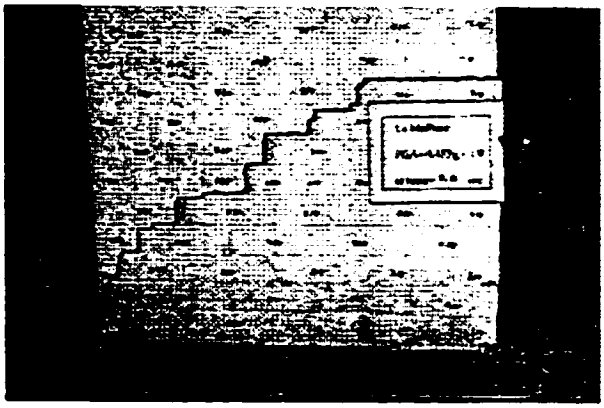

Figure 3.32(b) Pier rocking behavior

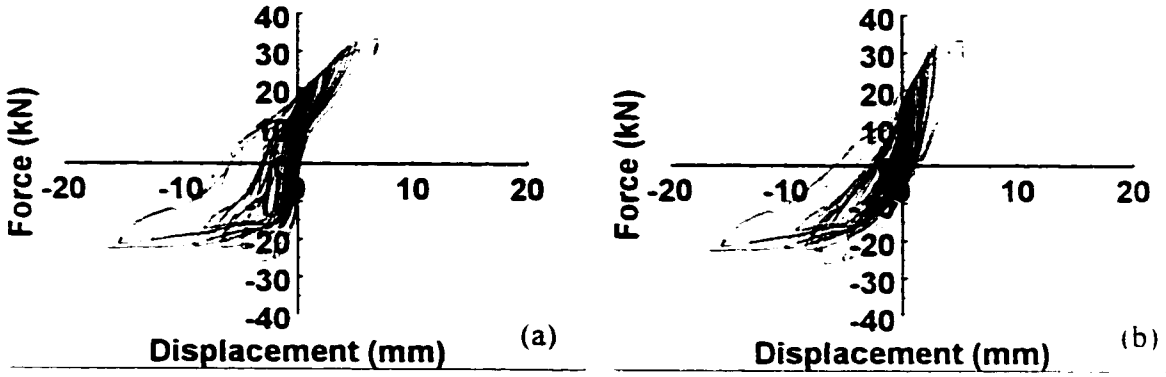

Figure 3.33 Hysteretic response during La Malbaie x 2.0 of: (a) West wall; (b) East wall.

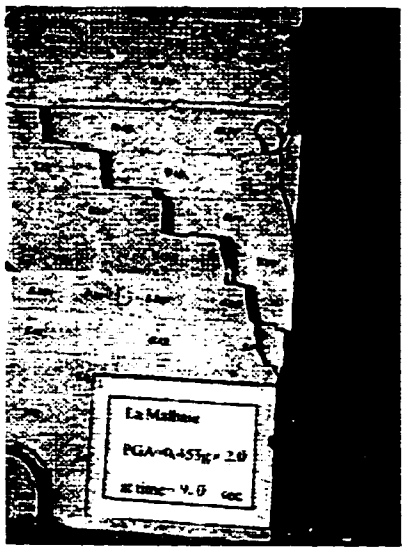

Figure 3.34 Triangular piece of bricks.

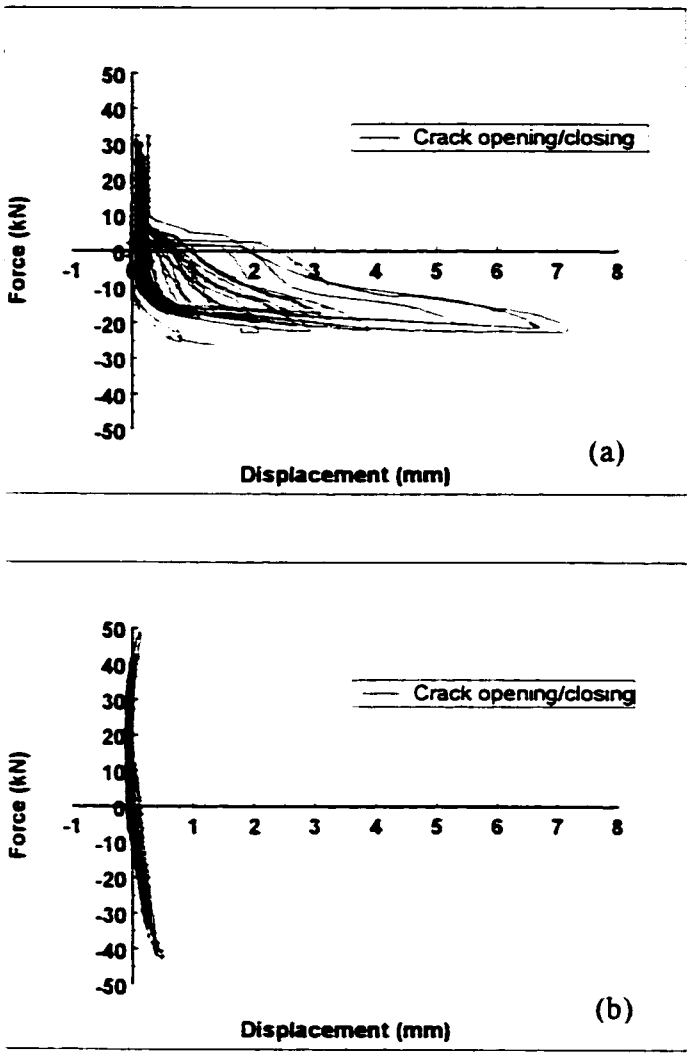

Figure 3.35 Door pier rocking response at the base: (a) before; and (b) after Tyfo repair for La Malbaie x 2.0.

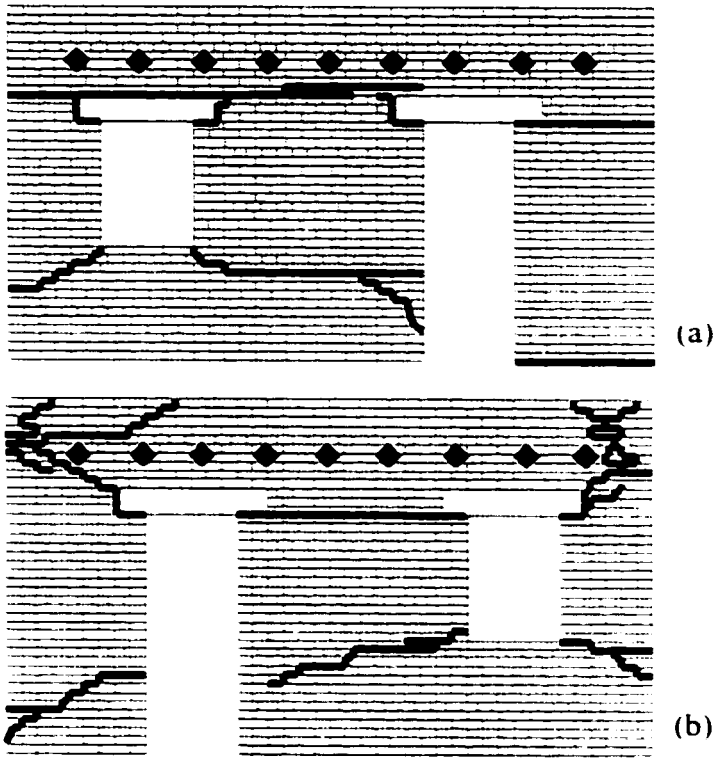

Figure 3.36 Crack pattern after La Malbaie x 2.0: (a) West wall, (b) East wall

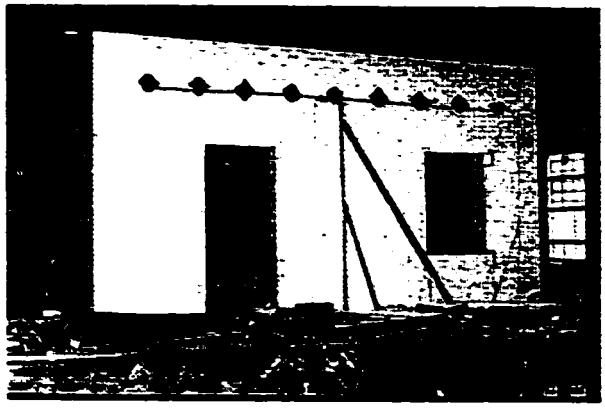

Figure 3.37 URM specimen after first series of tests.

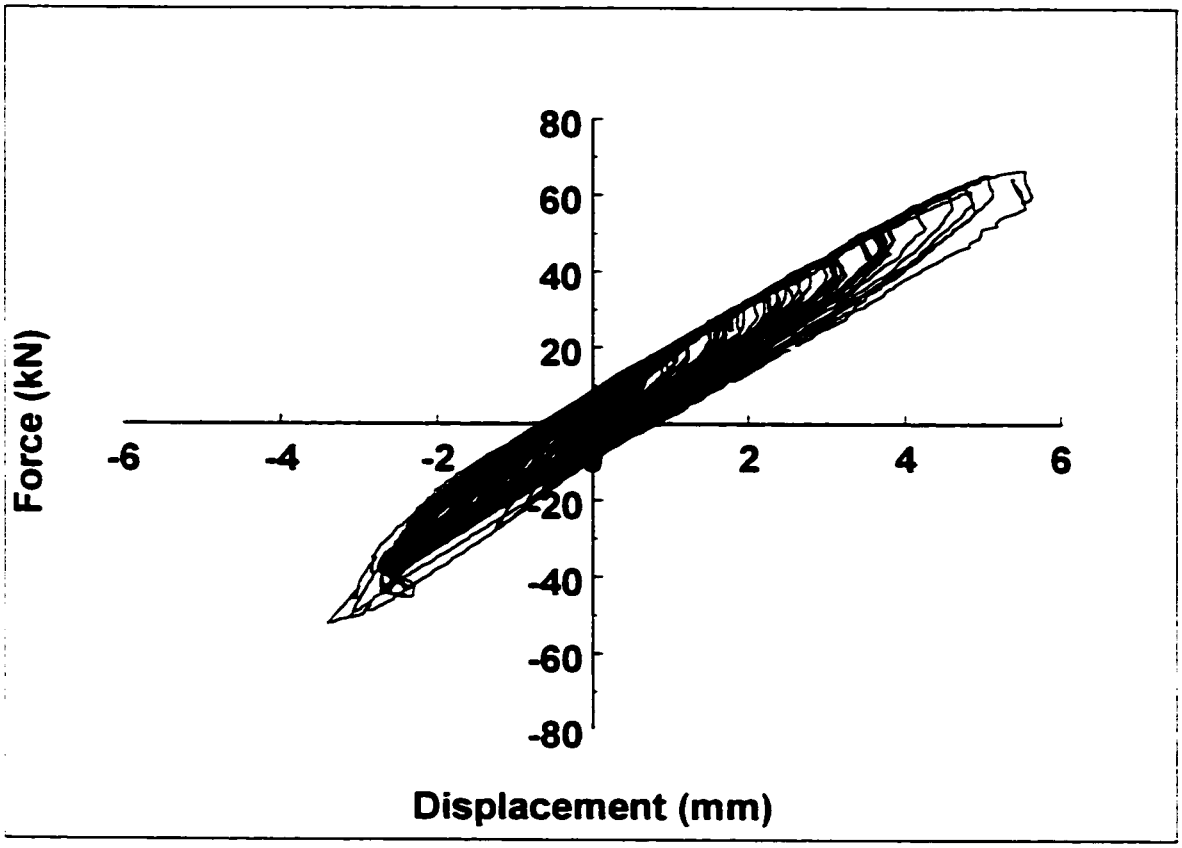

Figure 3.38 Hysteretic response of wood diaphragm at center-span during La Malbaie x 2.0.

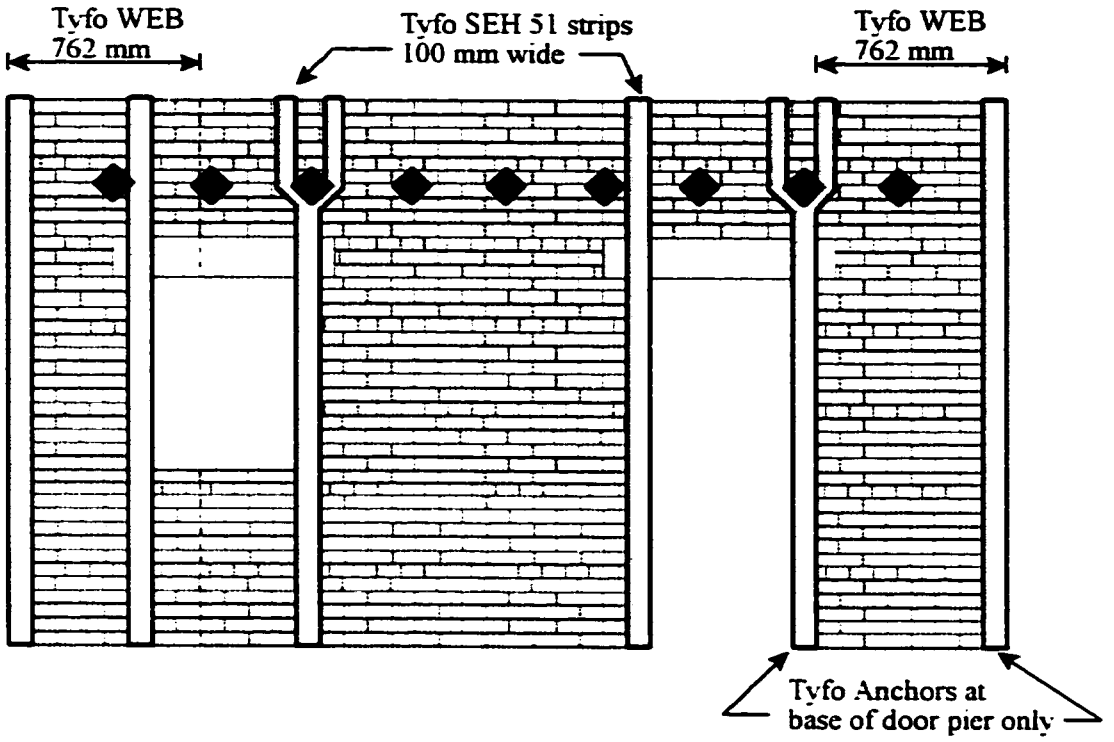

Figure 3.39 West wall elevation of URM specimen repaired with Tyfo SEH 51 and WEB. (the east wall is simply a mirror image).

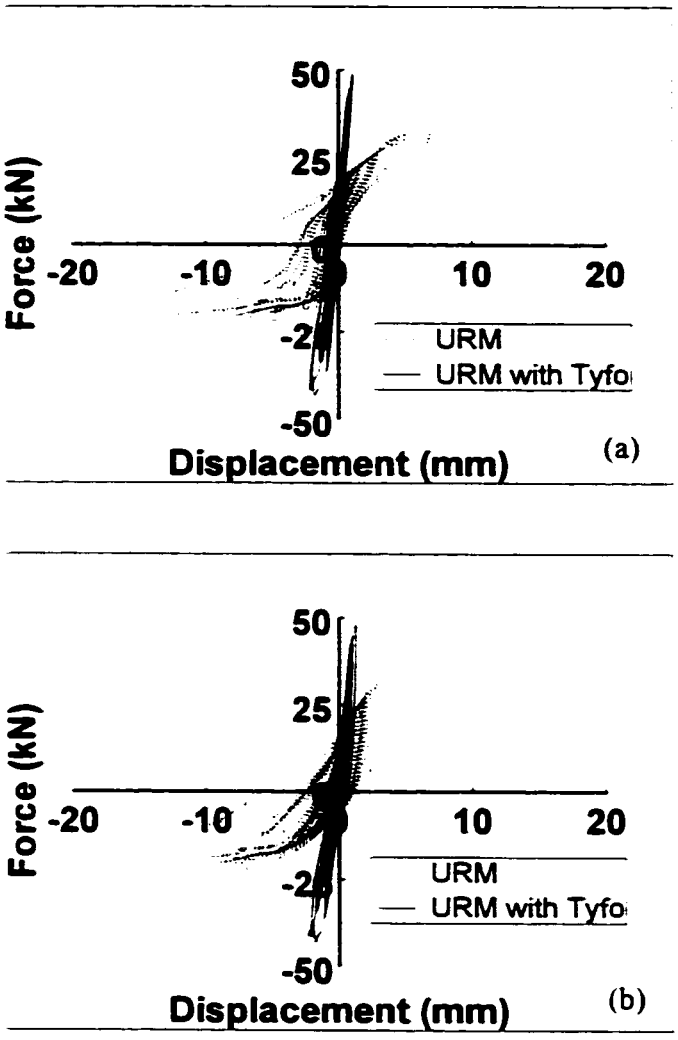

Figure 3.40 Hysteretic response of URM during La Malbaie x 2.0 before and after Tyfo repair: (a) West wall; (b) East wall.

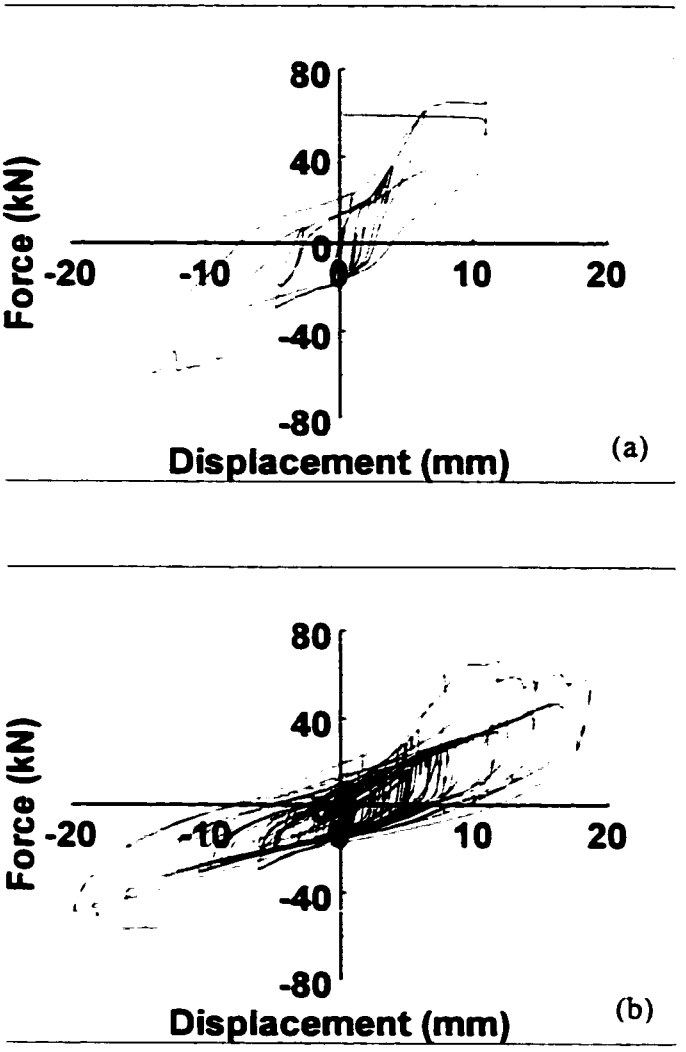

Figure 3.41 Hysteretic response of wall repaired with Tyfo during La Malbaie x 4.0: (a) West wall; (b) East wall.

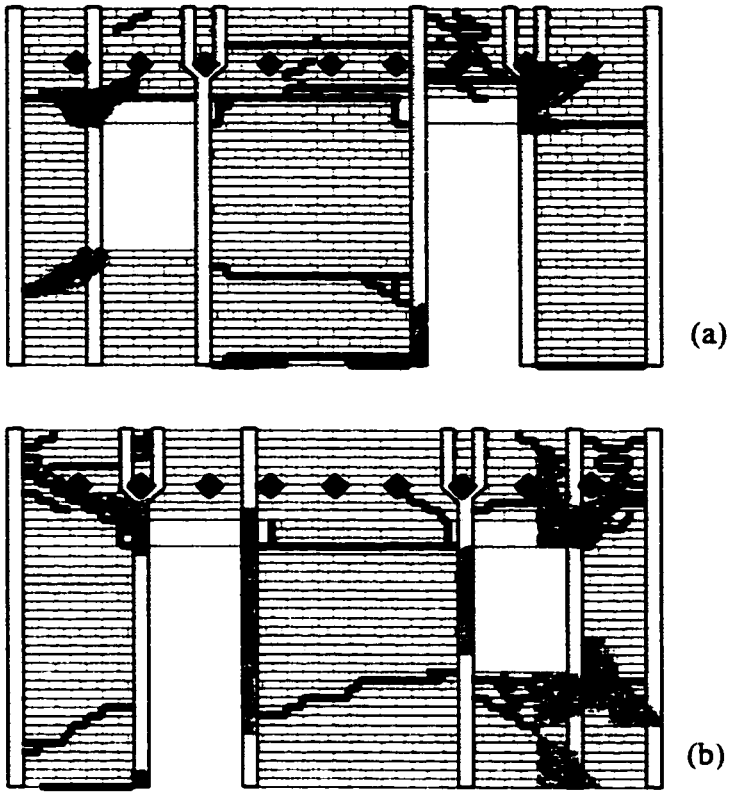

Figure 3.42 Crack pattern on repaired shear wall after La Malbaie x 4.0: (a) West wall; (b) East wall. (Shaded area indicates Tyfo material de-bonded).

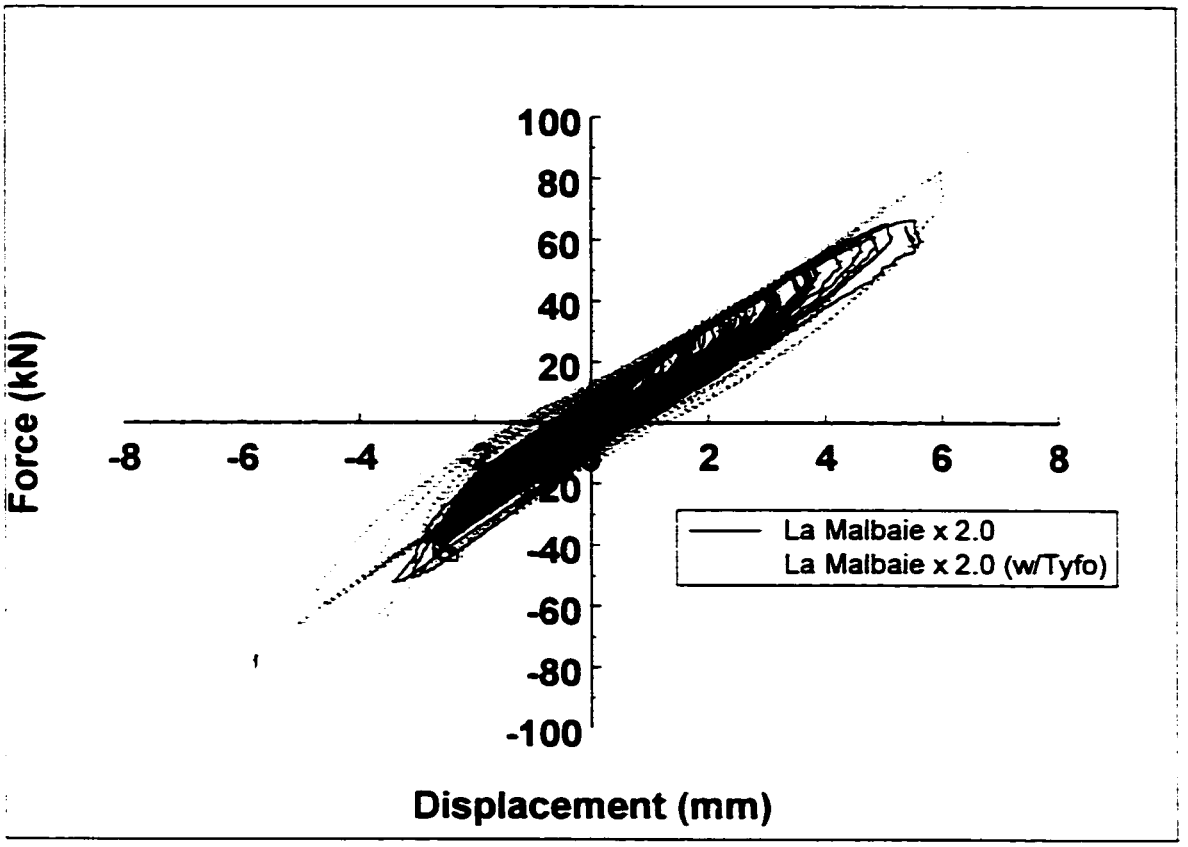

Figure 3.43 Comparison of hysteretic response of wood diaphragm with shear walls as-is and repaired with Tyfo, during La Malbaie x 2.0.

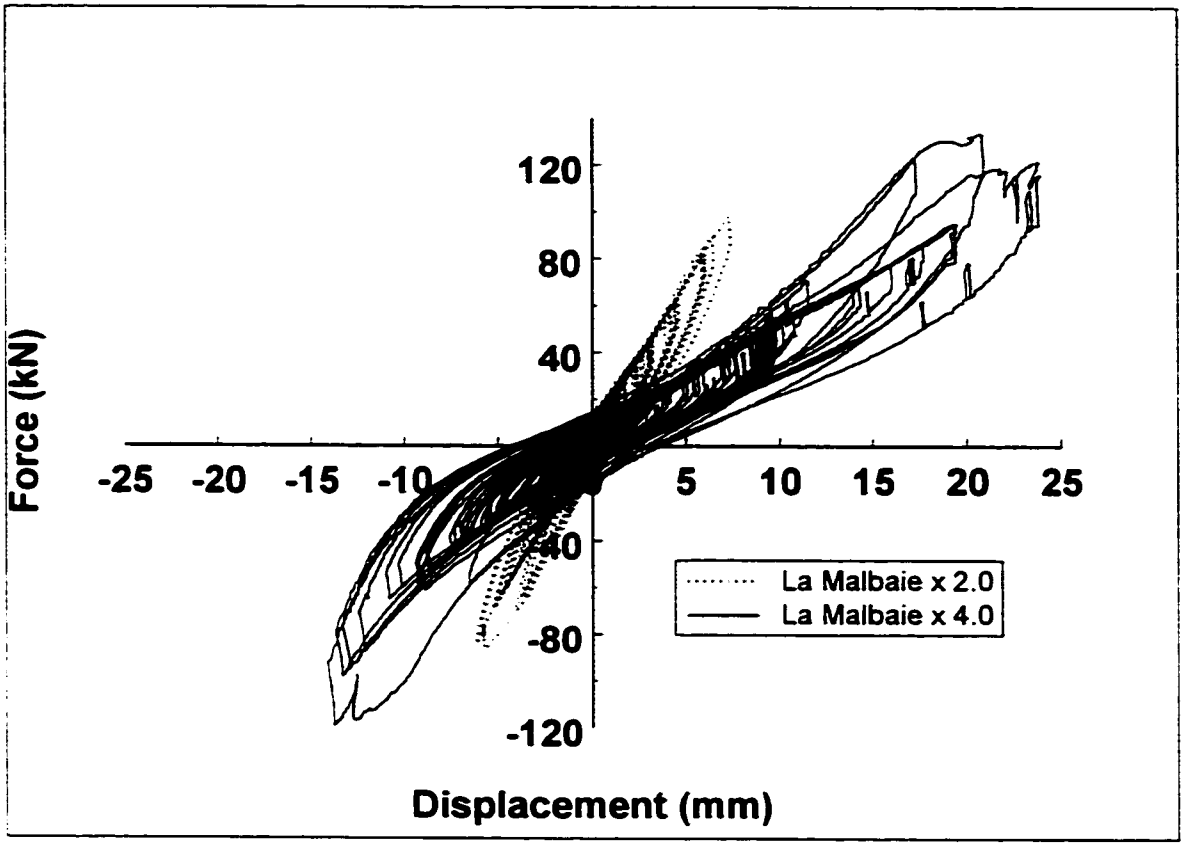

Figure 3.44 Comparison of diaphragm center-span hysteretic response with shear wall repaired with Tyfo material during La Malbaie x 2.0 and x 4.0.

Figure 3.45 URM specimen during cyclic testing.

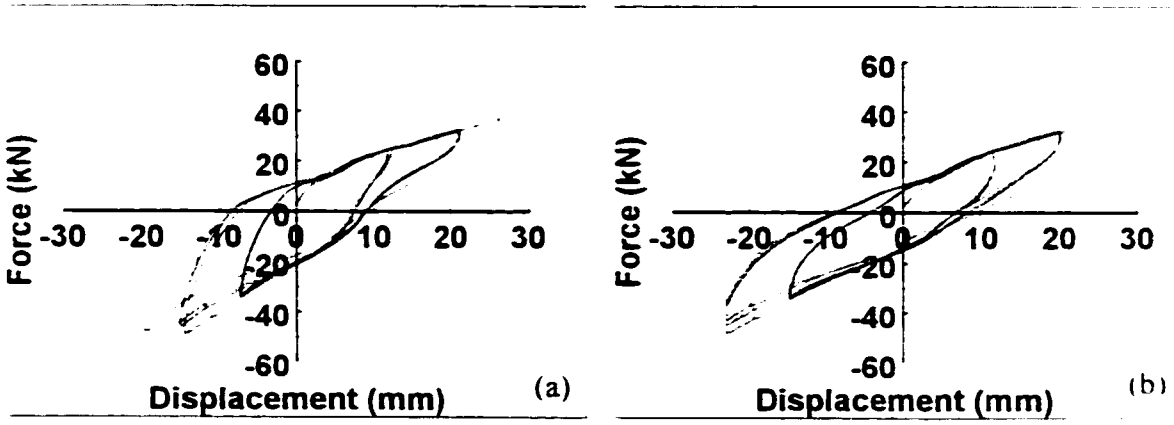

Figure 3.46 Hysteretic response during cyclic test: (a) West wall; (b) East wall

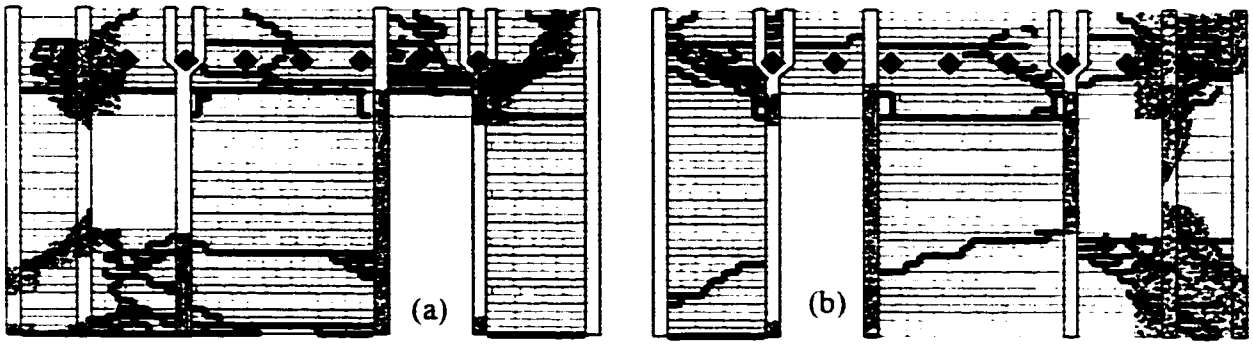

Figure 3.47 Crack pattern on shear wall repaired with Tyfo after cyclic test: (a) West wall; (b) East wall. (Shaded area indicates Tyfo material de-bonded).

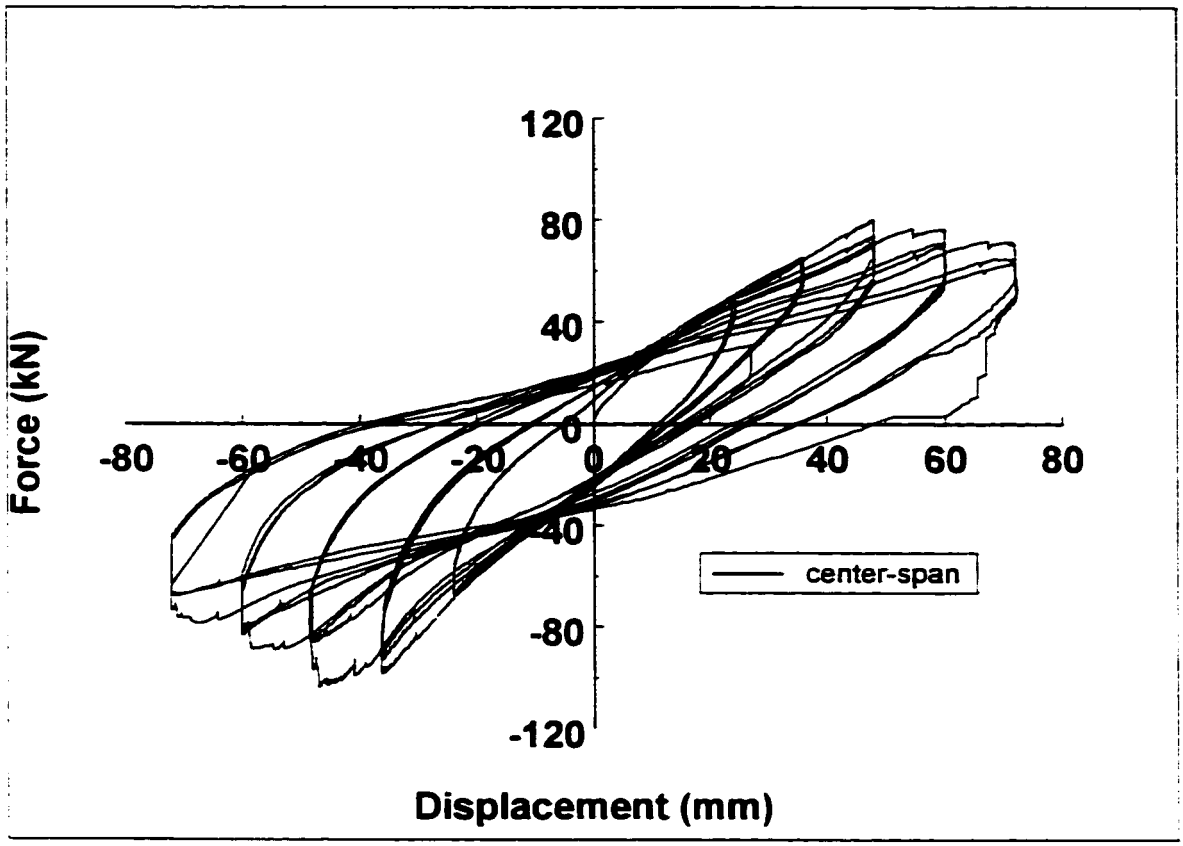

Figure 3.48 Hysteretic center-span displacement response of wood diaphragm during cyclic tests.

Figure 3.49 Popped out nails at ends of diaphragm.

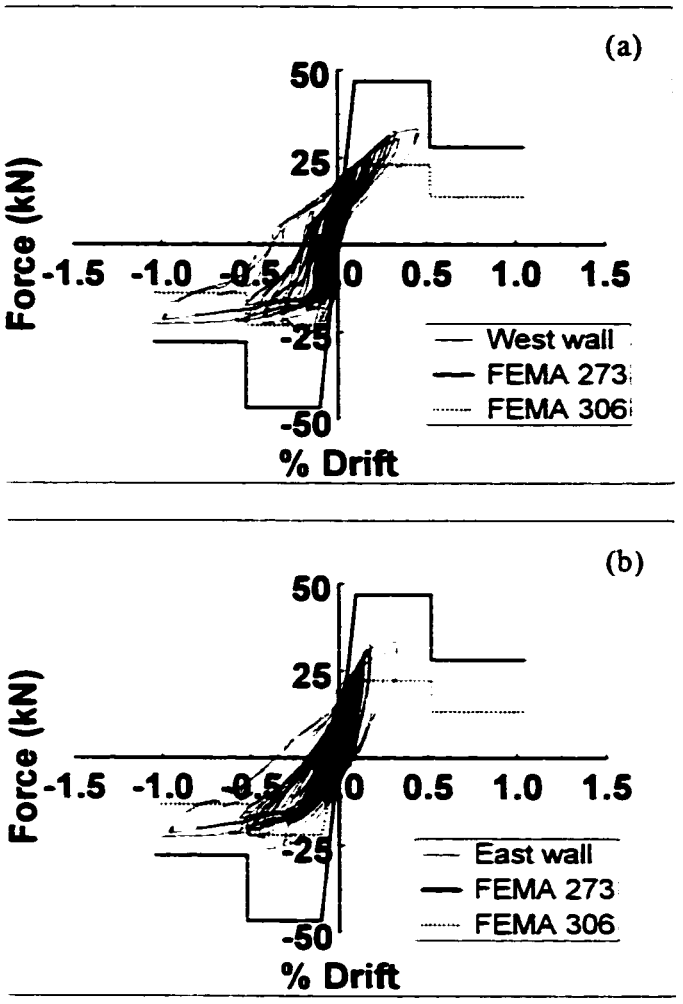

Figure 4.1 Comparison with idealized force-deflection model using expected capacities from FEMA 273 and FEMA 306 during La Malbaie x 2.0, for: (a) West wall; (b) East wall.

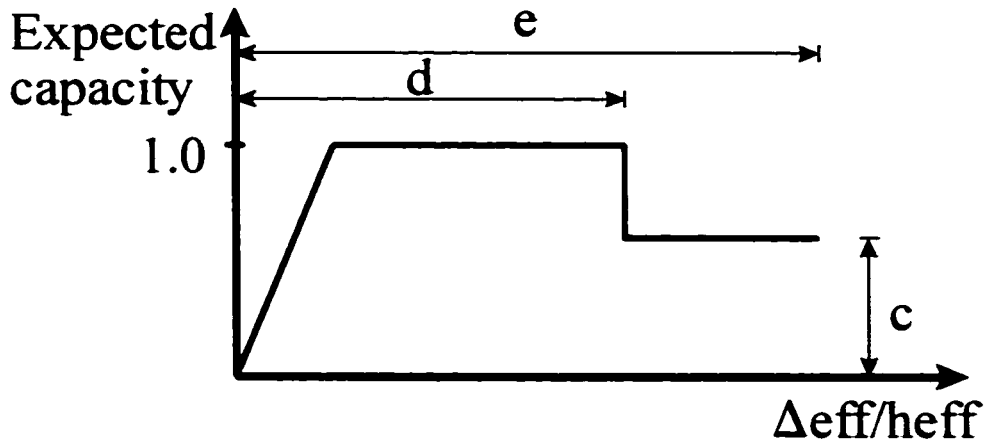

Figure 4.2 FEMA 273 idealized normalized force-deflection relation.
where c = fraction of strength loss for secondary element,
d = inelastic drift percentage deformation capacity for primary element,
e = inelastic drift percentage deformation capacity for secondary element.

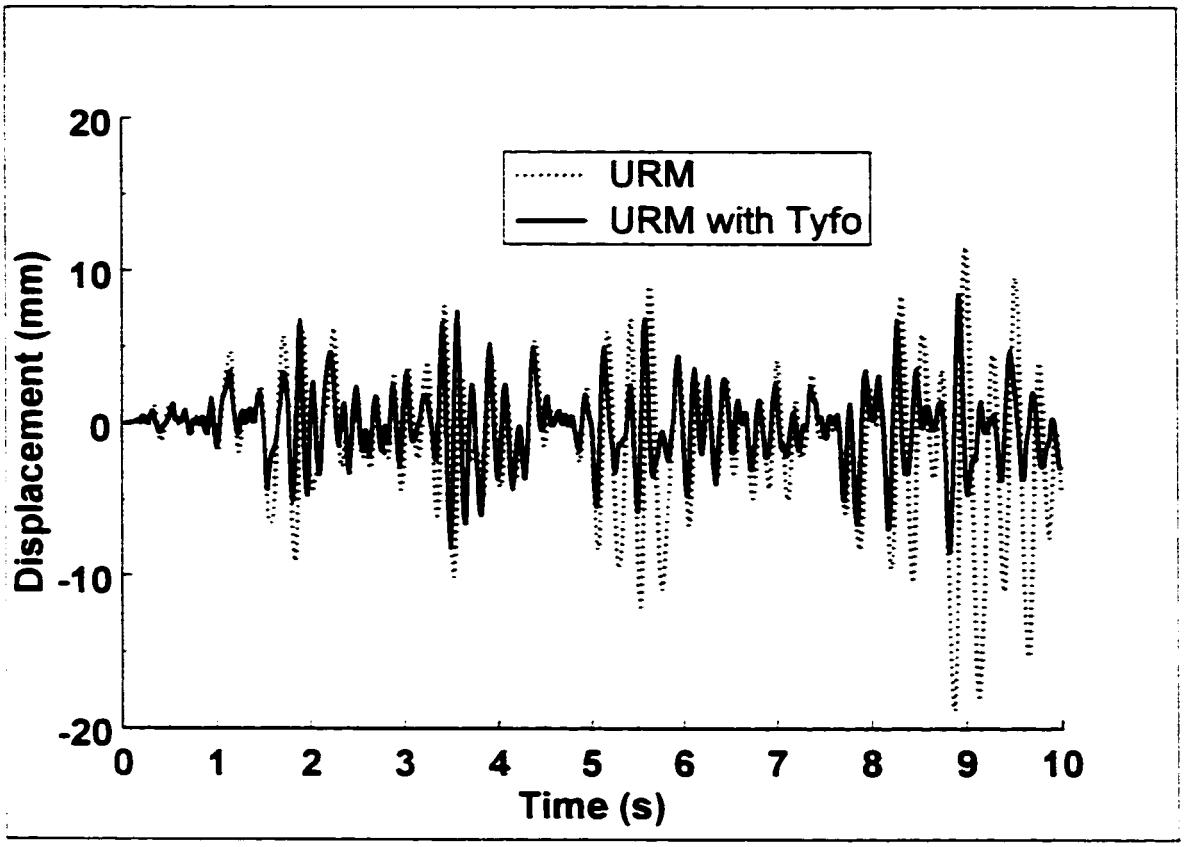

Figure 4.3 Comparison of diaphragm center-span response before and after Tyfo repair for La Malbaie x 2.0.

Figure 4.4 Pier rocking at base of central pier with Tyfo repair during La Malbaie x 4.0.

Figure 4.5 Tyfo strip failed in shear.

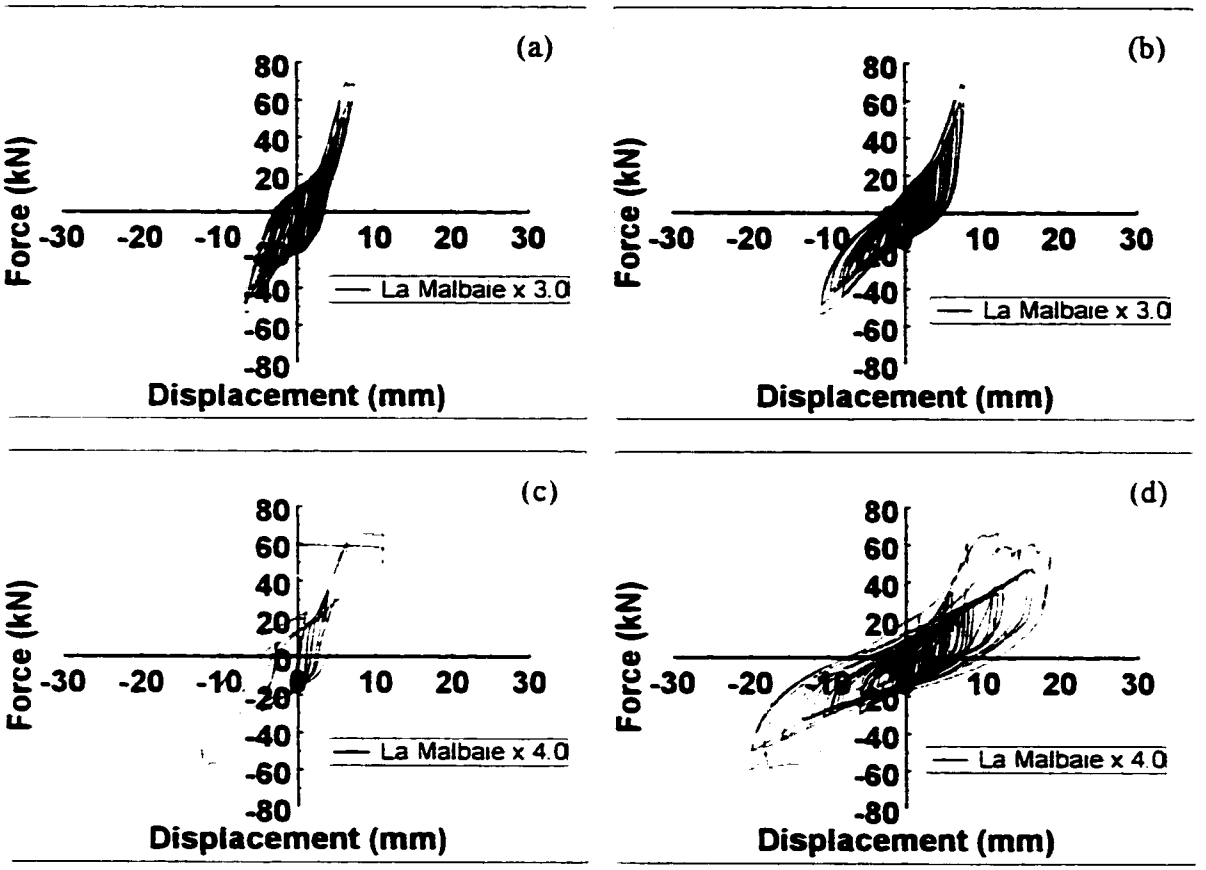

Figure 4.6 Hysteretic response of URM with Tyfo during: La Malbaie x 3.0: (a) West wall, (b) East wall; and La Malbaie x 4.0: (c) West wall, (d) East wall.

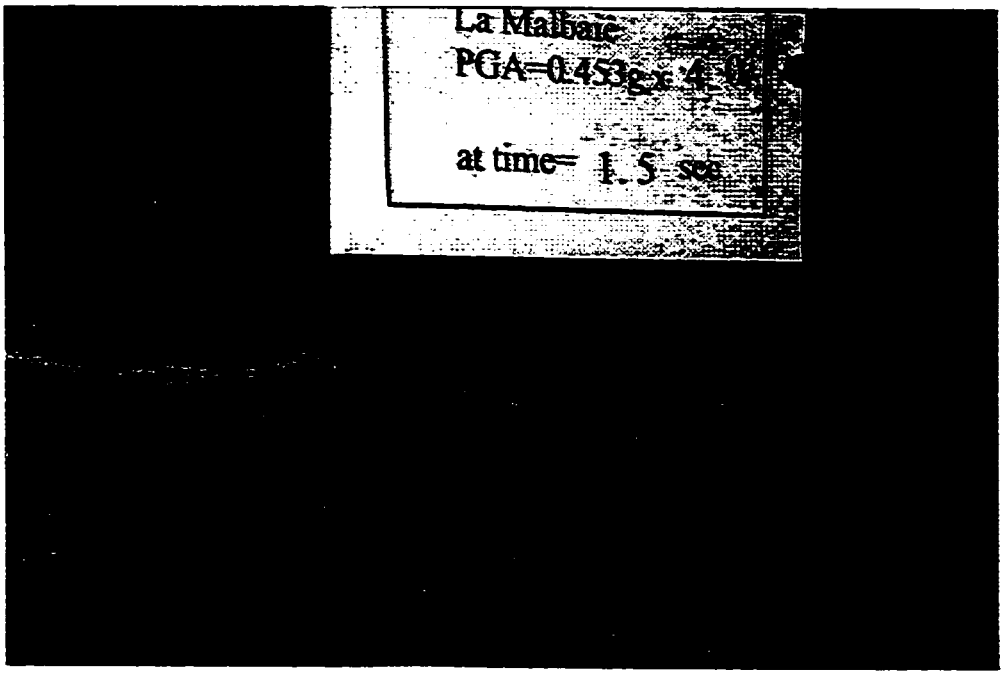

Figure 4.7 Tears in Tyfo WEB due to out-of-plane tensile cracks.

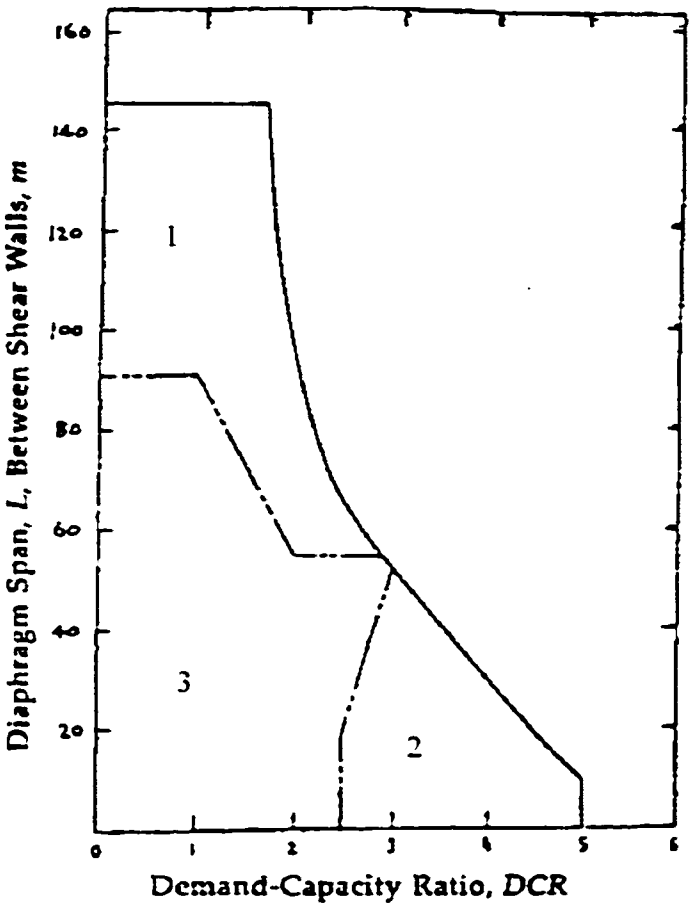

Figure 4.8 Figure of acceptable diaphragm span versus demand-capacity ratio (DCR) (CGSEEB 1992).

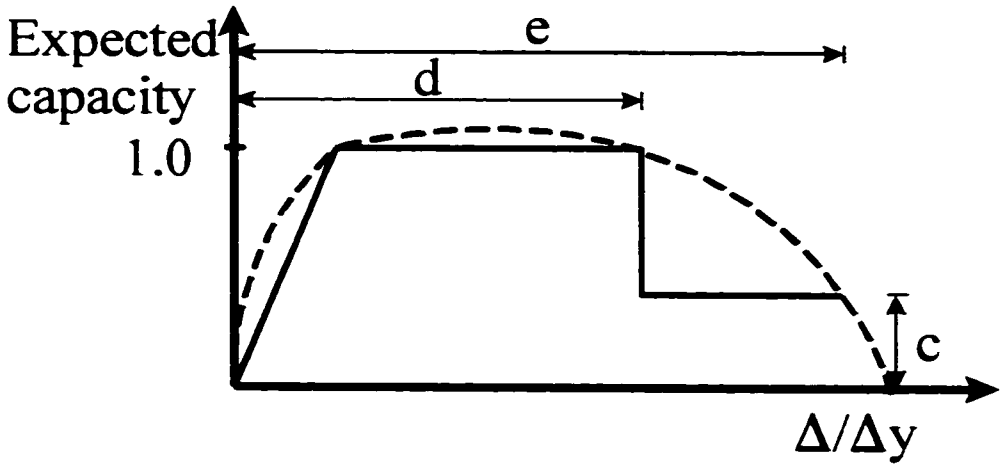

Figure 4.9 FEMA 273 normalized force-deformation curve for wood diaphragm.
where c = reduced strength parameter,
d = maximum possible deflection at yield strength,
e = maximum deflection at a reduced strength.

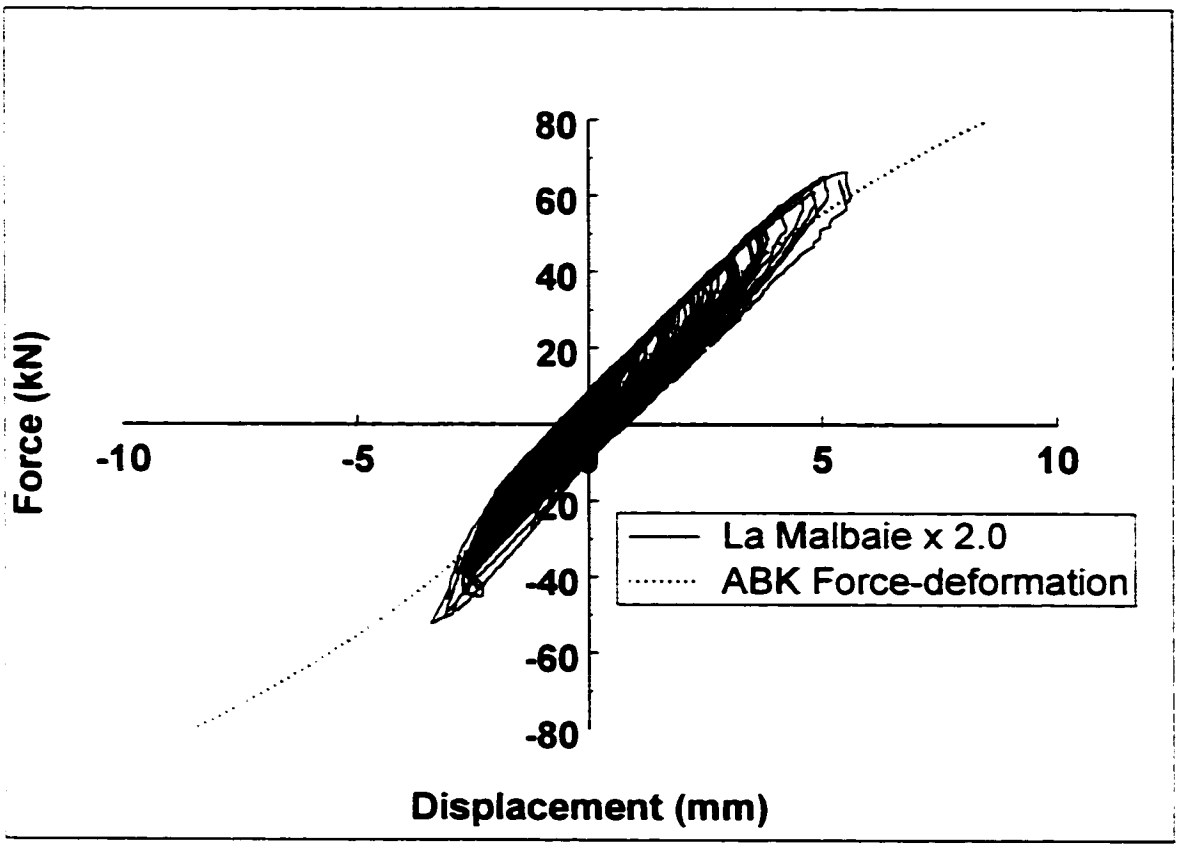

Figure 4.10 Comparison of hysteretic response of wood diaphragm during La Malbaie x 2.0 and ABK force-deformation envelope.

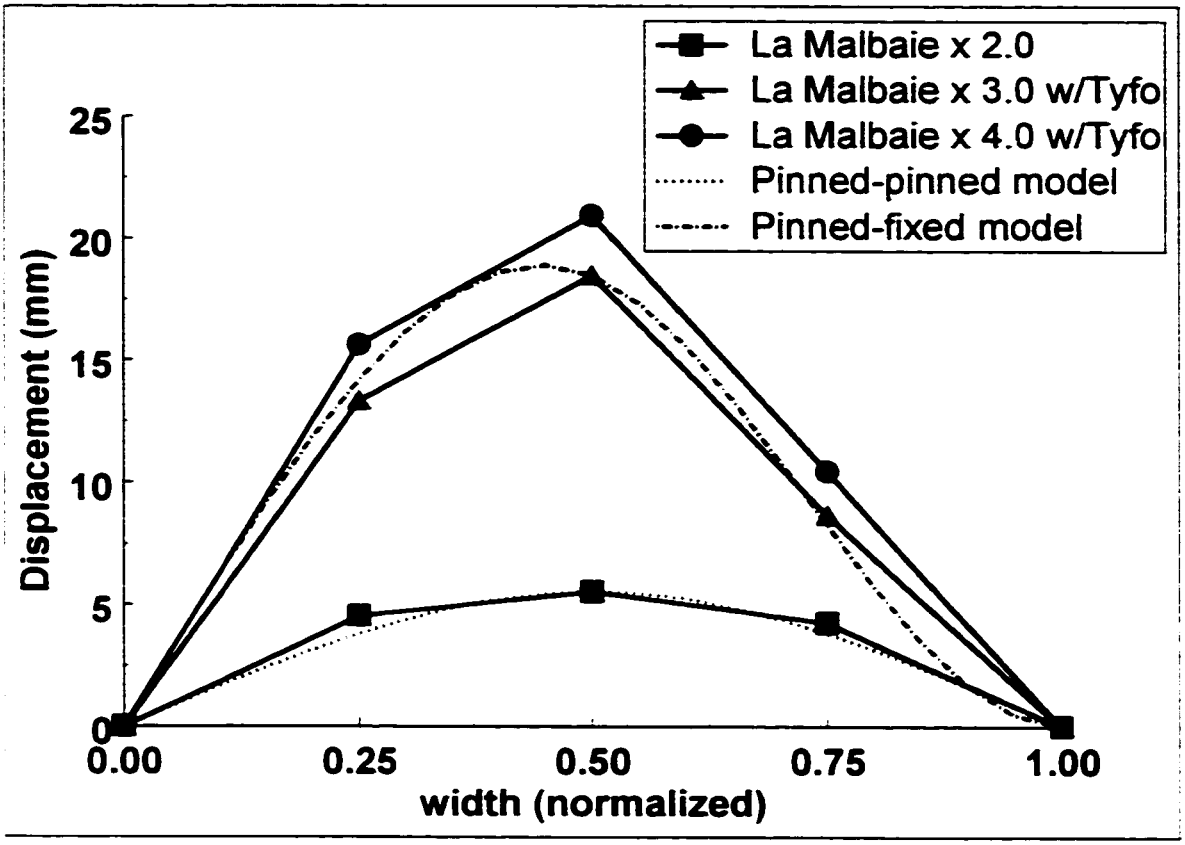

Figure 4.11 Deflected shape of wood diaphragm during La Malbaie x 2.0, 3.0, 4.0, and matching pinned-pinned, pinned-fixed beam models.

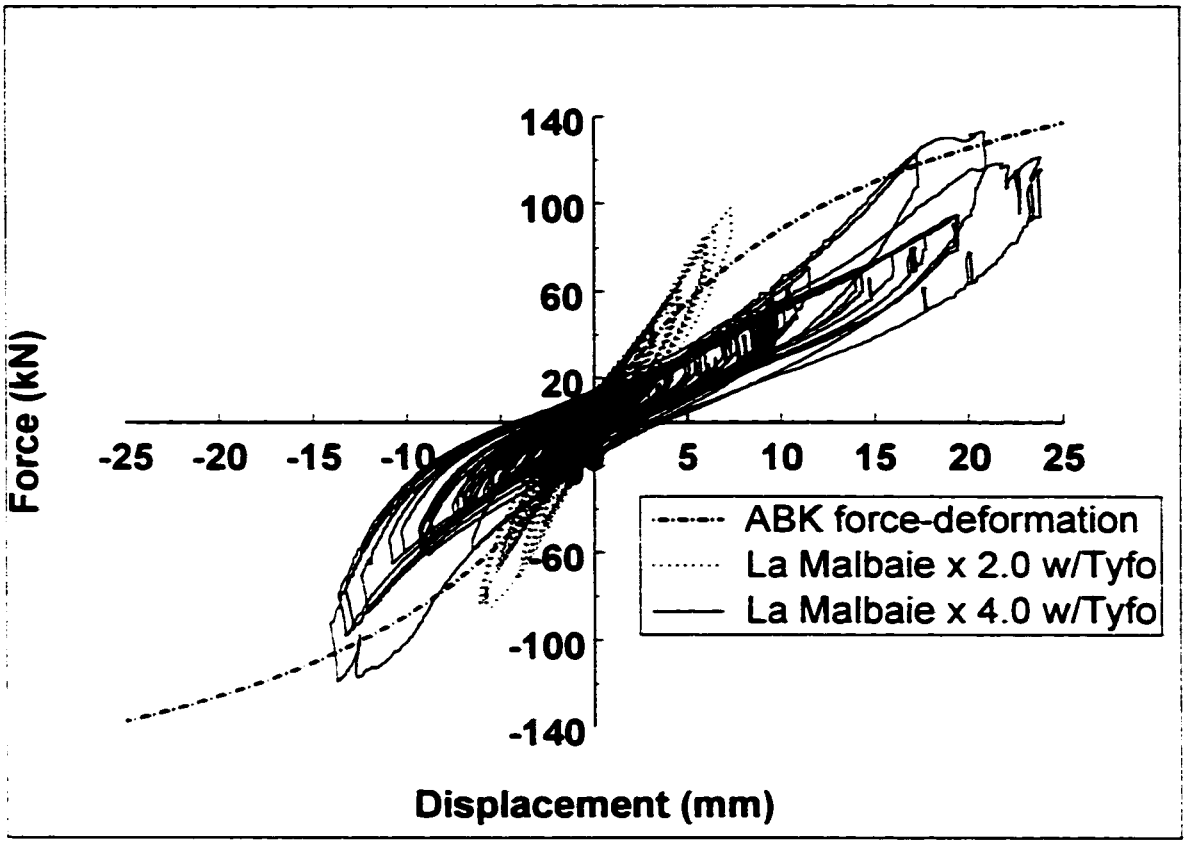

Figure 4.12 Hysteretic response of wood diaphragm with shear walls repaired with Tyfo for La Malbaie x 2.0, 4.0, and ABK force-deformation envelope.

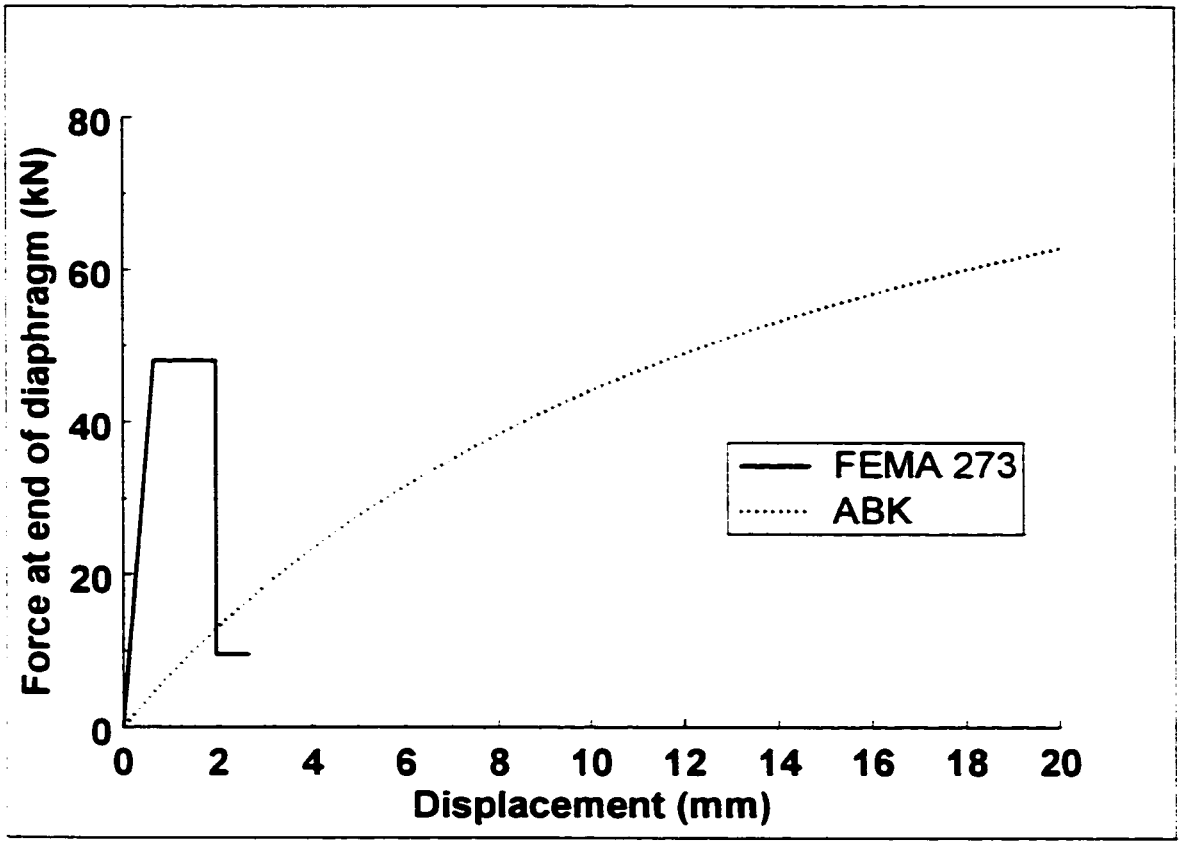

Figure 4.13 Force-deformation curves from FEMA 273 and ABK for a 3.66 m x 5.28 m wood diaphragm with straight sheathing over diagonal sheathing.

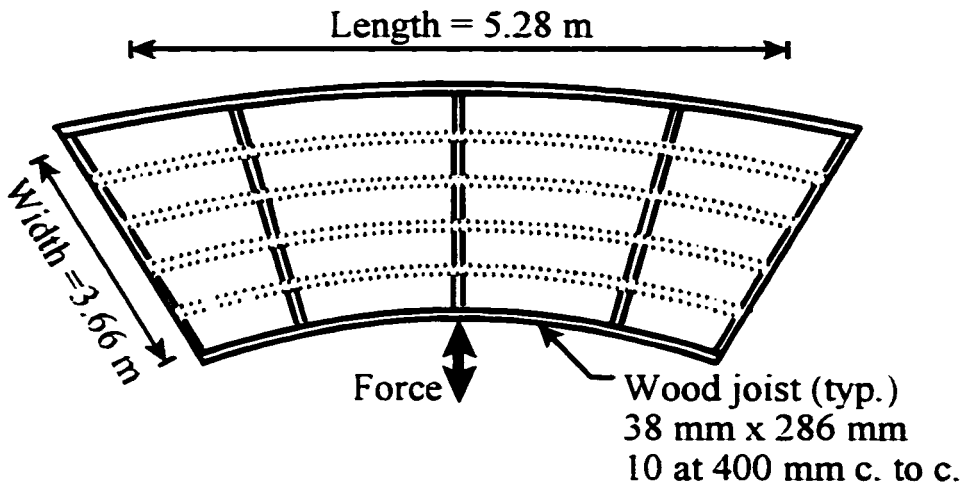

Figure 4.14 Wood diaphragm deflected shape (Model 1).

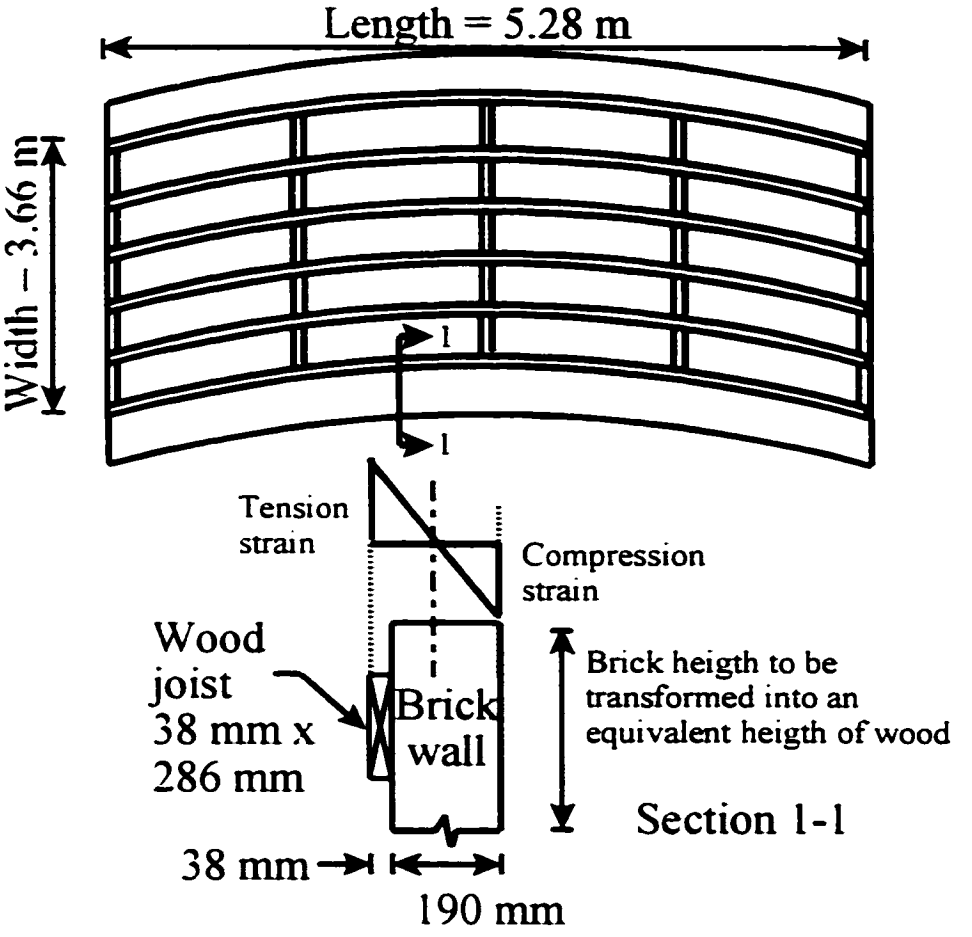

Figure 4.15 Wood diaphragm deflected shape (Model 2).

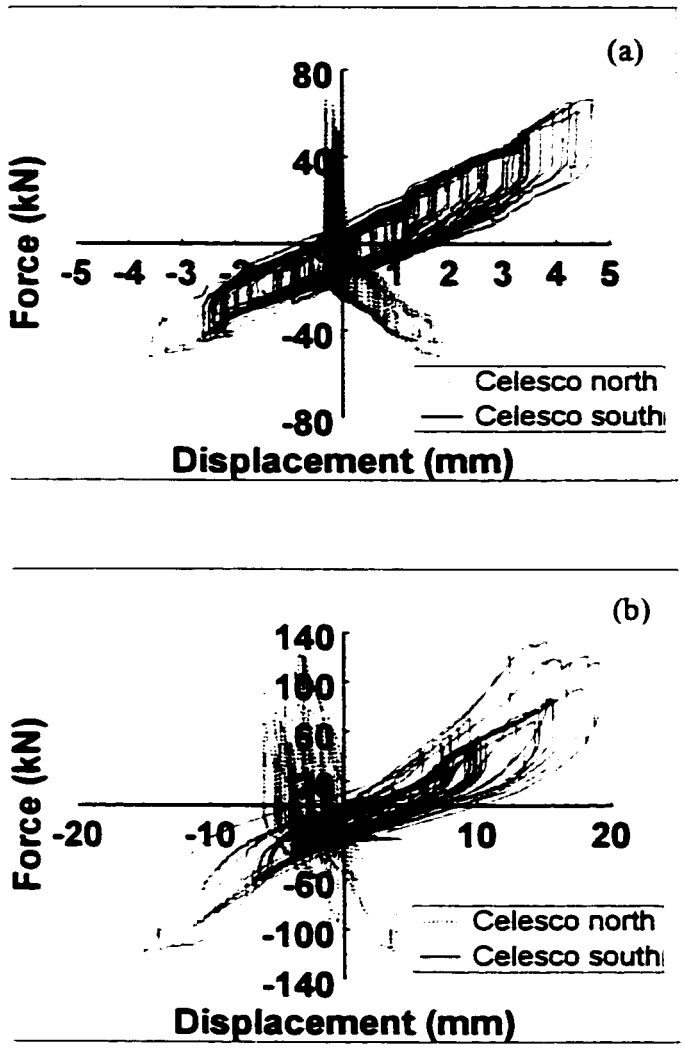

Figure 4.16. Hysteretic response of in-plane wood diaphragm deformation during: (a) La Malbaie x 2.0 without Tyfo; (b) La Malbaie x 4.0 with Tyfo.

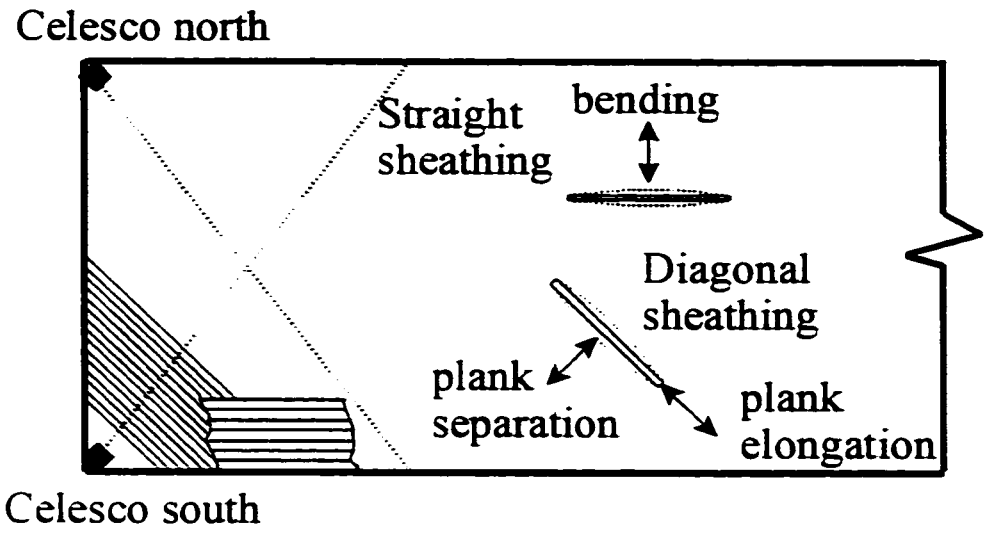

Figure 4.17 Schematic illustration of in-plane diaphragm deformation.

Figure 5.1 Three-story older residential building in Montreal, Canada from which wall specimens were retrieved.

Figure 5.2 Retrieval of test specimens from existing building.

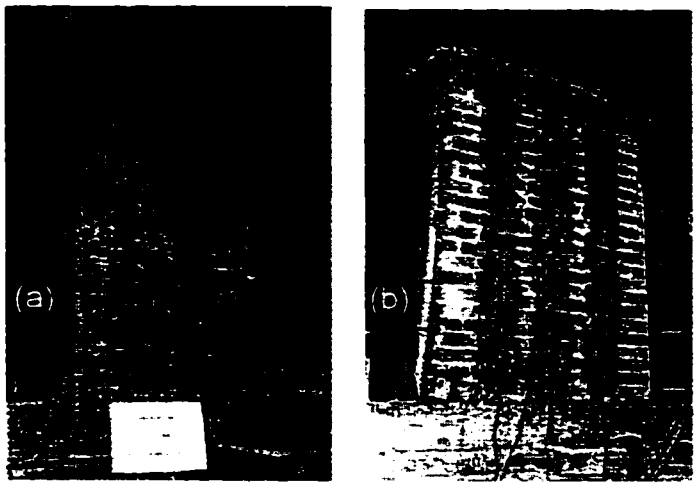

Figure 5.3 Specimens: (a) As-Built specimen, and; (b) Specimen retrofitted with Tyfo fiberglass strips.

Figure 5.4 Test set-up on shake table.

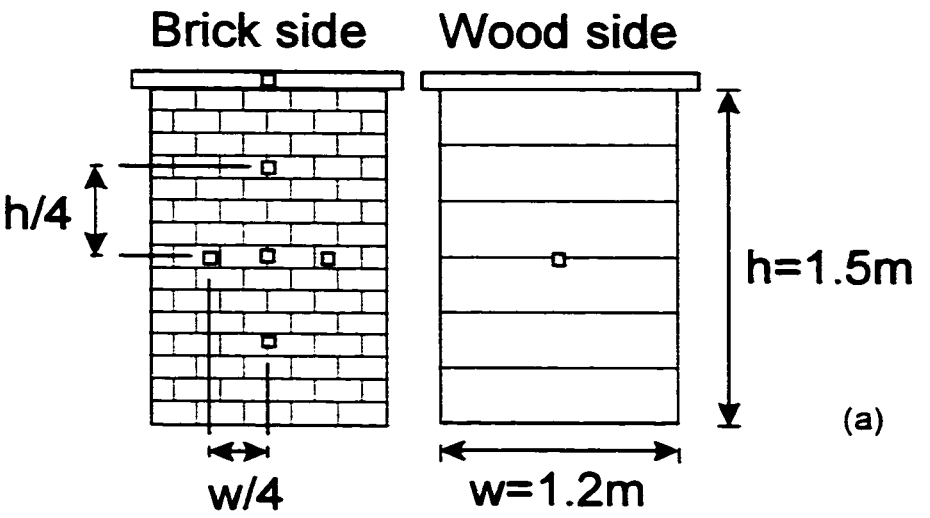

Brick wall thickness: 95 mm

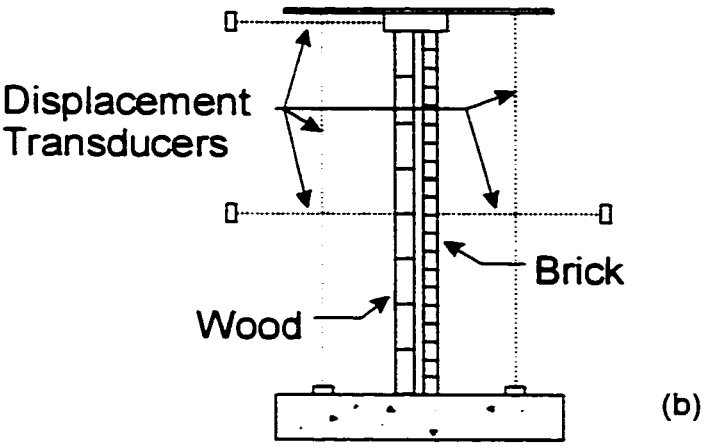

Figure 5.5 Location of: (a) Accelerometers, and; (b) Displacement transducers on specimens.

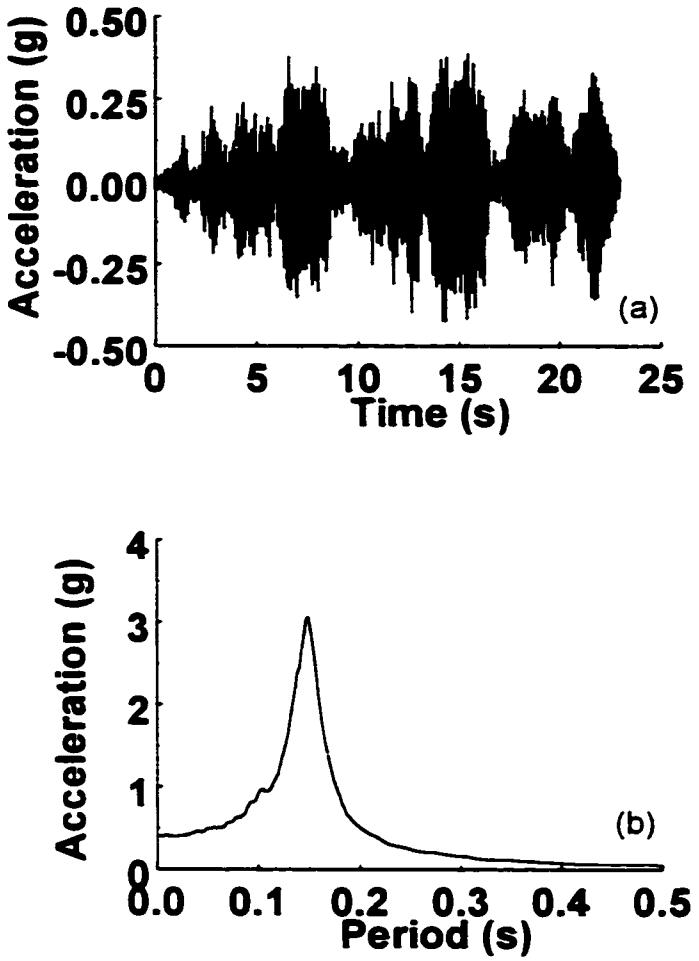

Figure 5.6 Floor-level seismic input motion for shake table tests: (a) Acceleration time-history, and; (b) Absolute acceleration response spectrum at 5% damping.

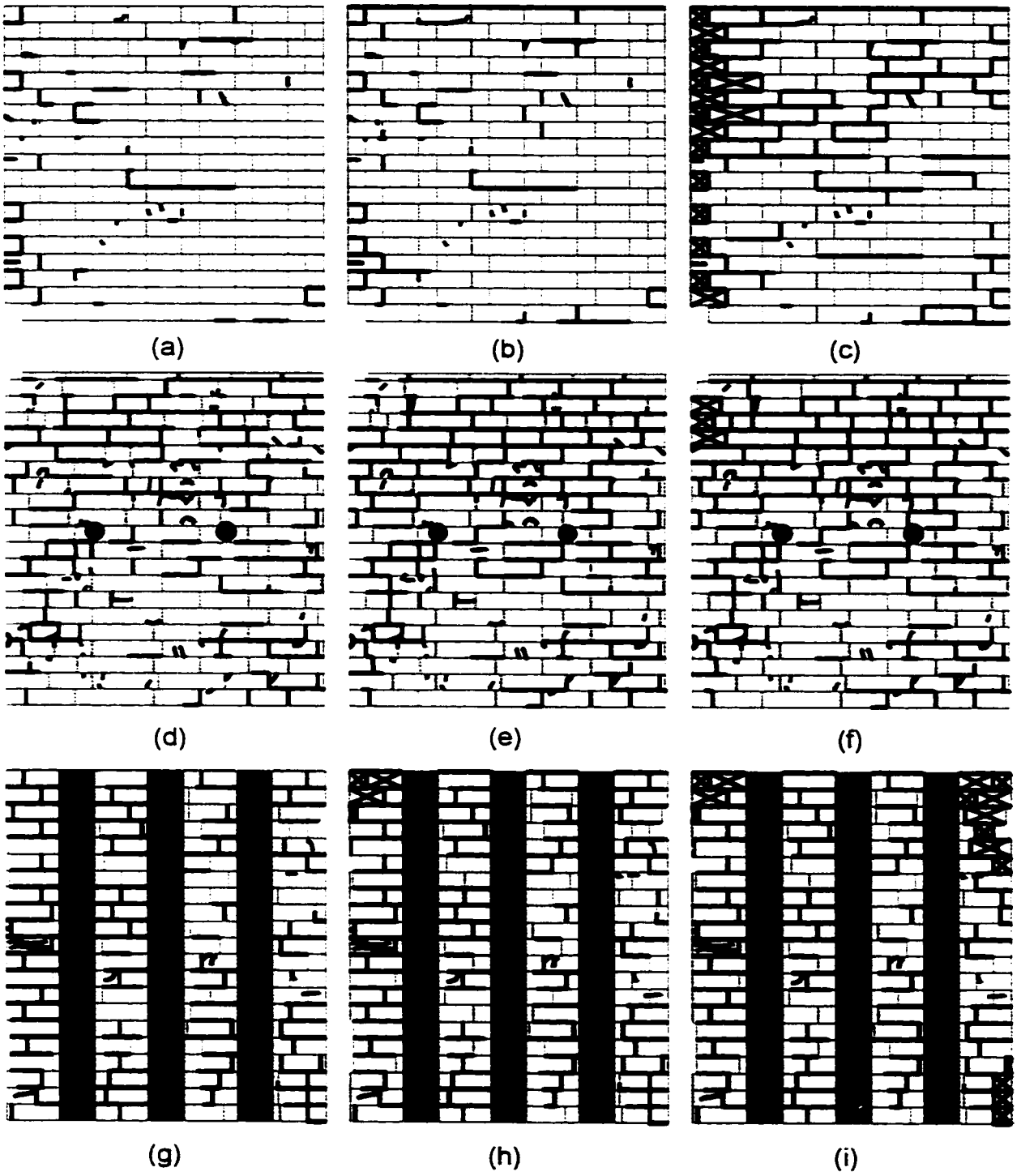

Figure 5.7 Crack pattern for as-built specimen at PHA of: (a) 0.4g, (b) 1.0g, (c) 1.5g; Cintec specimen at PHA of: (d) 0.4g, (e) 1.0g, (f) 1.5g; Tyfo specimen at PHA of: (g) 0.4g, (h) 1.0g, (i) 1.5g. (Fallen bricks are covered by an X, and solid circles in (d), (e), and (f) indicate anchors).

Figure 5.8 Failure mode of: (a) As-built specimen; (b) Cintec specimen, and; (c) Tyfo specimen.

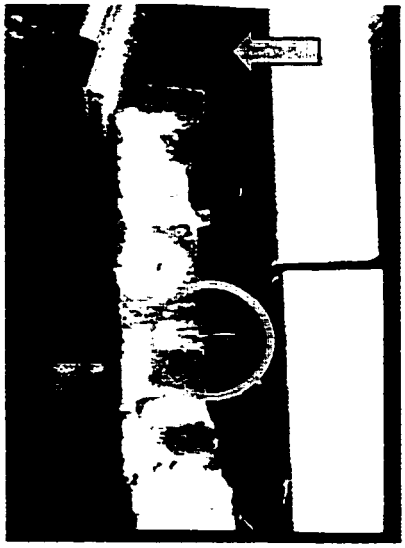

Figure 5.9 Lack of tight fit inside the wooden belt at the top of the wall due to repeated shaking (arrow), and connecting nails embedded in mortar joints (circle).

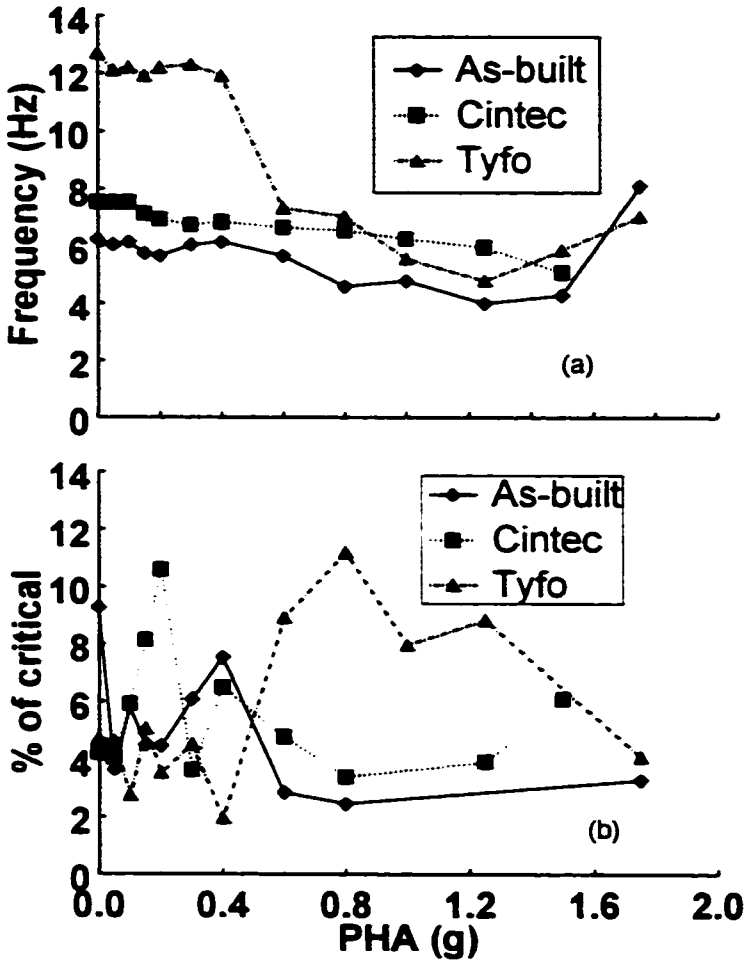

Figure 5.10 Variation of dynamic properties: (a) Fundamental frequencies, and; (b) Damping ratios.

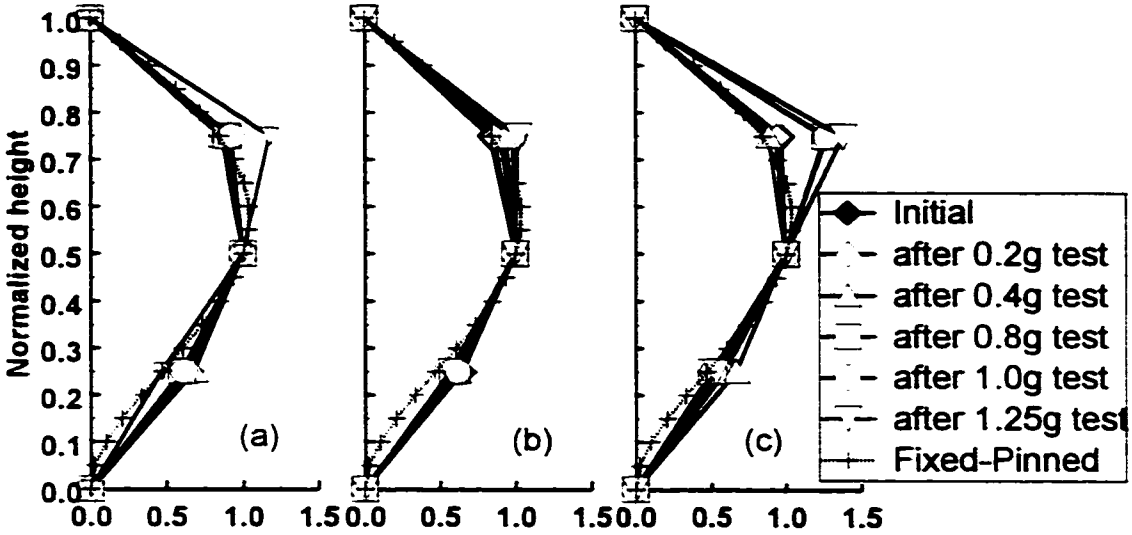

Figure 5.11 Mode shapes of: (a) As-built specimen; (b) Cintec specimen, and; (c) Tyfo specimen.

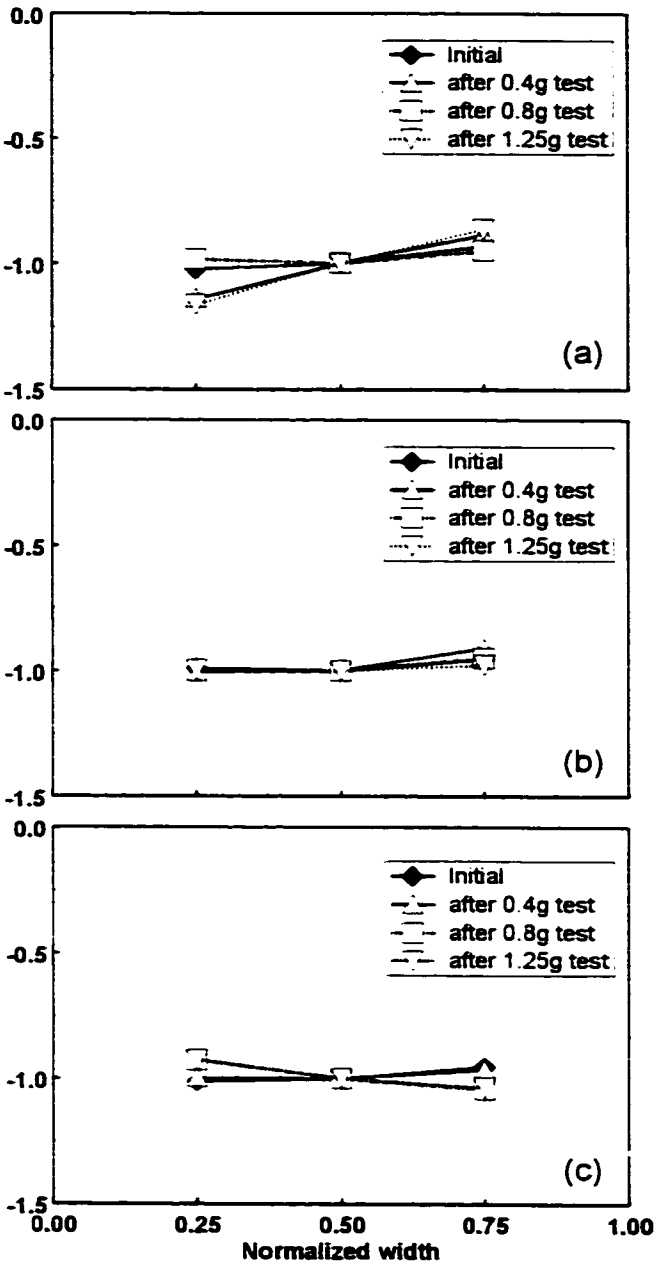

Figure 5.12 Mode shapes in-plan of: (a) As-built specimen; (b) Cintec specimen, and; (c) Tyfo specimen.

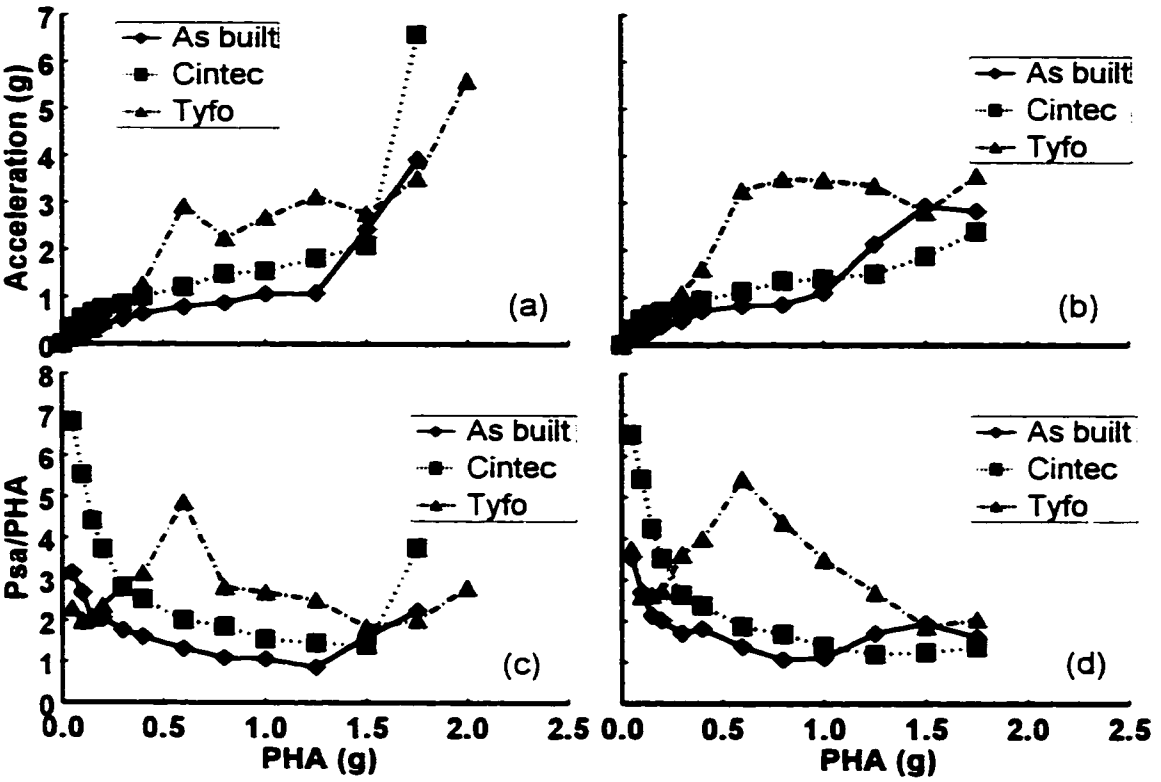

Figure 5.13 Peak acceleration at center of wall: (a) Brick side, (b) Wood side, and; Dynamic amplification factor at center of wall: (c) Brick side, (d) Wood side.

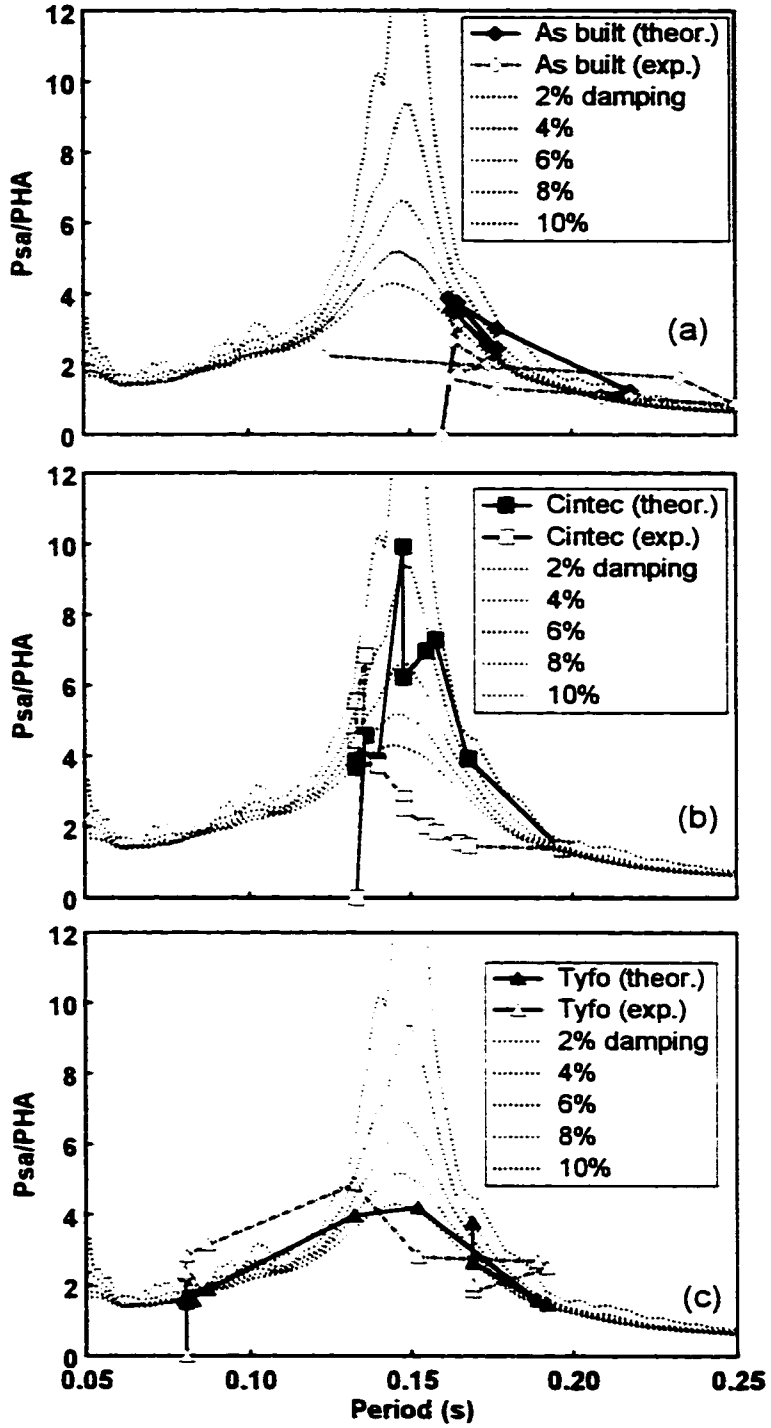

Figure 5.14 Response spectrum of: (a) As-built specimen; (b) Cintec specimen, and; (c) Tyfo specimen.

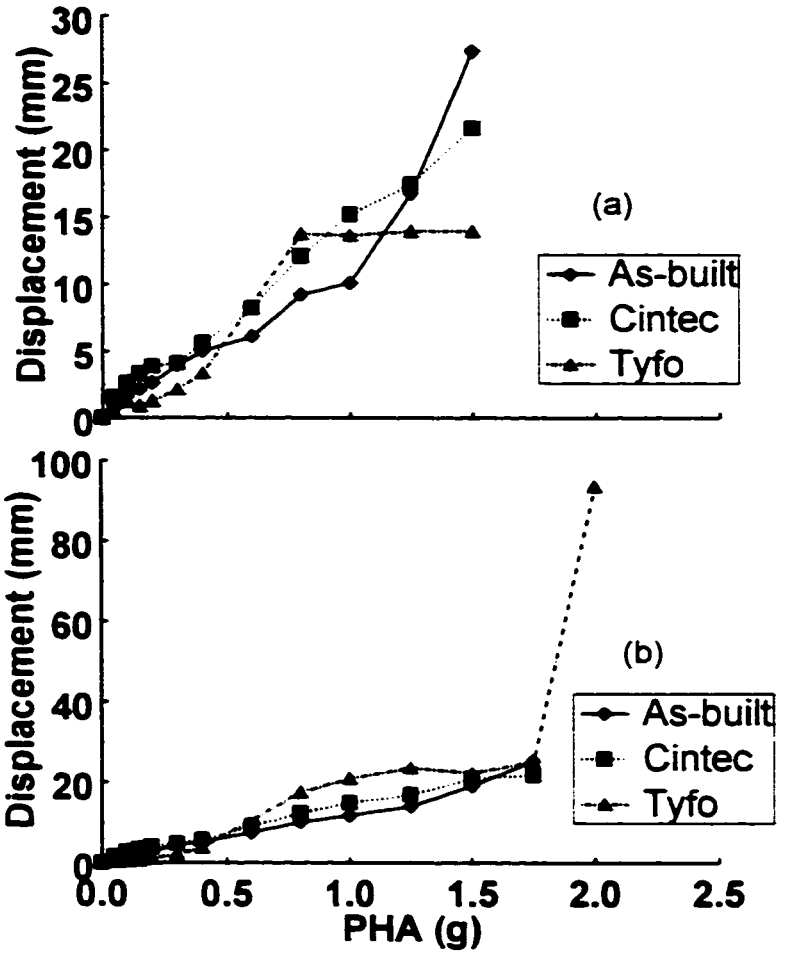

Figure 5.15 Peak displacement at center of wall: (a) Brick side, and; (b) Wood side.

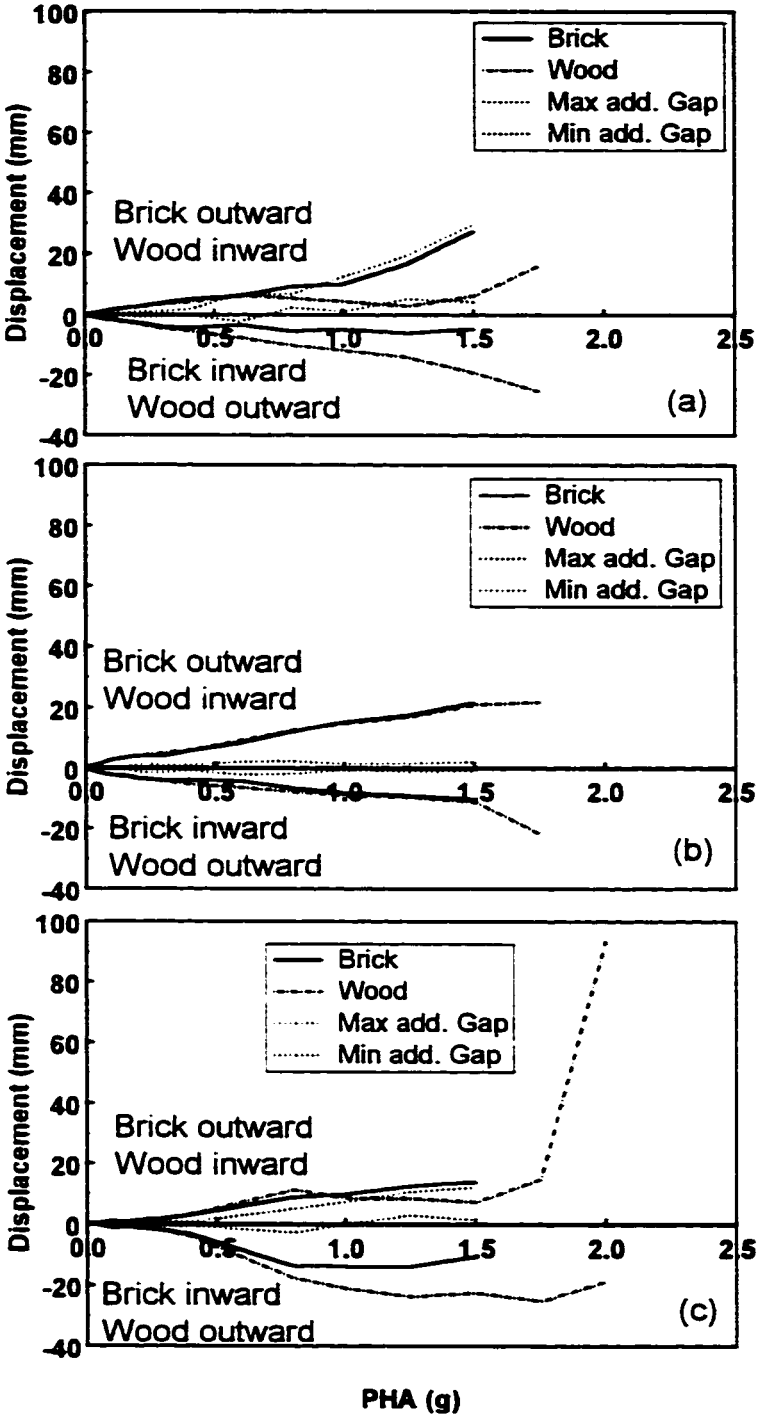

Figure 5.16 Maximum inward and outward displacement, and progression of additional gap between wood and brick wall at mid-height of wall for: (a) As-built specimen; (b) Cintec specimen, and; (c) Tyfo specimen. Maximum additional gap indicates the largest increase in the distance between the masonry and wood wall, at mid-height, at any time and in any direction during the response time history. Minimum additional gap is the corresponding smallest increase (if positive), or largest decrease (if negative).

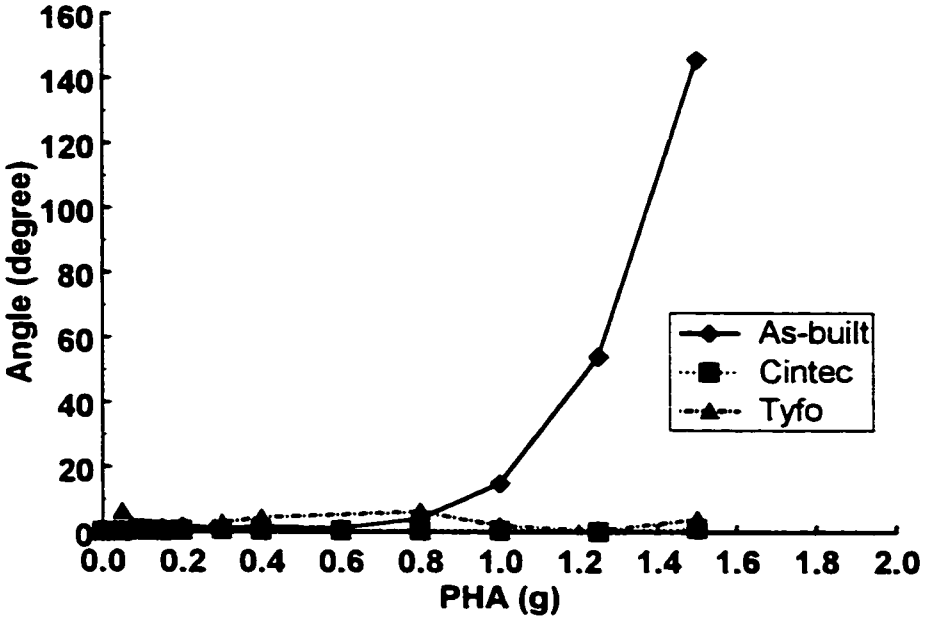

Figure 5.17 Variation of phase angle.

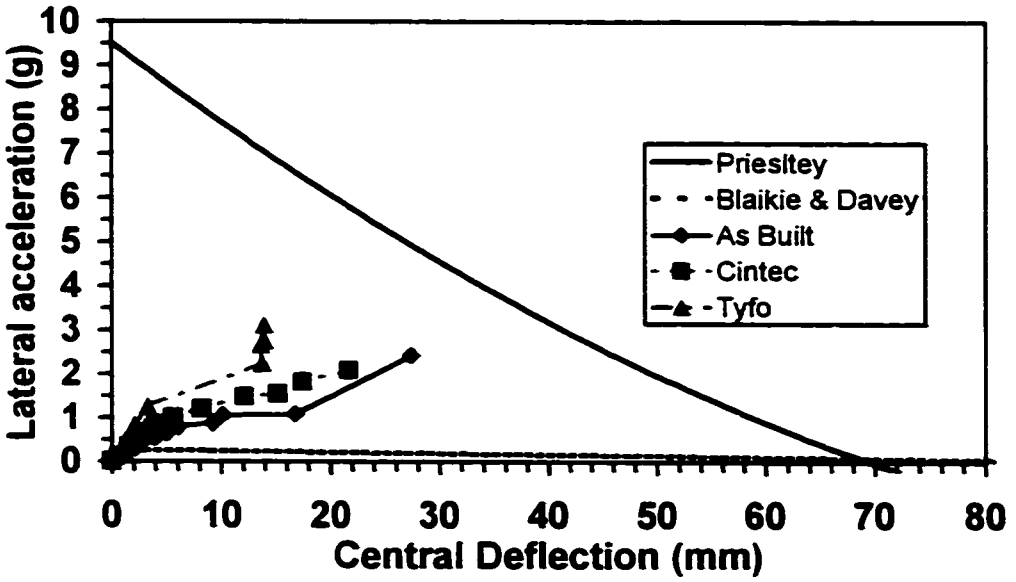

Figure 5.18 Comparison of lateral acceleration-displacement response at mid-height with various analytical models.

Appendix A

Seismic Evaluation of the URM Specimen Using the CGSEEB

A.1 Evaluation procedure

Recall that, according to the Canadian Guidelines for the Seismic Evaluation of Existing Buildings (CGSEEB) (NRC 1992), pier rocking is given by:

$$V_r = 0.9\frac{D}{H}P_D \tag{1}$$

where P_D is the axial load on the pier, and D and H are the pier's width and height, respectively.

The shear resistance is given by:

$$V_d = v_m D t / 1.5 \tag{2}$$

where t is the thickness of the wall, 190 mm, and v_m is the masonry shear strength given by:

$$v_m = 0.56 v_t + 0.75\frac{P_D}{A} \tag{3}$$

where v_t is the mortar shear strength determined by in-place shear tests (also known as "push-tests"), and A is the mortared area, or equivalently, the pier's width (D) times its thickness (t). The mortar shear strength, v_t, should not be less than 0.2 MPa otherwise the mortar should be removed, or pointed and retested, and it cannot exceed 0.7 MPa.

When designing the specimen, a value of 0.7 MPa for v_t was assumed. After construction of the specimen, the mortar shear strength along bed joints was obtained by triplet tests and in-place shear tests with values of 0.52 MPa and 0.418 MPa, respectively.

If (3) is substituted into (2), it yields:

$$V_d = 0.373 v_t A + 0.5P \tag{4}$$

Also, for an uncracked pier, the load required to initiate cracking at the pier's top and bottom based on strength of material principles, is given by:

$$V_{cr}=f_t\frac{tD^2}{3H}+\frac{P_D D}{3H} \tag{5}$$

where f_t is the tensile strength of the masonry. In (5), the first term of the equation represents the tensile capacity, while the second term is the axial load effect. When designing the specimen, a typical value of 0.5 MPa was used for f_t (CSA 1994). Flexural tension tests on masonry prisms gave a value of 0.18 MPa. Calculations were also performed for an unusually high masonry tensile strength of 1.26 MPa as reported by Abrams and Costley (1995).

For a pier fixed at the top and bottom, the pier's lateral stiffness is given by:

$$k=\frac{E_m t}{\left(\frac{H}{D}\right)^3+3\left(\frac{H}{D}\right)} \tag{6}$$

where E_m is the modulus of elasticity of masonry taken as $E_m = 850 f'_m$ MPa (but not greater than 20 000 MPa) (CSA 1994), and f'_m was assumed to be 17 MPa for design (CSA 1994), and was found to be 22.2 MPa from masonry prism tests. In (6), the first term in the denominator is the flexural deformation component, while the second term is the shear deformation contribution.

The self weight for a 190 mm thick clay brick wythe is 3.78 kPa (Drysdale et al. 1994). The dead load for the 3.66 m x 5.28 m diaphragm consists of the joists (0.120 kPa) plus diagonal sheathing (0.080 kPa) and straight sheathing (0.080 kPa).

A.2 Calculations based on design values

When using design values (i.e., $f'_m = 17$ MPa, $f_t = 0.5$ MPa, and $v_t = 0.7$ MPa) and assuming a wood diaphragm with no live load and shear walls that are not bearing walls, the following values can be calculated as shown in Table a.1.

Table a.1

Pier	Width D (m)	Height H (m)	Axial load P_D (kN)	Rocking V_r (kN)	Cracking V_{cr} (kN)	Shear V_s (kN)	Stiffness k (kN/mm)
Door	0.883	1.842	7.03	3.03	14.53	47.32	179.0
Central	1.410	0.953	11.60	15.45	71.78	75.75	1175.1
Window	0.578	0.953	4.96	2.71	12.10	31.15	291.0

A.2.1 Push over analysis

Based on the pier's individual lateral stiffness, the pier's share of the lateral load can be calculated. By gradually increasing the lateral force on the shear wall, the following behavior is expected:

-At a lateral load of 68.4 kN, the window pier will first reach its cracking load of 12.10 kN, while the lateral loads on the door pier and central pier are 7.46 kN and 48.8 kN, respectively. After cracks develop, the capacity of the window pier then drops to that of rocking, 2.71 kN. The difference in load (12.10 - 2.71) is redistributed to the door and central piers, they now resist 8.70 kN and 56.95 kN, respectively.

-The lateral load is then increased up to 85.4 kN, at which point the central pier reaches its cracking load of 71.78 kN. The lateral load on the door pier is now 10.92 kN, while the window pier resistance remains at its rocking capacity, 2.71 kN. Having cracked, the capacity of the central pier drops to that of rocking, 15.45 kN. The difference (71.78 - 15.45) is then redistributed to the door pier, which immediately reaches its cracking load, 14.53 kN, then drops to its rocking capacity, 3.03 kN.

Thus, after reaching a maximum load of 85.4 kN, the lateral capacity of the shear wall is then the summation of each pier's rocking capacity, i.e. 3.03 + 15.45 + 2.71 = 21.19 kN.

According to the CGSEEB, the expected in-plane seismic load, F_{wx}, on a shear wall is given by:

$$F_{wx} = v'(W_{wx} + W_d/2) \tag{7}$$

where W_d is the total load tributary to the diaphragm, including walls perpendicular to the direction of motion, and W_{wx} is the tributary load of each shear wall, which were calculated to be 68.1 kN, and 21.1 kN, respectively. v' is an effective velocity ratio, taken as 0.4 for the most severe seismic zone encountered in Canada.

Thus, from (7), the expected lateral load gives 22.1 kN, which is greater than 21.19 kN, the rocking capacity of the shear wall. Since pier rocking is a stable deformation-controlled energy dissipation mode, the CGSEEB states that only 60% of the lateral load need to be resisted. Thus the expected lateral load, 22.1 kN, can be reduced to 60%, 13.2 kN, which is less than the rocking capacity of the shear wall, 21.19 kN. This means that, theoretically, the shear wall is able to resist the highest seismic lateral force possible in Canada.

However, in (7), it is assumed that the ground motion applied at the diaphragm's edges is unamplified by the end-walls. Thus, (7) is simply "the inertia force produced by the tributary mass times the base ground acceleration or the zonal acceleration factor (or zonal velocity in the Canadian system) times the tributary weight" (Bruneau 1994a).

Knowing the maximum lateral load from the push over analysis, 85.4 kN, it is possible to calculate, using (7), the corresponding effective velocity ratio v'. This yields a value of 1.55. Interestingly, this means that a peak horizontal ground acceleration of 1.55g is required to crack all piers and induce a rocking mechanism in the shear wall. Because such a value is rather unrealistic, it was decided to provide additional mass on the diaphragm modeling the

effect of a live load. Also, it was decided to make the tested shear walls load-bearing to reduce their cracking to rocking ratios.

A.3 Calculations based on experimental values

After construction of the specimen, material test on masonry prisms were performed and actual values (i.e. f'_m = 22.2 MPa, f_t = 0.18 Mpa, and v_t = 0.52 MPa) were used to predict the shear wall behavior. Thus, with load bearing shear walls and a 2.4 kPa live load on the diaphragm, the previous values were re-calculated as shown in Table a.2.

Table a.2

Pier	Width D (m)	Height H (m)	Axial load P_D (kN)	Rocking V_r (kN)	Cracking V_{cr} (kN)	Shear V_s (kN)	Stiffness k (kN/mm)
Door	0.883	1.842	14.1	6.08	7.08	39.59	233.8
Central	1.410	0.953	25.9	34.49	36.56	64.91	1534.5
Window	0.578	0.953	11.2	6.11	6.26	26.90	380.0

A.3.1 Push over analysis

Similarly, from a push over analysis, a maximum lateral load of 48.3 kN is required for all piers to crack, then a full rocking mechanism will develop with a capacity of 46.7 kN (i.e. 6.08 + 34.49 + 6.11).

Again, from (7) using W_d = 114.5 kN and W_{ex} = 21.1 kN, the maximum expected lateral load for the most severe seismic zone in Canada (v' = 0.4), is calculated to be 31.3 kN. Which is less than the rocking capacity of the shear wall, 46.7 kN. Using the maximum lateral load of 48.3 kN, the corresponding effective zonal velocity ratio, v', is 0.62.

However, one must keep in mind that the force transmitted to the shear walls is limited by the shear strength of the diaphragm. Thus, the lateral load cannot exceed:

$$F_{wx}=v'W_{wx}+v_u D \tag{8}$$

where $v_u D$, is the maximum shear strength of the diaphragm. In this case, the unit shear strength of a diaphragm with diagonal with straight sheathing overlay is 29.8 kN/m based on values from the CGSEEB procedure. Thus, using (8), the lateral load cannot exceed 117.5 kN which is greater than the expected maximum load, 31.3 kN, and the maximum load to reach cracking, 48.3 kN, hence the diaphragm should be adequate.

Table a.3 below shows values for different cases of live load, and masonry tensile strengths.

Table a.3	Masonry properties based on material testing f_t = 0.18 MPa v_t = 0.52 MPa				CSA S304.1 f_t=0.5 MPa	f_t = 1.26 MPa
Pier	P_D (kN)	V_{cr} (kN)	V_r (kN)	V_a (kN)	V_{cr} (kN)	V_{cr} (kN)
	Shear NOT bearing wall					
Door	7.03	5.95	3.03	36.06	14.53	34.90
Central	11.60	29.5	15.45	57.76	71.78	172.20
Window	4.96	5.00	2.71	23.78	12.10	28.98
			Σ=21.19			
	Shear wall = bearing wall, Live load: 0.0 kPa					
Door	7.77	6.07	3.35	36.43	14.65	35.02
Central	13.09	30.24	17.43	58.51	72.52	172.93
Window	5.61	5.13	3.06	24.11	12.24	29.11
			Σ=23.84			
	Shear wall = bearing wall, Live load: 2.4 kPa					
Door	14.1	7.08	6.08	39.59	15.66	36.03
Central	25.9	36.56	34.49	64.91	78.83	179.25
Window	11.2	6.26	6.11	26.90	13.37	30.24
			Σ=46.68			
	Shear wall = bearing wall, Live load: 4.8 kPa					
Door	20.40	8.09	8.80	42.74	16.66	37.04
Central	38.70	42.87	51.53	71.31	85.15	185.56
Window	16.80	7.39	9.17	29.70	14.50	31.37
			Σ=69.50			
	Shear wall = bearing wall, Live load: 6.0 kPa					
Door	23.60	8.60	10.18	44.34	17.18	37.55
Central	45.10	46.02	60.05	74.51	88.30	188.72
Window	19.60	7.96	10.70	31.10	15.06	31.94
			Σ=80.94			

Appendix B

Analytical modeling

Prior to testing, analytical modeling provided some valuable observations on expected seismic behavior of the specimen, particularly on diaphragm response respective to wall response.

B.1 Elastic analyses

First, using a linear elastic program such as SAP 90, the stiffness and dynamic properties of the diaphragm and shear walls were investigated. Both the diaphragm and the shear walls were modeled using frame elements as shown in Fig. b.1. The period of vibration of the shear wall and the diaphragm was found to be 0.00684 s and 0.278 s, respectively. Results were confirmed by using the same model with a different program, DRAIN-2DX and 3DX.

The specimen was then modeled as a three degrees of freedom (3DOF) "stick" model with lumped masses, as shown in Fig. b.2a. In order to closely match the fundamental period of the specimen determined using SAP 90 and DRAIN-2DX (T = 0.278 s), it was found that the effective tributary mass was to be distributed as follow:
-50% of the wall's mass + 20% of the floor's mass acting at the top of each shear wall, i.e., m_1
-60% of the floor's mass acting at mid-span, i.e., m_2.
This gave a fundamental period of 0.282 s.

This mass distribution was used instead of the more typical:
-50% of the wall's mass + 25% of the floor's mass acting at the top of each shear wall,
-50% of the floor's mass acting at mid-span, giving a period of 0.257 s.

Analyses were also done using a single-degree-of-freedom model (1 DOF) i.e. with 60% of the floor's mass acting at mid-span only, as shown in Fig. b.2b. As shown in this document (see Fig. 3.9), a sufficiently accurate seismic response can be captured by using only a single actuator acting at the diaphragm center-span, i.e. using a 1 DOF model.

B.2 Nonlinear analyses

Nonlinear elastic analysis was performed using a FORTRAN program by Costley and Abrams (1995). This time step integration program uses a 3 DOF model with bilinear force-displacement curves for the shear wall. As shown in Fig. b.3, the initial portion of the curve is the linear elastic stiffness of the shear wall, while the second portion has a zero slope representing the rocking behavior of the piers in the shear wall. It is assumed that all piers developed the same rocking strength at the same time even though the specimen possesses piers with different aspect ratio and strength. However, the diaphragm is assumed to remain linearly elastic. Among noteworthy features, the program was able to determine when rocking occurred, and estimate the peak wall displacement due to rocking. It was found that the diaphragm governs the response, since the shear wall displacements are in phase with the diaphragm mid-span's displacements.

Similarly, inelastic nonlinear analyses were performed using the "stick" model with DRAIN-2DX. Spring elements were used at the top and bottom of the frame modeling the shear walls to model rotational flexibility at joints, as shown in Fig. b.4. The rotational stiffness of the springs used bilinear force-displacement curves as in the FORTRAN program from Costley and Abrams. A first series of analysis was performed with a linear elastic diaphragm. Excellent agreement was found with the results obtained from the Costley and Abrams program. Then, inelastic response of the diaphragm was considered using an inelastic force-displacement relationship as shown in Fig. b.5. Results showed that yielding of the diaphragm reduces the peak displacements of the shear walls during rocking, (for example, see Fig. 3.8).

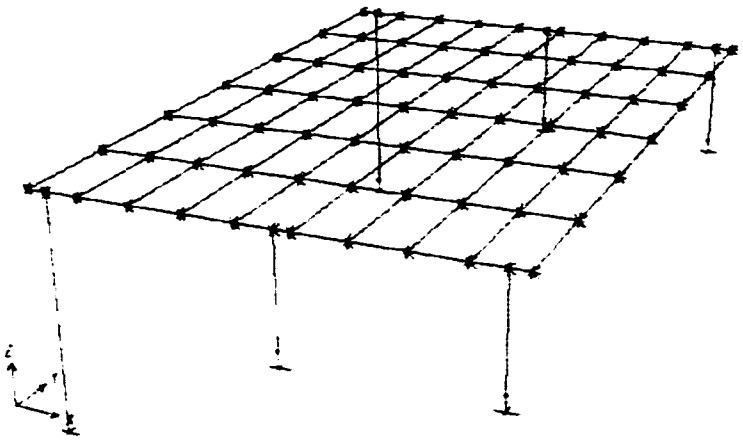

Figure b.1 Sap 90 linear elastic model for shear walls and diaphragm.

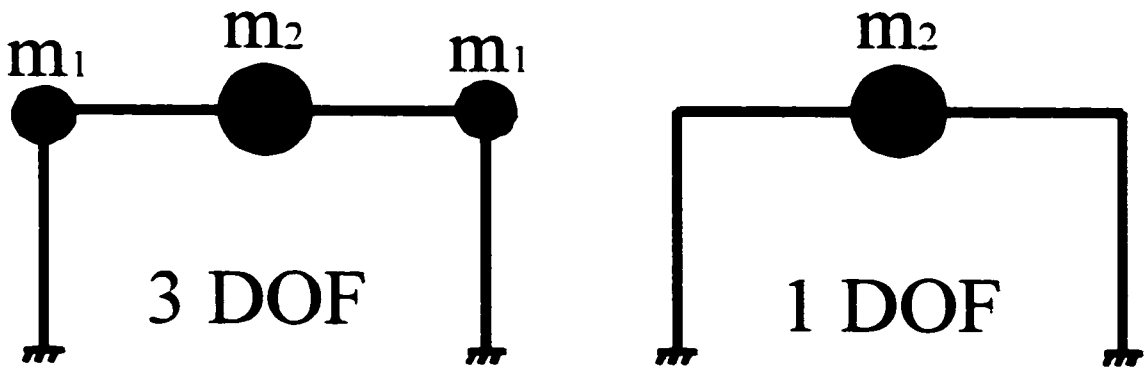

Figure b.2 3 DOF and 1 DOF models for URM specimen.

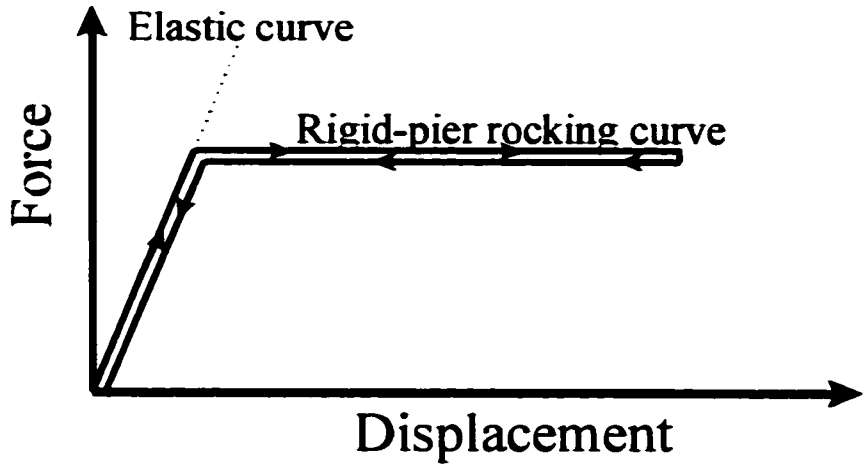

Figure b.3 Bilinear force-displacement curve for shear wall rocking motion.

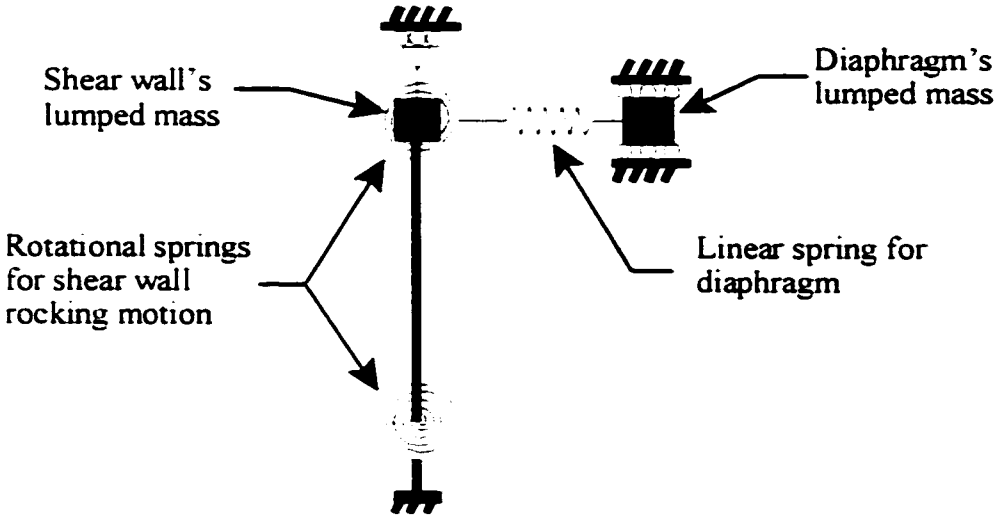

Figure b.4 DRAIN-2DX model.

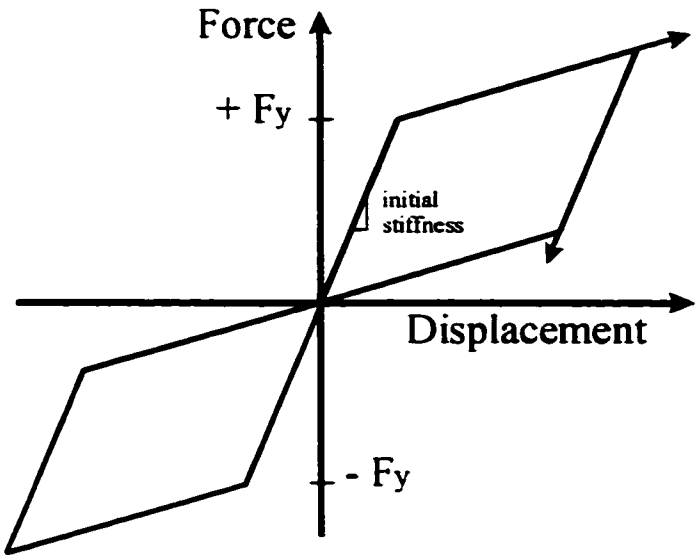

Figure b.5 Inelastic force-displacement curve for flexible wood diaphragm.

Appendix C

Schedule and list of materials

C.1 Construction and testing schedule

December 1997 - January 1998:	Construction of reinforced concrete foundation.
March 12, 1998 - March 23, 1998:	Construction of URM specimen.
May 20, 1998 - May 27, 1998:	Drilling holes and installation of anchor bolts securing the wood floor to the masonry walls.
July 27, 1998 - August 1, 1998:	Installation of diagonal and straight sheathings.
August 3, 1998 - August 16, 1998:	Preparation for out-of-plane testing of URM walls with wood backing at Ecole Polytechnique in Montreal.
August 10, 1998:	Testing of as-built specimen.
August 13, 1998:	Testing of Cintec specimen.
August 16, 1998:	Testing of Tyfo specimen.
July 6, 1999:	Test of URM specimen for La Malbaie x 0.25, 0.5, 1.0, 1.5, and 2.0 with clip gages on west wall.
July 12, 1999:	Test of URM specimen for La Malbaie x 1.0, and 1.5 with clip gages on east wall.
August 24, 1999:	Test of repaired URM specimen with fiberglass for La Malbaie x 1.0, 2.0, and 3.0 with clip gages on west wall.

August 25, 1999:	Test of repaired URM specimen with fiberglass for La Malbaie x 3.0, and 4.0 with clip gages on west wall.
August 27, 1999:	Test of repaired URM specimen with fiberglass for La Malbaie x 3.0, and 4.0 with clip gages on east wall.
September 2, 1999:	Test of repaired URM specimen with fiberglass. Cyclic tests.

C.2 List of materials

- Standard metric modular brick 90 mm x 57 mm x 190 mm	Qty: 7700
- Type O mortar 1 part cement: 2 parts lime: 9 parts sand	635 kg of cement 540 kg of lime 4868 kg of sand
- Joists construction grade spruce 38 mm x 286 mm x 6100 mm	Qty: 10
- Blockings 38 mm x 286 mm x 6100 mm	Qty: 1
- Blockings 38 mm x 89 mm x 6100 mm	Qty: 2
- Diagonal and straight sheathings construction grade spruce 19 mm x 140 mm x 3658 mm	Qty: 60
- Anchor bolts 19 mm diameter	Qty: 26
- Bearing plates 150 mm x 150 mm x 6 mm	Qty: 52

Appendix D

Pseudo-Dynamic Algorithm

D.1 Pseudo-dynamic testing

A real-time dynamic behavior of a test structure can be observed during a shake table test. However, the main disadvantage is the limit on the shake table's payload capacity. In most cases, scale models of structures are used. Thus, pseudo-dynamic testing was developed as an alternative to real-time dynamic testing.

The pseudo-dynamic method is an on-line computer-controlled testing technique in which the dynamic characteristics of a structure (mass and damping), being usually well known, are numerically simulated on a computer model, while the usually complex (and unknown) restoring force characteristics are directly measured from the tested specimens. This allows for the testing of structures or components under real earthquake excitations but at a relatively slow speed, thus allowing to observe the evolution of damage. The schematic of the test method is shown in Fig. d.1.

While the pseudo-dynamic testing concept is simple, the equipment required must be of stringent accuracy, high capacity, and extremely modular to answer the needs of large-scale structural engineering testing. The University of Ottawa pseudo-dynamic system is a unique facility in Canada, and one of the few available worldwide. Using this facility, structures and components can be loaded in any direction using three actuators of 1000 kN capacity each. The extreme flexibility of this pseudo-dynamic equipment permits to conduct experiments that yield as much information on the inelastic seismic behavior of structures subjected to realistic earthquake excitations as could be obtained using shake table testing. However, using this new experimental technique, these results can be obtained at a much slower speed (thus easily allowing to visually observe the progression of damage), and using large scale or full scale specimens.

Over the years, various algorithms and schemes were developed to improve accuracy and testing strategies for pseudo-dynamic tests. Here, the pseudo-dynamic testing algorithm by

Shing et al. (1991) based on an implicit algorithm and proven to be reliable, was implemented in the MTS controller system at the University of Ottawa.

The time integration method adopted for pseudo-dynamic testing in this program is the same as the Newmark method but with the equations of motion modified as follows:

$$Ma_{i+1} + (1+\alpha)Cv_{i+1} - \alpha Cv_i + (1+\alpha)r_{i+1} - \alpha r_i = (1+\alpha)f_{i+1} - \alpha f_i \quad (1)$$

$$d_{i+1} = d_i + \Delta t v_i + \Delta t^2[(1/2-\beta)a_i + \beta a_{i+1}] \quad (2)$$

$$v_{i+1} = v_i + \Delta t[(1-\gamma)a_i + \gamma a_{i+1}] \quad (3)$$

where M and C are the mass and damping matrices of the structure, d_i, v_i, and a_i are vectors of nodal displacements, velocities, and accelerations at time equal to $i\Delta t$, Δt is the integration time step, r_i is the nodal restoring force vector, and f_i is the external force excitation vector. α, β and γ are parameters that govern the numerical properties of the algorithm. The algorithm is unconditionally stable when $-0.5 \le \alpha \le 0$, $\beta = (1+\alpha)^2/4$ and $\gamma = \frac{1}{2} - \alpha$. When $\alpha = 0$, the algorithm degenerates to the constant-average-acceleration method, which has zero damping.

D.2 Input parameters needed

-The specimen characteristics, i.e. the number of degrees of freedom, the initial stiffness, mass and damping matrices.

-The integration parameters, i.e. the value of the α parameter, time interval, the minimum time interval, the parameter for the divergence check, the convergence tolerance for each DOF, and the total time span for dynamic simulation.

-The excitation type, i.e. ground motion record, sine or cosine function, free vibration, and the characteristics of the excitation. For earthquake ground motions, one needs to specify the name of the file in which the record is stored, the number of data points in the record, the time interval with which the data is recorded, and the amplification factor for the ground motion. A ground motion data file contains two columns. First for digitized ground acceleration readings and second for the number of the reading.

-The initial conditions, i.e. a zero starting position with zero initial displacements and velocities, or a non-zero starting position for which the values of initial displacements and velocities must be entered.

-The information related to the control or data acquisition channels, i.e. the control channel for each degree of freedom, the channels acquiring the displacements and restoring forces, the maximum actuator velocity, and specifying if an external data acquisition system will be used.

-The name for the output file, and the plotting information.

When all the information is entered, the test can start.

D.3 Pseudo-dynamic algorithm

The structure of the algorithm is shown in Fig. d.2, and is as follow:

1. Select an initial value for Δt.
   Set $\Delta t_{max} = \Delta t$.
   Select values for Δt_{min}.
   Select the displacement tolerance Δd^n for each DOF n.
   Set value for the reduction factor to reduce the chance of displacement overshoot.
   Set $i = 0$ and $t_i = 0$.

Initialize d_0, $d^{\cdot}_0$, d^{m}_0, v_0, r_0, r^{m}_0, a_0, and f_0.

2. Evaluate K^{*} and M^{*} with the following equations

$K^{*} = M^{*} + (1+\alpha)\beta\Delta t^{2} K.$

$M^{*} = M + (1+\alpha)\gamma\Delta t\, C.$

3. Set $t_{t-1} = t_t + \Delta t$ and get the excitation vector $f_{t-1} = f(t_{t-1})$.

4. Compute $M^{*}d_{t-1}$ with the following equations

$M^{*}d_{t-1} = M^{*}\tilde{d}_{t-1} + \Delta t^{2}\beta\{(1+\alpha)f_{t-1} - \alpha f_t - (1+\alpha)C\,\dot{v}_{t-1} + \alpha C v_t + \alpha r_t\}$

where

$\tilde{d}_{t-1} = d_t + \Delta t\, v_t + (\tfrac{1}{2} - \beta)\,\Delta t^{2} a_t$

and

$\dot{v}_{t-1} = v_t + (1-\gamma)\,\Delta t\, a_t$

5. Set $k = 0$ (beginning of iteration loop).

6. Set $r^{(k)}_{t-1} = r_t$

Set $r^{m(k)}_{t-1} = r^{m}_t$

Set $d^{r(k)}_{t-1} = d^{r}_t$

Set $d^{m(k)}_{t-1} = d^{m}_t$

7. Evaluate $M^{*}e^{R(k)}_{t-1}$ with the following equation:

$M^{*}e^{R(k)}_{t-1} = -M^{*}d_{t-1} + M^{*}d^{m(k)}_{t-1} + \Delta t^{2}\beta(1+\alpha)r^{m(k)}_{t-1}$

8. Solve $K^{*}\Delta d^{(k)}_{t-1} = -M^{*}e^{R(k)}_{t-1}$ for $\Delta d^{(k)}_{t-1}$

9. If $|\Delta d^{m(k)}_{t-1}| \le \Delta d^{m}$, go to step 15

10. Evaluate $d^{E(k+1)}_{i+1} = d^{E(k)}_{i+1}$ + (reduction factor)$\Delta d^{(k)}_{i+1}$

11. Impose $d^{E(k+1)}_{i+1}$ on the test structure.

12. Measure $r^{m(k+1)}_{i+1}$ and $d^{m(k+1)}_{i+1}$ developed by the structure.

13. Set $k = k+1$

14. Go to step 7.

15. $d_{i+1} = d^{m(k)}_{i+1} + \Delta d^{(k)}_{i+1}$

$r_{i+1} = r^{m(k)}_{i+1} + K \Delta d^{(k)}_{i+1}$

$d^{E}_{i+1} = d^{E(k)}_{i+1}$

$d^{m}_{i+1} = d^{m(k)}_{i+1}$

16. $a_{i+1} = 1/(\Delta t^2 \beta) [d_{i+1} - d_i - \Delta t\, v_i - \Delta t^2 (½ - \beta)\, a_i]$

$v_{i+1} = v_i + \Delta t [(1- \gamma)\, a_i + \gamma a_{i+1}]$

17. Set $i = i + 1$, go to step 3.

D.4 Simulated free vibration test

It is possible to perform a simulated free vibration test with the pseudo-dynamic algorithm. When entering the initial conditions, a non-zero starting position for which the values of initial displacements and velocities must be specified, and when entering the load type, the free vibration option should be selected. Then, upon starting the test, the actuators will impose on the specimen the specified displacements and the resulting simulated free vibration response as per the pseudo-dynamic algorithm.

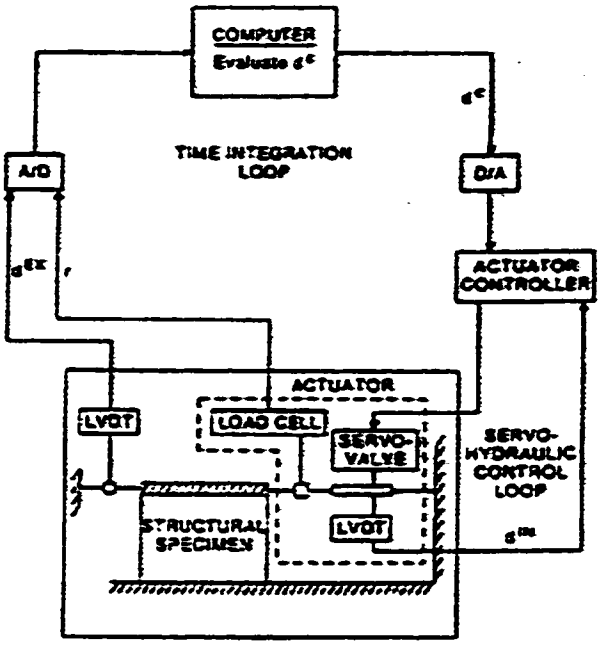

Figure d.1 Schematic of the Pseudo-dynamic test method (Shing et al. 1991).

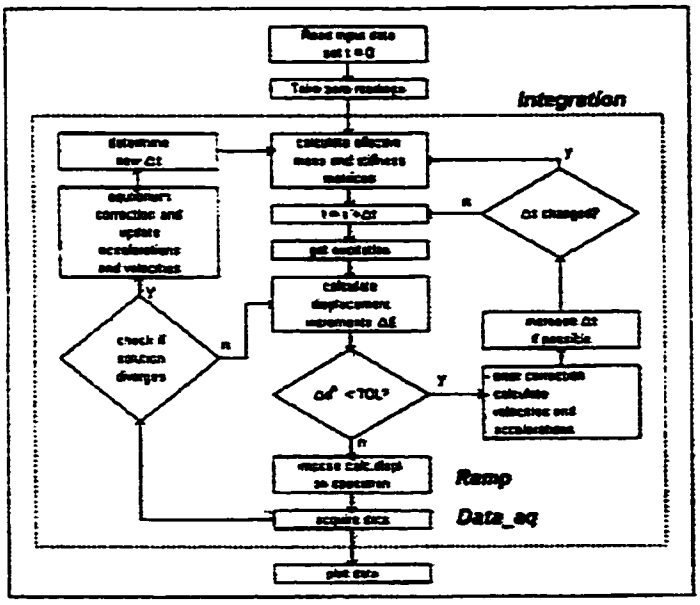

Figure d.2 Structure of the pseudo-dynamic testing algorithm (MTS Pseudo-dynamic software user's manual 1995).

Appendix E

Design of Clip Gages

E.1 Clip gages design

To record crack opening and closing during the pier's rocking cycle, twelve special clip gages were installed at expected crack location around all the piers. The clip gage itself is like a portal frame with a strain gage attached to the top beam, as shown in Fig. e.1. If the columns are chosen to be much stiffer than the beam, i.e., being infinitely rigid relative to the beam, then any changes in distance between the supports result in changes in curvature and, consequently, variation of strain at the top fibre of the beam. If the stresses in the beam remain within the elastic range, a linear relationship can be developed between the change in the distance and the strain at the beam top fibre. Thus, from Fig. e.2, the top beam is under constant moment, therefore:

$$\theta = \frac{ML}{2EI} \tag{1}$$

also, from the rigid legs:

$$\theta = \frac{\Delta}{2H} \tag{2}$$

Thus, from strength of material,

$$\sigma = \frac{Mc}{I} \tag{3}$$

the following relationship can be established:

$$\varepsilon = \frac{c}{LH}\Delta \tag{4}$$

Using L = 140 mm, H = 82 mm, c = 0.8/2 mm, it can be calculated that for 1 mm, the corresponding strain is 34.8 microns. Before testing the URM specimen, the clip gages were calibrated, and it was found that the corresponding strain was actually 30.8 microns.

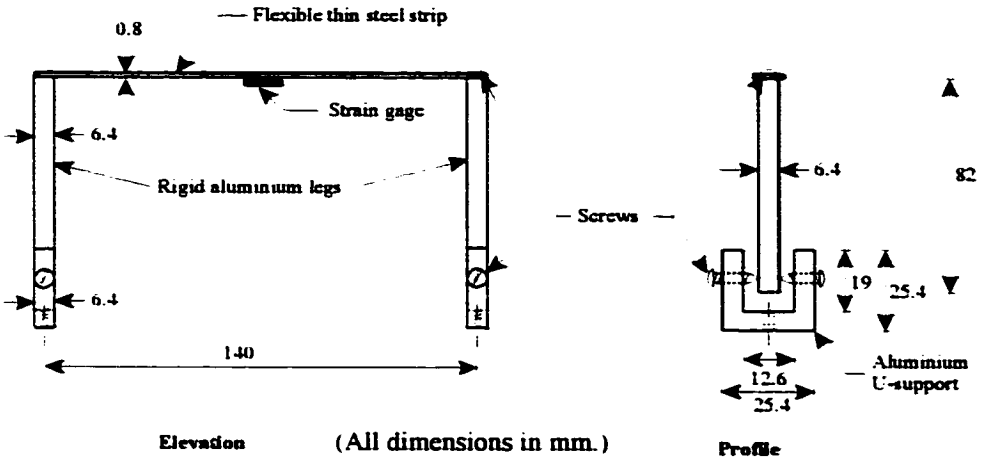

Figure e.1 Clip gage dimensions.

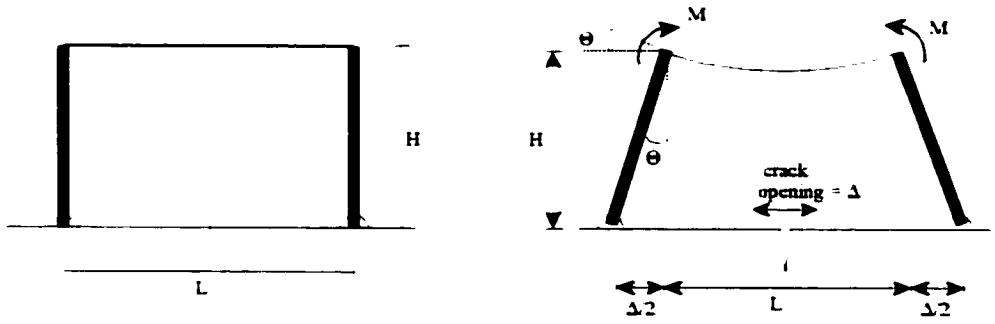

Figure e.2 Clip gage measuring crack opening.

Appendix F

Design of Tyfo Repair

F.1 Masonry rehabilitation with Tyfo fiberglass strips

In this retrofit strategy, piers are assumed to have failed in a rocking mode. This mode of failure is a desirable one, as it is a deformation-controlled mode allowing for energy dissipation by rocking motion of the piers. Damage is limited to horizontal cracks at the ends, top and bottom of the pier. The objective is to use the Tyfo strips to preserve the desirable pier rocking mode and avoid the possibility of changing the mode of failure from rocking (deformation-controlled mode) to diagonal tension (force-controlled mode).

However, there exists no accepted design procedure that could be used to design the strips to achieve this objective. A 100 mm strip was arbitrarily selected. The following calculations attempt to assess what would be the corresponding stresses and whether the intended results could have been predicted.

Material properties:

Tyfo SEH 51

- Ultimate tension strength: 552 MPa
- Ultimate elongation strain: 0.02
- Elastic Modulus: 27579 MPa
- Thickness: 1.3 mm

Masonry

- Compressive strength: 22.2 MPa
- Ultimate compressive strain: 0.003
- Elastic Modulus: 850 f_m' MPa

Using the CGSEEB values calculated in Chapter 3 (Table 3.2) and the free body diagrams from Figs f.1 to f.4, the following calculations (shown in details, at first, for the central pier)

can be performed. It is assumed that 100 mm wide strips are installed on both sides, i.e., inside and outside each pier.

If the strip is assumed to have reached its ultimate strength, then the tension force is:
$T = \phi_f f_u A = 0.75(552)(1.3 \times 2 \times 100) = 107.6$ kN
where ϕ_f is taken as 0.75, based on the resistance factor for Fiber Reinforced Polymers (FRP) from a draft version of the proposed Canadian Standards Association (CSA) S806-00 for Design and Construction of Building Components with Fibre Reinforced Polymers (CSA 1999).

Thus, from Fig. f.2, it can be found that: $P = Q + T$, or $P = P_D + C + T$
The axial load, P_D for the central pier is 25.9 kN. For equilibrium: $C = T$,
therefore $P = 25.9 + 2(107.6) = 241.2$ kN
Substituting this value into the pier rocking capacity equation:

$$V_r = 0.9\frac{D}{H}P \qquad (1)$$

where D = 1410 mm, H = 953 mm for the central pier, the maximum rocking capacity, V_r is calculated to be 321 kN which is greater than the pier diagonal tension capacity, V_{dt}, 59.8 kN. Therefore, a diagonal tension failure should occur first.

To avoid changing the mode of failure from rocking to diagonal tension, the maximum rocking value with Tyfo strips, V_r, was assumed to be less or equal to the pier diagonal tension capacity, V_{dt}.

Thus, for the central pier: $V_r \leq 59.8$ kN $= V_{dt}$,
therefore, from (1): $P = 44.9$ kN, and C or $T = (P - P_D)/2 = 9.5$ kN

The stress in each strip, is $f_f = T/\phi_f A = 9.5 \times 10^3/(0.75)(2x100x1.3) = 48.7$ MPa.
The corresponding strain is $\varepsilon_f = f_f / E_f = 48.7/27579 = 0.00177 < \varepsilon_{fy} = 0.02$.

For the masonry in compression, after trial and errors, the depth of the compressive zone, c, is found to be 156 mm. Then from strain compatibility, $\varepsilon_m = \varepsilon_f c/(d-c)$, where d is the distance to the centroid of the fiberglass strip and is: D-(100/2) = 1360 mm.
Thus, $\varepsilon_m = 0.00023$, which is still in the linear elastic range. Therefore, $f_m = E_m \varepsilon_m = 4.33$ MPa.

The total compressive force from the triangular stress prism is:
$C_m = \phi_m (½) f_m b c = (0.55)(0.5)(4.33)(190)(156) = 35.3$ kN
which is the same as $Q = P_D + C = 25.9 + 9.5 = 35.4$ kN OK

Similarly, for the window pier: $V_r \leq V_{dt} = 16.6$ kN
Thus P = 30.2 kN, and C = T = 9.5 kN
For the Tyfo strip, $f_f = 48.7$ MPa, and the corresponding strain is 0.00177.
The masonry compression depth, c, is found to be 73 mm. Using d = 528 mm, the masonry compression strain and the corresponding stress are 0.000284 and 5.36 MPa, respectively.
The total compressive force is 20.4 kN, and $Q = P_D + C = 20.7$ kN. OK

Finally, for the door pier: $V_r \leq V_d = 24.5$ kN
Thus P = 57.9 kN, and C = T = 21.9 kN
For the Tyfo strip, $f_f = 112.4$ MPa, and the corresponding strain is 0.00407.
The masonry compression depth, c, is found to be 82 mm. Using d = 833 mm, the masonry compression strain and the corresponding stress are 0.000444 and 8.39 MPa, respectively.
The total compressive force is 35.9 kN, and $Q = P_D + C = 36.0$ kN. OK

From the above calculations, the door pier governs the design because it produces the largest stress in the masonry and fiberglass strips. Therefore, a repair solution using Tyfo strips SEH 51, 100 mm wide on the left and right sides of each pier, and on both wall faces (i.e. both inside and outside the building) should be adequate.

However, the capacity of the bond between the epoxied strips and the wall surface is not known. During pier rocking, as the crack opens, the strip may debond from the wall surface around this location. Assuming the strip elongation to be equal to the crack opening, the required length over which the strip may debond can be calculated.

Using the strains previously calculated and assuming a crack opening of 10 mm, the length of strip over which debonding may occur is: $L = \Delta L/\varepsilon$

Hence, for the central pier, L = 10/0.00177 = 5650 mm, a value larger than the pier's height, 953 mm. Thus, it is expected that the strips may debond from the wall surface before reaching their ultimate strength. Similarly, for the window pier, L = 10/0.00177 = 5650 mm, and door pier, L = 10/0.00407 = 2457 mm.

F.2 Design of Tyfo WEB for corner wrap

It has been observed that masonry walls can develop vertical cracks in the corners during earthquakes. Therefore, the corners of the URM specimen were wrapped with Tyfo WEB. This fabric has fibers in both directions of weave for added in-plane shear capacity.

Material properties:

Tyfo WEB

- Ultimate tension strength: 207 MPa
- Ultimate elongation strain: 0.015
- Elastic Modulus: 13790 MPa
- Thickness: 0.4 mm

The expected shear stress at the flange-to-web interface (where flange = cross wall, web = shear wall) of the URM specimen was calculated, as shown in Fig. f.5.

The effective wall flange length, x_2, was taken as six times the flange thickness, t_2 (CSA S304.1-94 1994). Thus, $x_2 = 6\ t_2 = 6\ (190) = 1140$ mm.

From strength of materials, the shear flow at the interface is given by:

$$v = \frac{VQ}{I} \tag{2}$$

Thus $Q = A\ \bar{y} = 1140 \times 190 \times (4091-190)/2 = 4.225 \times 10^8$ mm^3, and $I = 2.733 \times 10^{12}$ mm^4. V is taken as the total rocking resistance calculated by the CGSEEB i.e., $\Sigma V_r = 46.7$ kN. Therefore, from (2) v is 7.22 N/mm.

The strength per length of Tyfo WEB was assumed to be: $T_f = \phi_f f_{fu} t_f$
where f_{fu} and t_f are the fiber ultimate tension strength and the fiber's thickness, respectively.

Thus, T_f is 62.1 N/mm, a value greater than the expected shear flow at the corner interface. Therefore, it was recommended to wrap the specimen's corners with Tyfo WEB, both inside and outside the building, to increase their shear resistance and maintain their structural integrity, as shown in Fig. f.6.

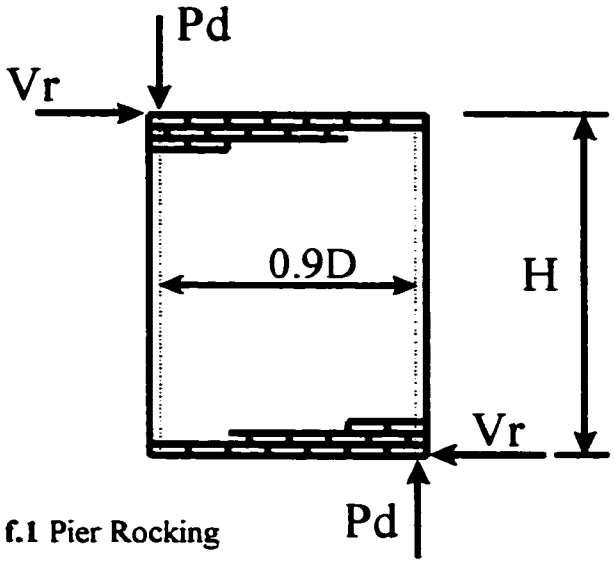

Figure f.1 Pier Rocking

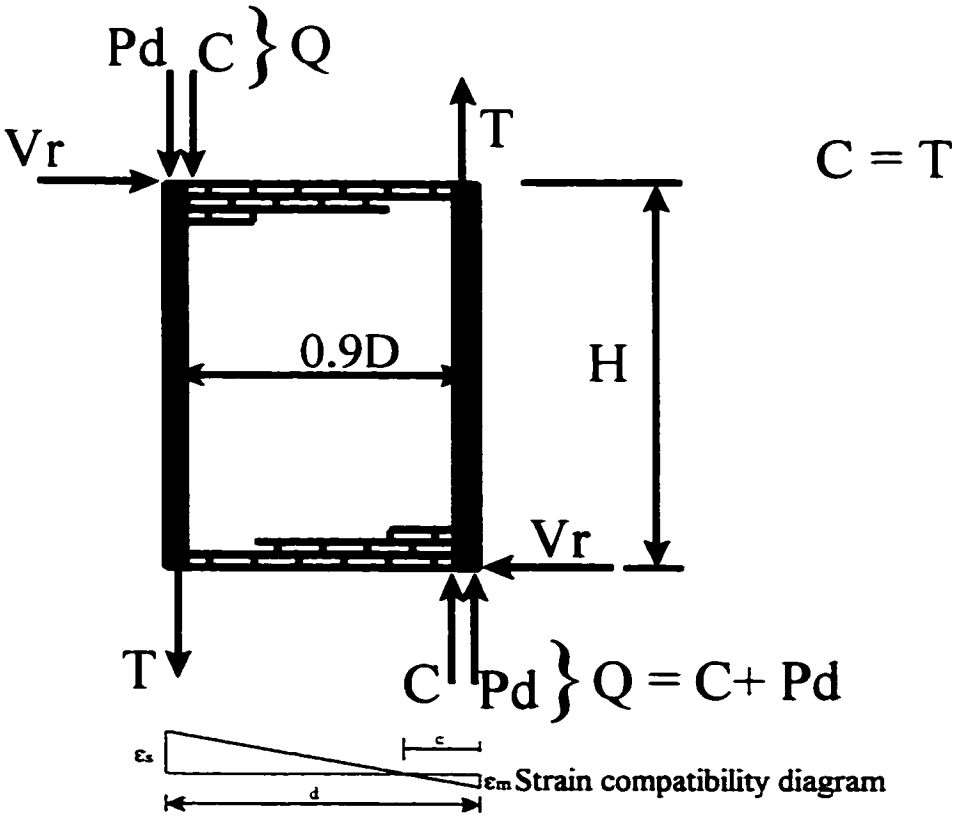

Figure f.2 Pier Rocking with Tyfo strips and strain compatibility diagram.

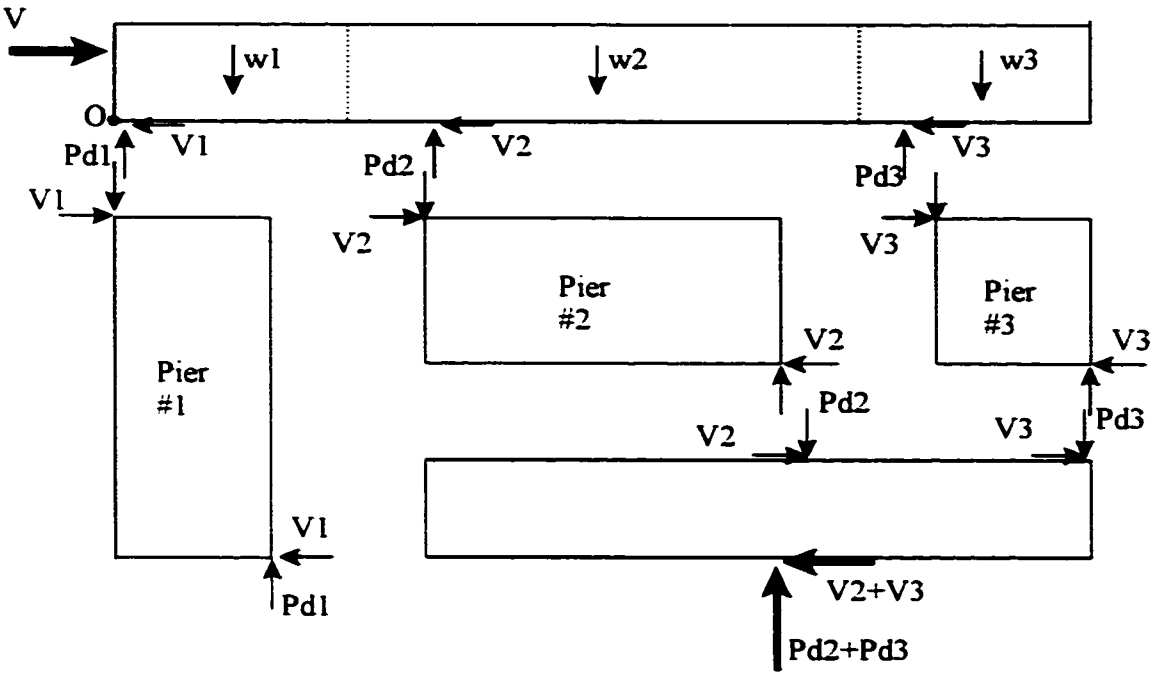

Figure f.3 Free body diagram of URM.

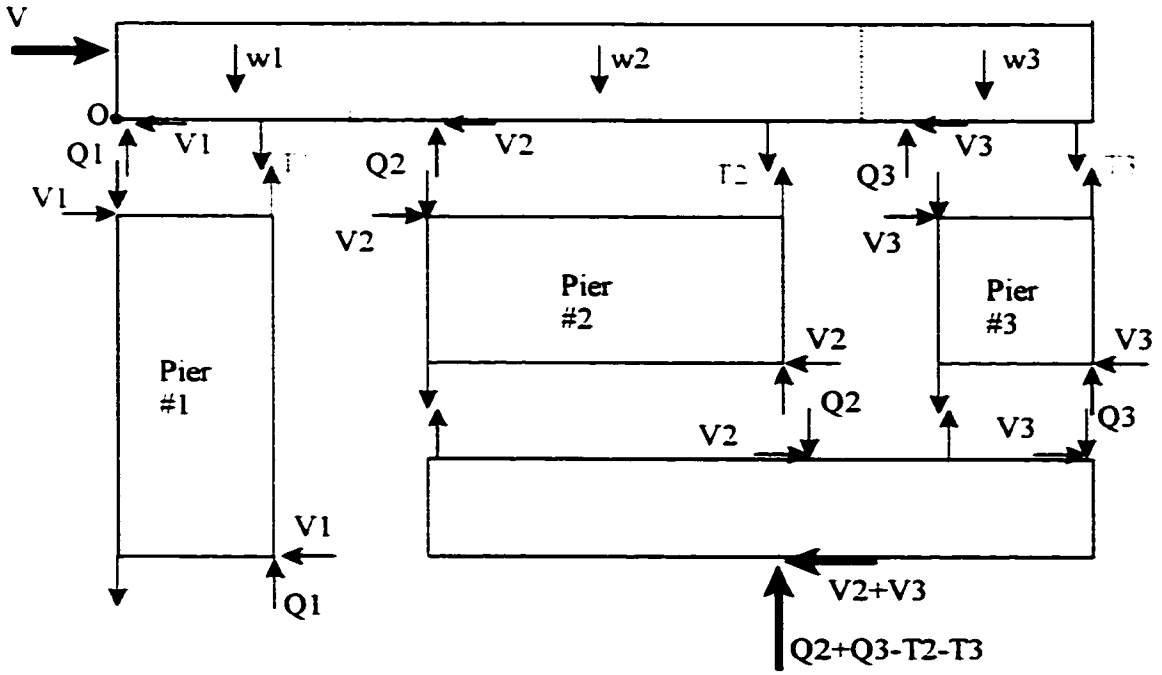

Figure f.4 Free body diagram of URM with Tyfo strips.

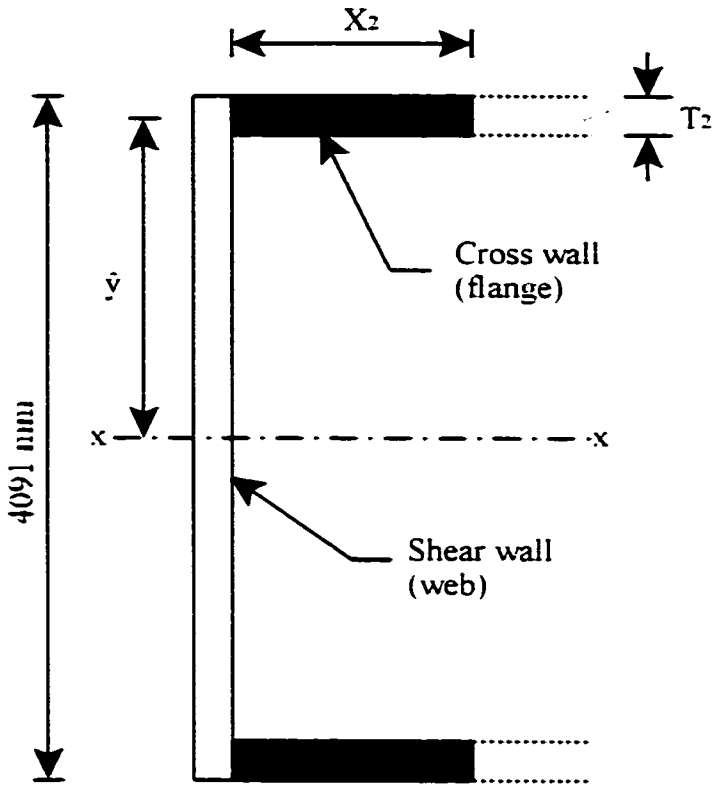

Figure f.5 Assumed model used for calculation of the shear flow at the corner interface.

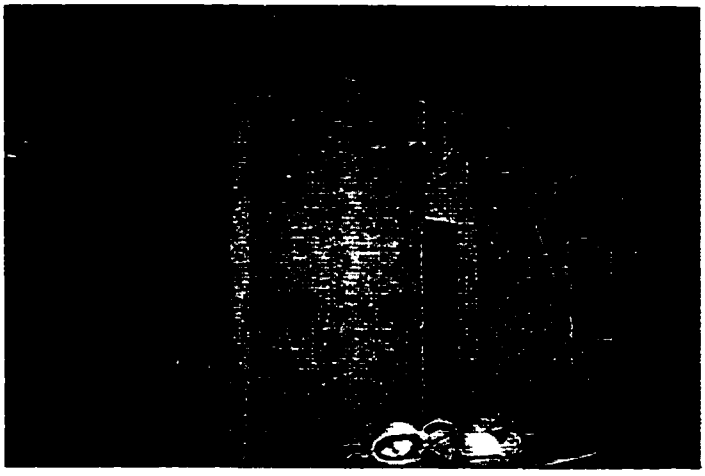

Figure f.6 URM specimen repaired with Tyfo material.

Appendix G

Dynamic out-of-plane wall stability

G.1 Dynamic out-of-plane wall stability

The following calculations are based directly on the method presented in "Seismic design of reinforced concrete and masonry buildings" section 7.8.2, by T. Paulay and M.J.N. Priestley:

The forces acting on the wall and the moments at the center are shown in Figs. g.1 and g.2, respectively.

Data:

-wall width, height, and thickness: 1295 mm, 1448 mm, and 95 mm, respectively.

-masonry compressive strength: $f'_m = 2.50$ MPa

-Elastic modulus: $E_m = 2125$ MPa

-wall mass: 357 kg

-moment of inertia = $bt^3/12 = 1295(95)^3/12 = 9.253 \times 10^7$ mm^4

Conditions at: *cracking*

$M_{cr} = Rt/6$

with $R = P + 0.5W_i$

where R is the resulting gravity load acting on the upper half of the wall, P is the applied gravity load, and W_i is the self-weight.

Since no additional gravity load were considered, P = 0, thus $R = 0.5(357 \times 9.81) = 1751$ N

$M_{cr} = Rt/6 = 1751(95)/6 = 27.7$ kN.mm

The distributed lateral forces required to cause M_{cr} is given by: $M_{cr} = w_r h^2/8$ or, $w_r = 8M_{cr}/h^2$

Since $w_r = ma_r$, the acceleration required to cause cracking can be readily calculated:

$w_r = 8(27.7 \times 10^3)/(1448)^2 = 0.106$ N/mm

$a_r = 0.106/(0.357/1448) = 0.106/(2.465 \times 10^{-4}) = 429$ mm/s^2 $= 0.044g$

The displacement at the center is given by: $\Delta = 5w_r h^4/384EI$

$5(0.106)(1448)^4/384(2125)(9.253 \times 10^7) = 0.0309$ mm

Alternatively, the acceleration required to develop a displacement Δ is given by:

$a_r = (8/mh^2) R(x - \Delta)$ where x is the location of the resultant force R from the centroid.

At cracking $x = t/6 = 95/6 = 15.8$ mm

Hence, $a_r = \{8/(2.465 \times 10^{-4})(1448)^2\} 1751(15.8 - 0.0309) = 427$ mm/s^2 = 0.044g, same as before.

Half cracked

$M = 2M_{cr} = 55.4$ kN.mm

$\Delta = 4\Delta_{cr} = 0.124$ mm

$x = t/3 = 31.7$ mm

$a_r = (8/mh^2) R(x - \Delta) = 856$ mm/s^2 = 0.0872g

3/4 cracked

$M = 2.5M_{cr} = 69.3$ kN.mm

$\Delta = 16\Delta_{cr} = 0.494$ mm

$x = 5t/12 = 39.6$ mm

$a_r = (8/mh^2) R(x - \Delta) = 1060$ mm/s^2 = 0.108g

At ultimate

The maximum value for x will occur when the resultant R is at the edge of the wall. Instability will occur when $\Delta = x_{max}$.

$x_{max} = (t - a)/2$

where $a = R/0.85f'_m t$

Thus, $a = 1751/\{(0.85)(2.50)(95)\} = 8.67$ mm

and $x_{max} = (95 - 8.67)/2 = 43.2$ mm

Using the equal energy approach, as shown in Fig. g.3,

$a_e = (2kA)^{1/2} = [(2)(0.044/0.0309)(0.108)(43.2)(½)]^{1/2} = 2.58$g

G.2 Out-of-plane strength of URM confined by stiff members

In this section the out-of-plane strength of unreinforced masonry panels confined by stiff frame members is calculated following the method presented in section 7.4.2 (d) from Paulay and Priestley (1992). The forces acting on the wall panel are shown in Fig. g.4.

The compression membrane strength envelope can be calculated from the following set of equations:

Compressive zone depth: $c = t/2 - \Delta/4$

Compression strut force per unit width: $C = 0.72 f'_m c$

Moment capacity at hinges per unit width: $m_i = (C/2)(t - 0.85c)$

Equivalent response acceleration: $a = (8/mh^2)(2m_i - C\Delta)$

Thus, the acceleration required for a central displacement can be calculated and is plotted in Fig. 5.18.

G.3 Face loaded URM walls

In this section, the seismic behavior of face loaded unreinforced masonry walls is assessed using a model proposed by Blaikie and Davey (2000).

From the free body diagram shown in Fig. g.5, and using simple statics,

$V = 2/H\{W(t - Y) + O(3t/2 - 2Y)\}$

where V is a point load acting at mid-height, W is the total wall weight, O is the overburden load, Y is the central displacement, and H and t are the wall height and thickness, respectively.

When $Y = 0$, V is max, then $V_{max} = (t/H)\{2W + 3O\}$

and $Y_{max} = t\,(W + 1.5O)/(W + 2O)$ thus, the load deformation relationship for a point load acting at mid-height is $V = V_{max}\,(1 - Y/Y_{max})$.

Since no overburden load was applied on the specimen, $Y_{max} = t$

For a uniformly distributed load, V need to be replaced by wH/2. Thus V_{max} becomes $w_{max}H/2 = (t/H)(2W)$ or $w_{max} = 4tW/H^2$,

and V becomes $wH/2 = (4tW/H^2)(H/2)(1 - Y/Y_{max})$ or $w = (4W/H^2)(t - Y)$

Since $w = ma$, the acceleration required can be calculated for a given central displacement as follow: $a = 4W(t - Y)/(H^2m)$, and the curve is plotted in Fig. 5.18.

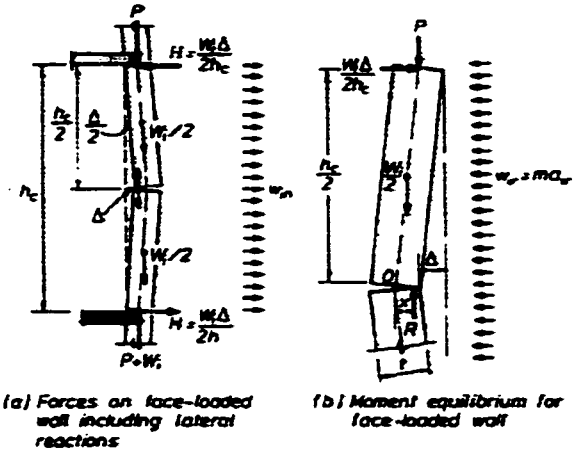

Figure g.1 Out-of-plane response of unreinforced wall (Pauley and Priestley 1992).

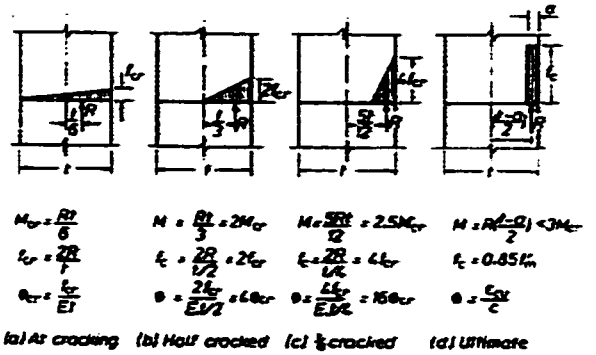

Figure g.2 Moments and curvatures at center of face-loaded wall (Pauley and Priestley 1992).

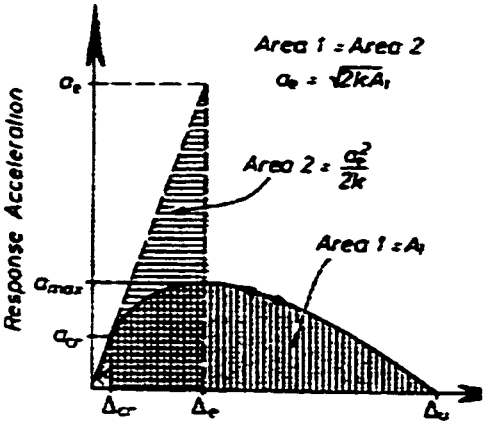

Figure g.3 Equal-energy principle for equivalent elastic stiffness (Pauley and Priestley 1992).

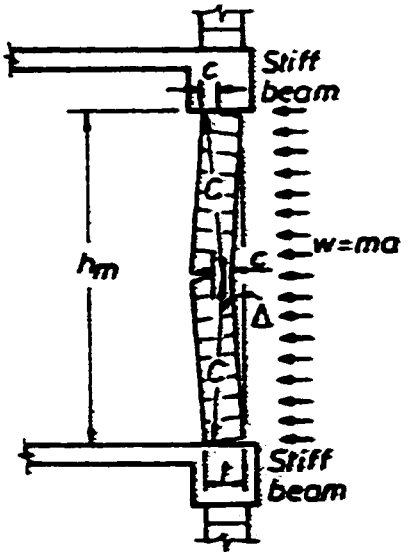

Figure g.4 Compression membrane action in infill panels (Pauley and Priestley 1992).

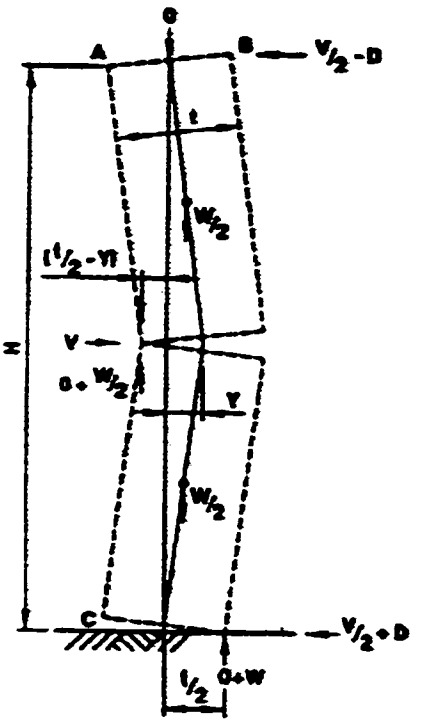

Figure g.5 Face loaded wall under static loading (Blaikie and Davey 2000).